Fundamental Studies on Propagation Mechanisms and Deposit Characteristics of Rock Avalanches

by

Qingqing Yang

A dissertation submitted in partial fulfillment of the requirements
for the degree of doctor of philosophy
to

Gunma University

September, 2012

CONTENTS

CHAPTER 1

INTRODUCTION

1.1 GENERAL INTRODUCTION

Long run-out rock avalanches, or Sturzstroms as called by Heim (1932), are defined as extremely rapid, massive, flow-like motion of fragmented rock derived from a bed-rock failure. They travel vast horizontal distances compared with its comparatively small vertical drop in height—as much as 20 or 30 times the vertical drop. Their extraordinary mobility appears to be a consequence of sustained fluid-like behavior during motion (Collins and Melosh, 2003). Rock avalanches flow across land fairly easily, and their mobility increases with the volume. That is, the deposit of a large rock avalanche with a volume larger than 10^6-10^7 m^3 will usually extend much farther than smaller one (e.g. Scheidegger, 1973; Hsü, 1975; Legros, 2002). The large deposit also extend much farther than would be expected using a friction model (Hungr et al. 2001).

Rock avalanches have been extremely costly in terms of human lives and of engineering developments (Davies, 1982). Some historic rock avalanches in the world are listed in Table 1.1. One of the most notorious events is the Vaiont rockslide of 1963, which involved a mass of approximately 2.7×10^8 m^3 collapsed into the reservoir generating a wave which overtopped the dam and hit the town of Longarone and other villages: almost 2,000 people lost their lives (Genevois and Ghirotti, 2005). The Val Pola rock avalanche that occurred close to Bormio in northern Italy caused 29 deaths and resulted in the Valtellina disaster (destruction of villages, road closure, and floodability threat) with the total cost of 400 million euro. The Frank rock avalanche with a volume of 4×10^7 m^3 collapsed from the peak called the Turtle Mountain and killed more than 76 people. The great Good Friday earthquake of 1964 triggered a large rock avalanche that fell 600 m and then spread 5 km across the Sherman Glacier, resulting in a blanket 3-6 m thick. An Ms 8.0 earthquake triggered a huge avalanche from the summit of Nevado Huascarán, the highest peak in Peru. Part of the avalanche jumped a 300 m ridge, wiping out the town of Yungay and killing 18,000 inhabitants, and this is the worst avalanche disaster in history.

Table 1.1 Historic rock avalanches in the world

Event	Location	Date	Volume (10^6 m^3)	Apparent friction coefficient	Fatalities	Remark
Flims	Switzerland	Prehistoric	12,000	0.13	/	/
Köfels	Austria	Prehistoric	2,200	0.18	/	Frictionite observed
Bandai	Japan	1888	1,500	0.11	500	Volcanic eruption
Daguangbao	China	2008	750	0.23	38	/
Tombi	Japan	1858	410	0.13	40	/
Blackhawk	USA	Prehistoric	300	0.13	/	/
Vaiont	Italy	1963	270	0.34	2,000	Flood wave
Silver Reef	USA	Prehistoric	220	0.13	/	/
Huascarán	Peru	1970	80	0.07	18,000	Giant bounces
Hope (BC)	Canada	1965	50	0.37	2	/
Goldau	Switzerland	1806	40	0.21	457	/
Val Pola	Italy	1987	40	0.46	29	Flood wave
Frank	Canada	1903	40	0.25	76	/
Sherman	USA	1964	30	0.21	/	Run-out on glacier
Donghekou	China	2008	15	0.24	780	/
Elm	Switzerland	1881	10	0.31	120	/

1.2 BACKGROUND AND MOTIVATION

Numerous hypotheses have been put forward to explain the extraordinary high mobility of rock avalanches. Some of these have invoked the presence of a lubricating/fluidizing medium. Air as a means was first considered by Kent (1966) in the sense of fluidization of a solid mass in advanced state of disintegration by the action of thin air layers ‘trapped’ between the particles. Shreve (1968a, 1968b) formulated an alternative by assuming a comparatively thin layer of compressed air supporting the mass from below. Instead of air lubrication/fluidization, high pore pressure generation is often a necessary condition to trigger mass collapse under undrained conditions. Sassa et al. (1996) proposed a

conception of sliding-surface liquefaction as the reason of the high mobility of landslides. Water can further be added to the base of landslides by incorporation of saturated valley sediments or directly by mixing with water from a river (Goguel, 1978). Vapor (Habib, 1976), volcanic gases (Voight et al., 1983), or a suspension of fine particles (Hsü, 1975) was also treated as a medium for the fluidization of landslides. Other authors proposed fluid-absent, granular models, e.g. acoustic fluidization (Melosh, 1979), spreading of a rapid granular flow (Davies, 1982), self-lubrication (Campbell, 1989), or spreading of a granular flow in a transition between frictional and collisional regime (Campbell et al., 1995). A continuum model with bulk rheological properties was presented by Voight et al. (1983). Though many of the invoked mechanisms may be important in some specific events, no general agreement has been achieved and the debate continues (Davies and McSaveney, 1999; McSaveney, 2002; Legros, 2002).

Unless the avalanches are artificially triggered, avalanche motion is difficult to observe and systematically record in nature because these events are devastating and their initiation is unpredictable. This is the reason why the dynamics of natural avalanches remain enigmatic and only the deposit morphology is generally known. If experimental flows are able to be up-scaled based on similarity law, the measurements in the laboratory allow inferences for the dynamics of natural avalanches. Furthermore, theoretical solution and numerical simulation provide a tool to predict the motion along its track from initiation to rest. The comparison between the predicted quantities by theoretical and numerical models and measured counterparts in the laboratory can verify the applicability of the theory and efficiency of numerical method. This, ultimately, can establish a nice and strong correlation among the theory, numeric, and experiment.

The well-known depth-integrated avalanche model by Savage and Hutter (1989) has been generalized in different stages since the early nineties of the last century from simple to arbitrary channelized topographies. Today these are available in different versions of comparable performance and have brought the science of avalanche modeling an important step ahead (Pudasaini and Hutter, 2007).

A number of researchers have contributed to numerical simulations of avalanching flows associated with demonstrate fundamental, physically interesting, and practically applicable results (e.g. Bouchut and Westdickenberg, 2004; Pudasaini et al., 2005b). The ultimate aim of all models is to establish numerical solution techniques in mountainous

avalanche prone regions, in which geographical information system (GIS) can be directly applied.

In spite of these efforts devoted to the physical understanding of avalanche formation and motion, rock avalanches are by no means fully investigated even the fundamental mechanisms of motion are partially unknown, and a realistic prediction of future catastrophic events is far from being attempted (Erismann, 1979; Legros, 2002; Evans et al., 2009).

1.3 SCOPE AND OBJECTIVES OF RESEARCH

One of the most important physical quantities of rock avalanches is their velocity distribution. From a structural engineering and planning point of view, one must know the velocity field of rock avalanches in order to design buildings, roadways, and rail transportation and appropriately estimate impact pressures on obstructing buildings that may hit by an avalanche along its track down a mountain valley (Pudasaini and Hutter, 2007). Equally important quantity is deposit characteristics. The information about the covered extent and impacted pressure of avalanches is the basis for hazard map, which is the primary tool that researchers and officials use for protection against rock avalanches.

Remote sensing techniques have been used to record the front velocity of moving snow (Fily ea al., 1997). However, the disadvantage of such in-situ experiments is uncontrollable. Laboratory experiments are able to overcome this disadvantage, and thus errors may be more easily estimated. Many researchers (e.g. Manzella and Labiouse, 2009; Valentino et al., 2008; Okura, 2000a) have conducted laboratory experiments to investigate the effects of potential factors on associated parameters—velocity and deposit characteristics of granular flows.

In order to investigate propagation mechanisms and deposit characteristics involved in rock avalanches, a series of fundamental studies, including laboratory experiments, theoretic predictions, and numerical simulations, was conducted. Figure 1.1 shows technical roadmap. Small flume tests were carried out to investigate the effects of some factors, i.e., interactions between constitute particles, lower slope inclination, and seismic waves, on deposit characteristics of granular flows. Large flume tests were also performed to examine some potential factors, i.e., released material, material volume,

initial arrangement, consecutive release, obstacle, and bottom roughness, influencing the mass-front velocity and deposit characteristics of granular flows. A simple lumped mass model based on energy approach was proposed to describe the velocity of granular flows by which relatively complex topography can be considered. Discontinuous deformation analysis was applied to simulate the experimental flows in the large flume and three large rock avalanches triggered by the 2008 Wenchuan earthquake. Furthermore, shaking table tests for jointed rock slopes were used to study their failure mode and dynamic behavior.

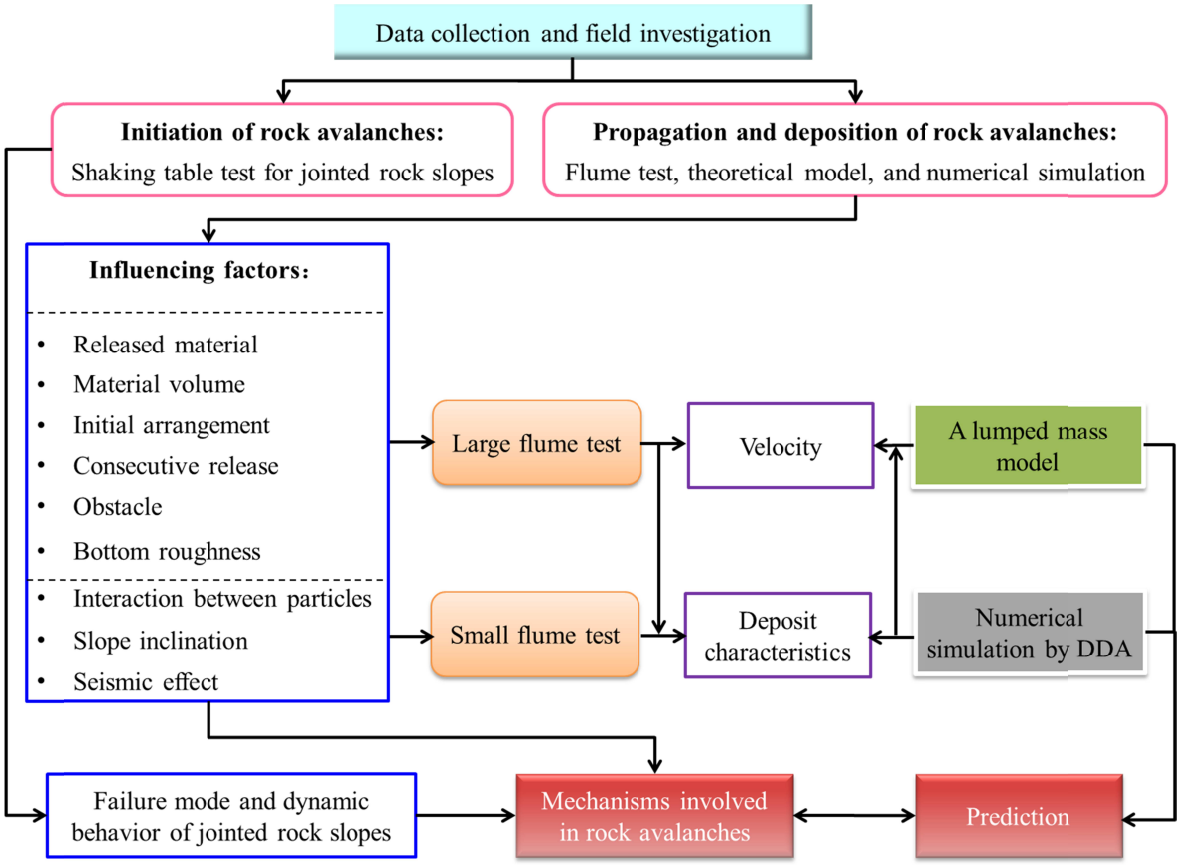

Figure 1.1 Technical roadmap of this dissertation

1.4 DISSERTATION ORGANIZATION

This dissertation is organized into seven chapters in addition to this introductory chapter. The contents of each chapter are briefly described as follows.

In Chapter 2, small flume tests of granular flows are presented. Mono-materials and composites of them were released, and their run-outs and deposition height were measured. The effect of interactions between constitute particles on enhancing the mobility of granular flows was examined.

Small flume tests of granular flows on a shaking table are presented in Chapter 3, in order to investigate the propagation mechanisms and deposit characteristics of earthquake-induced rock avalanches and debris avalanches. Released material, input sinusoidal wave, and shaking subsequence were varied to study the dynamic behavior and response of these granular flows.

Chapter 4 focuses on some factors (such as released material, material volume, initial arrangement, consecutive release, obstacle, and bottom roughness) influencing the mass-front velocity and deposit characteristics of granular flows released in a large flume.

A simple lumped mass model, based on energy approach, to describe the velocity of granular flows is proposed in Chapter 5. Predicted velocity by this model was compared with the measured velocity of granular flows in the large flume presented in Chapter 4, to verify the applicability of the simple model.

In Chapter 6, numerical simulations by discontinuous deformation analysis are presented. Granular flows in the large flume and three large rock avalanches triggered by the 2008 Wenchuan earthquake were reproduced, and the key parameter used in the numerical analysis was discussed.

Shaking table tests for jointed rock slopes are presented in Chapter 7. The failure mode and dynamic behavior of the jointed rock slopes under dynamic conditions is described briefly.

Chapter 8, the final chapter of this dissertation contains a brief review of major contributions and conclusions of this research.

CHAPTER 2

SMALL FLUME TESTS OF GRANULAR FLOWS

2.1 INTRODUCTION

Granular flows are widespread in nature as rockslides, volcanic block-and-ash pyroclastic flows, and dry rock and debris avalanches. An important feature of these flows is their extremely high mobility (up to tens of kilometers), which is capable of moving freely from their sources. Many researchers (e.g. Heim, 1932; Scheidegger, 1973; Hsü, 1975) claimed that the mobility of these flows is dependent on their volume, namely large events travel farther than smaller ones. However, the long run-out granular flows moved far beyond the distance that could have been expected when considering the size effect alone (Erismann and Abele, 2001). The fundamental understanding of the propagation mechanisms of granular flows remains an outstanding issue, in particular when geomorphological circumstances and mechanical properties of involved materials are varied according to different specific events.

The physical behavior of dense granular flows has attracted considerable attention from laboratory experiment and numerical modeling points of view. The dynamics of the collapses of axisymmetric and two-dimensional granular columns onto a horizontal surface and the subsequent granular propagation were well investigated experimentally (e.g. Balmforth and Kerswell, 2005; Savage and Hutter, 1989; Lajeunesse et al., 2004, 2005; Lube et al., 2004, 2005). The test results challenged the traditional view that the run-out depends only on the volume of the materials involved, and emphasized the importance of the initial aspect ratio of the column instead. Other researchers presented some numerical simulations to reproduce natural mass flows over complex terrains (e.g. Iverson and Denlinger, 2001; Denlinger and Iverson, 2001) and experimental flows (e.g. Crosta et al., 2009; Deangeli, 2008). Parameters used in the numerical simulations are usually obtained by back analyses of occurred events or by calibration, as a result of the extreme complexity of such phenomena and the still incomplete knowledge of the governing laws controlling the behavior of these materials (Crosta et al., 2009).

Experiment plays a significant role in contributing a better understanding of propagation mechanisms and factors influencing velocity and deposit characteristics (Manzella and Labiouse, 2009). A majority of previous experiments have focused on the case of mono-materials down inclined roughened slope (e.g. Davies and McSaveney, 1999; Manzella and Labiouse, 2009) and particle segregation of binary mixtures (e.g. Savage and Lun, 1988; Möbius et al., 2001). The research accounting for interactions between constitute particles with different grain sizes and shapes is still out of reach. At present, some researchers have claimed that experimental granular flows containing a range of particle sizes can exhibit macro-scale properties that differ from flows containing a single particle size (Phillips et al., 2006; Roche et al., 2006). The variety of mechanical properties can lead to a diversity and complication of behavior due to the interaction of composite components. Actually, natural flows generally contain particles of a fairly wide range of sizes; in some cases, the size range of particles can vary from tens of micrometers up to the order of a meter (Roche et al., 2006). Fragmentation, which is a prominent process in the emplacement of field rock avalanches, causes materials extensively fractured/shattered (e.g. Davies and McSaveney et al., 1999; Davies and McSaveney, 2002, 2009; Crosta et al., 2007). Therefore, considering size grades as many as possible is important for realistically reflecting and understanding natural granular flows.

Roche et al. (2006) performed experiments on a column of fluidized particles that were released into an enclosed channel, and the behavior of fine particles is distinct from that of larger ones. They concluded that the mobility is modified when the mixture of different-sized particles was used, especially with 30% fine particles in mass proportion. Another interesting work was conducted by Phillips et al. (2006). They presented laboratory measurements of flows of binary mixtures of fine and coarse granular materials, and showed that the interaction between them can result in significantly increased mobility. They used heuristic models to illustrate that some mechanisms are likely to occur in granular flows containing a wide range of grain sizes.

In this chapter, the run-out and deposition height of granular composites moving over a rough inclined flume were investigated by conducting a series of laboratory experiments, and the effect of the interactions between composite components on the mobility of the granular flows was examined. These granular flows contained a range of particle sizes from 0.1 mm to 10 mm, which was limited relative to the materials

involved in natural flows. Determining the chief interactions with a wide size distribution are difficult, and the choice of the particle sizes in this study was helpful to easily understand propagation mechanisms of rock avalanches.

2.2 EXPERIMENTS AND METHODS

2.2.1 Experimental set-up

The two-part flume used in the tests was consisted of two slopes, which were called upper and lower slope, respectively (Figure 2.1). Each slope was 1.5 m in length. The two slopes were connected by hinges in convenience of adjusting their inclinations. The angle of the upper slope was fixed at 45°, and the lower slope was inclined at angles of 0°, 5°, 10°, and 15° to the horizon in these experiments. The width of the flume was 0.18 m, which was sufficiently small for the flows to be one-dimensional; it was also sufficiently large for negligible the effect of side walls. A gate, perpendicular to the upper slope, can be lifted manually (but rapidly). The flows started moving down the flume immediately after granular materials behind the gate were released.

Figure 2.1 Experimental set-up

2.2.2 Employed materials

Compositional effects in flows containing more than one particle size were examined.

Three granular materials were used. The photos of them are shown in Figure 2.2.

a) Gravel: coarse particles; the grain size is 4.75~9.5 mm;

b) Coarse sand: fine particles; grain size is 0.42~2.0 mm;

c) Fine sand: Toyoura sand, which is a very fine material. The grain size is 0.1~0.3 mm.

(a) Gravel

(b) Coarse sand

Figure 2.2 Granular materials used (to be continued)

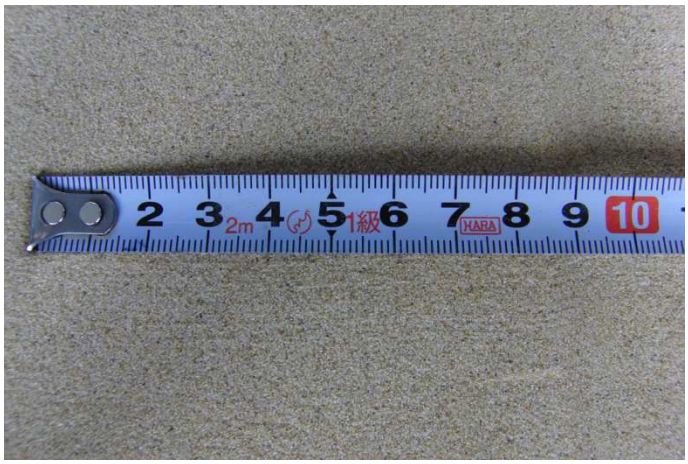

(c) Fine sand

Figure 2.2 Granular materials used (continued)

2.2.3 Data acquisition

Each test was filmed by a video camera. The run-out and deposition height were measured manually after each test. The deposit was divided into two parts based on the accumulation of particles (Figure 2.3). The first part, i.e. the main part of the deposit, represented the coherent main mass of the deposit. The second part, the deposit which was a layer one particle height, was discontinuous from the first part and easy to distinguish. The measurements were conducted by taking into account only the main part of the deposit. Individual particles moved beyond the flume were also not considered in this study. In the literature, the run-out is commonly defined as the total horizontal travel distance from the top of the breakaway scar to the distal end of the deposit, or the horizontal distance travelled by the center of moving mass. In this chapter, the run-out was the length of the main part of the deposit accumulated on the lower slope. This choice facilitated to obtain homogeneous results easy to compare. The deposition height of the main part, perpendicular to the lower slope, was measured at the interval of 10 cm in length along the midstream path of the lower slope.

A total of 88 cases were carried out. Each case was repeated at least three times to evaluate the repeatability and assess the validity of the corresponding measurements.

After the test, the total mass of the deposit was weighted, and the loss of particles was estimated to be less than 1 g.

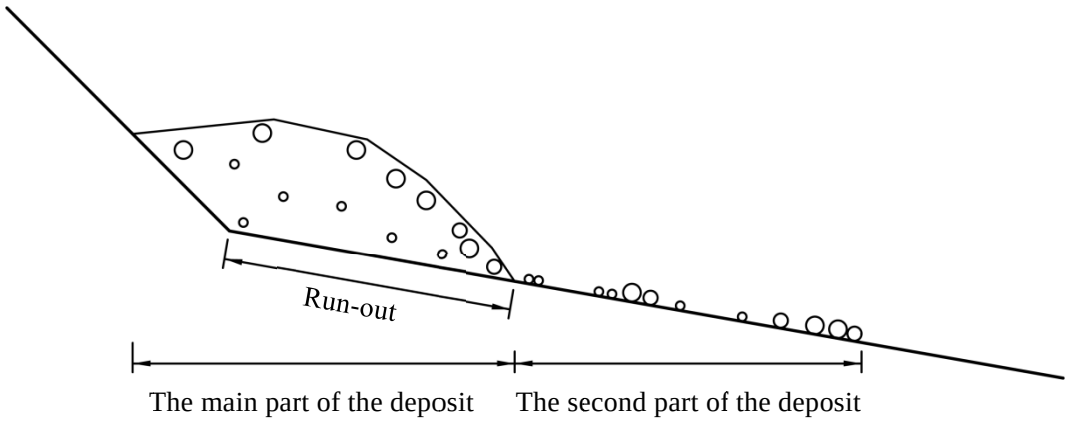

Figure 2.3 Deposit morphology

2.3 EXPERIMENTAL RESULTS

Mono-materials or composites of them with a range of grain sizes were used. These granular composites varied the proportion of constitute particles but maintained the same total mass of 3.0 kg.

2.3.1 Mono-materials

The run-outs of the mono-materials increased with the inclination of the lower slope (Figure 2.4). It is easy to understand that the materials had a higher mobility on steeper slopes. However, it is surprising that the run-outs of the three mono-materials were almost identical on the slope with the same inclination. Coarse materials would move farther than fine materials due to less energy consumption caused by intergranular friction.

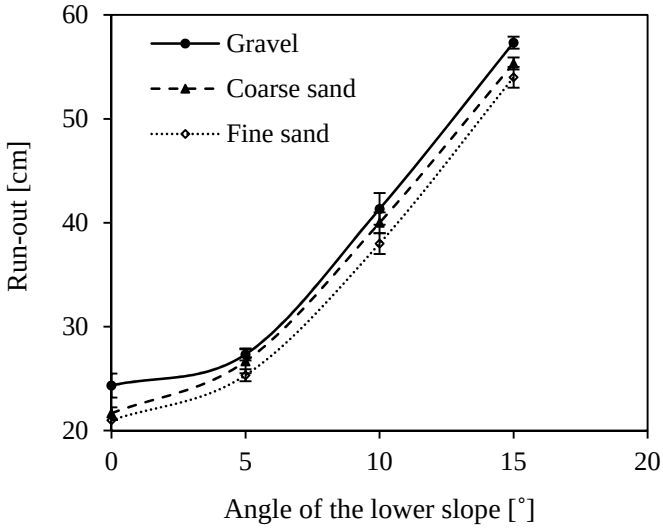

Figure 2.4 Run-out of the main part of the deposit for the three mono-materials on the slopes with different inclinations. The error bars show standard error of the average run-out for each test.

Figures 2.5, 2.6 2.7 and 2.8 show the deposit morphology of the main part of the deposit for the three mono-materials on the 0°, 5°, 10°, and 15° slope, respectively. The deposit morphology of the three mono-materials was similar on the slope with the same inclination.

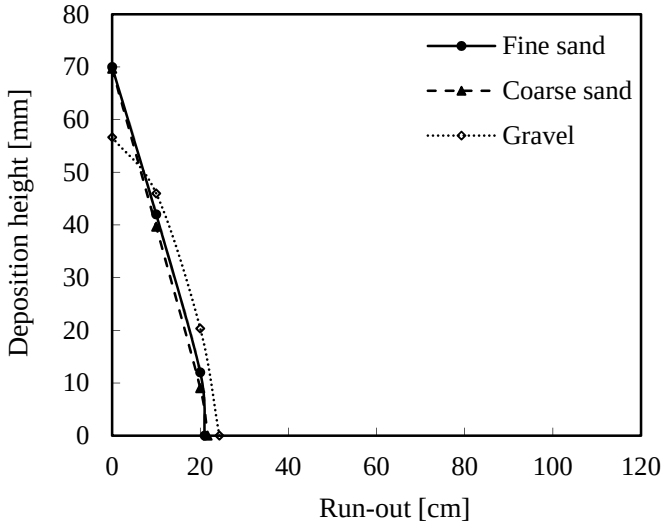

Figure 2.5 Deposit morphologies of the main part of the deposit for the three mono-materials on the 0° slope

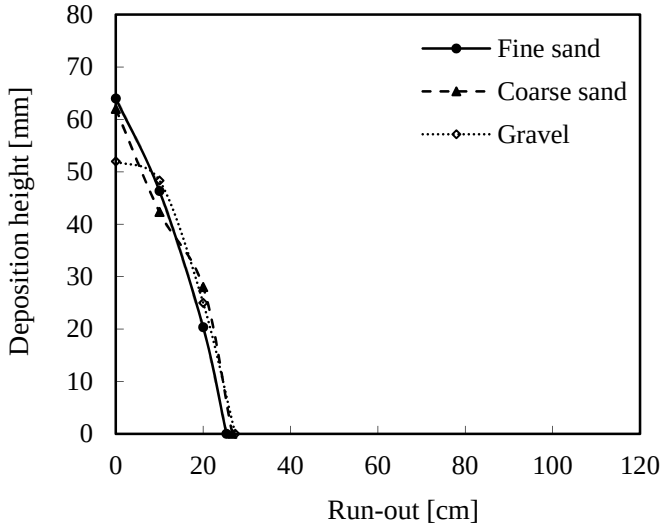

Figure 2.6 Deposit morphologies of the main part of the deposit for the three mono-materials on the 5° slope

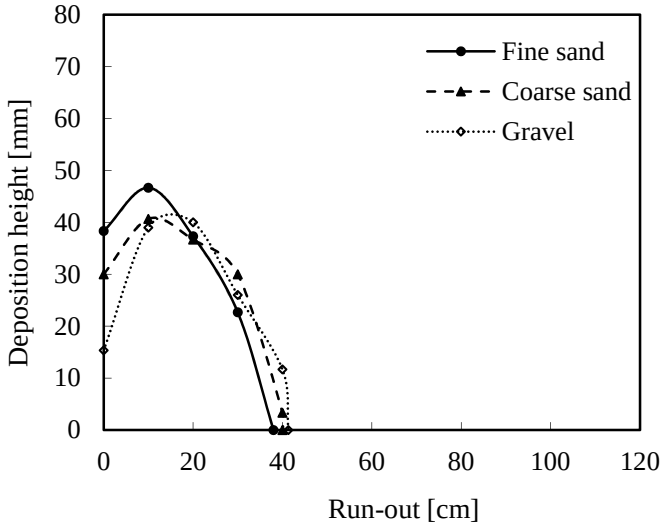

Figure 2.7 Deposit morphologies of the main part of the deposit for the three mono-materials on the 10° slope

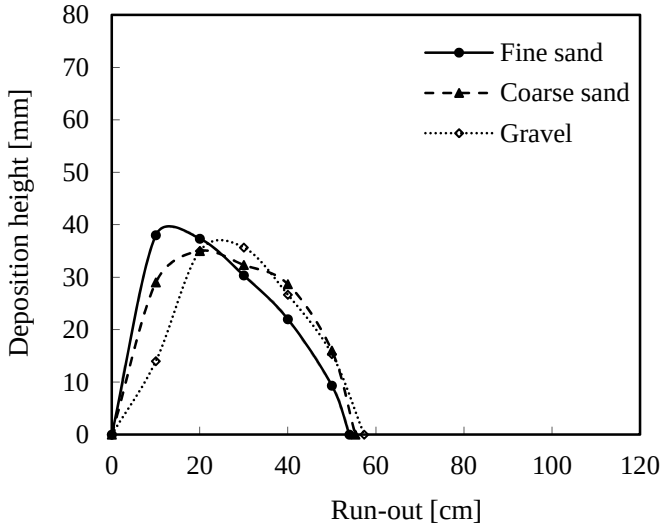

Figure 2.8 Deposit morphologies of the main part of the deposit for the three mono-materials on the 15° slope

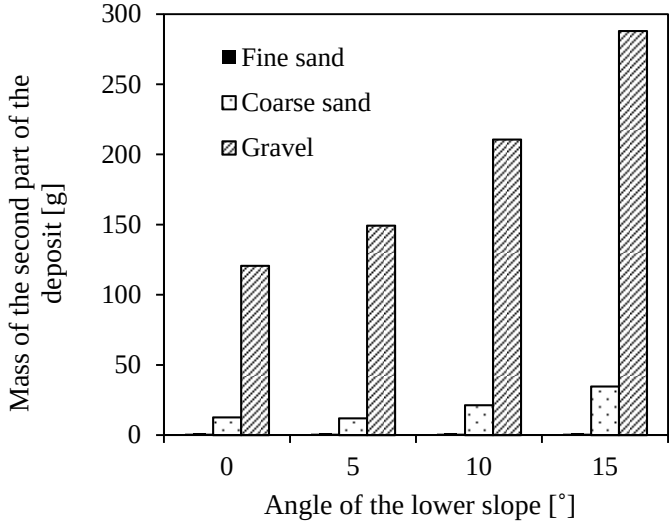

Figure 2.9 Mass of the materials accumulated on the second part of the deposit

The mass of the second part of the deposit was weighted. The coarser the particles were, the more particles accumulated on the second part of the deposit (Figure 2.9). This means that coarse particles were easier to travel a long distance. The mass of the fine sand accumulated on the second part of the deposit was 1.0 g regardless of the inclination of the lower slope. With the increasing angle of the lower slope, more coarse sand and gravel moved far and deposited on the second part, especially for the gravel. This implies

that coarse particles were prone to travel farther than fine particles on the steep slope. In the next section, a series of tests is carried out to examine the interactions between coarse and fine particles by releasing composites containing various proportion of constitute particles.

2.3.2 A composite with the same mass of gravel, coarse sand, and fine sand

A composite was used, which consisted of 1.0 kg gravel (M_g=1.0 kg), 1.0 kg coarse sand (M_c=1.0 kg), and 1.0 kg fine sand (M_f=1.0 kg). The run-out of this composite is shown in Figure 2.10, combined with those of the three mono-materials. The mobility of the composite was significantly higher than the mono-materials. This implies that the interactions between coarse and fine particles were helpful to enhance the mobility of granular flows.

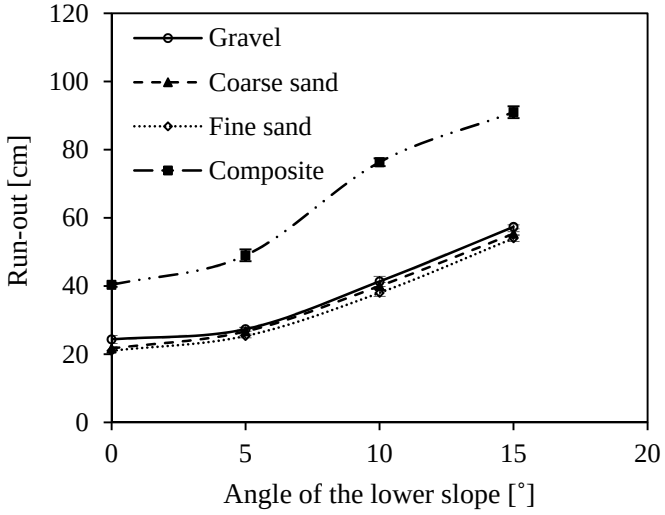

Figure 2.10 Run-out of the main part of the deposit for the composite (M_g=M_c=M_f=1.0 kg) on different slopes, comparing with the run-outs for the three mono-materials. The error bars show standard error of the average run-out for each test.

Figure 2.11 shows the deposit morphology of this composite (M_g=M_c=M_f=1.0 kg) on the 0°, 5°, 10°, and 15° slope, respectively. Comparing with the mono-materials, the

deposit shape of this composite was low and long.

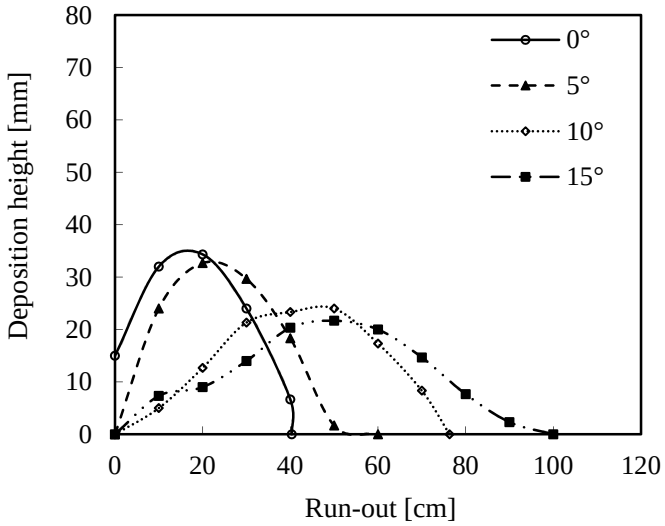

Figure 2.11 Deposit morphology of the main part of the deposit for the composite (M_g=M_c=M_f=1.0 kg) on the different slopes

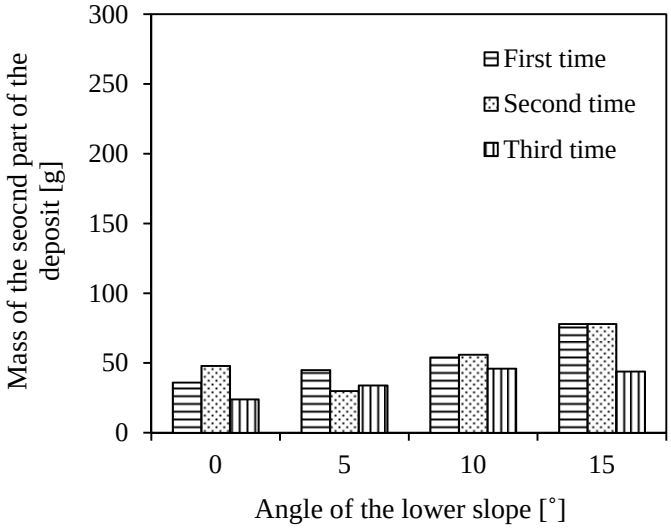

Figure 2.12 Mass of the second part of the deposit for the composite (M_g=M_c=M_f=1.0 kg) over three runs on different slopes

Each case was repeated three times with this composite (M_g=M_c=M_f=1.0 kg), and the second part of the deposit were weighted for each time (Figure 2.12). Less than 100 g of

the materials accumulated on the second part of the deposit, and a majority of particles travelled a long distance. This implies that this situation was more destructive for human habitation and environmental protection.

2.3.3 Composites with various fractions of fine sand

In order to further confirm the effect of the interactions between particles on enhancing the mobility of granular flows, composites with various fractions of fine sand were released. In each series, the mass of the gravel was maintained (1.0 kg, 1.4 kg, or 1.8 kg), and the rest was consisting of coarse sand and fine sand at different mixing proportions. Fine sand mass fraction F_f was defined as the proportion of fine sand in total mass, ranging from 0 (no fine sand) to 0.67 (all fine sand).

Figure 2.13 shows the run-outs of flows on the 15° slope consisting of composites of coarse and fine particles: gravel as the coarse particle, and coarse and fine sand as the fine particle. The mobility was enhanced due to the interactions between particles on the 15° slope, except in the case with 1.0 kg gravel and 2.0 kg fine sand where the run-out of this composite was significantly smaller than that of the three mono-materials.

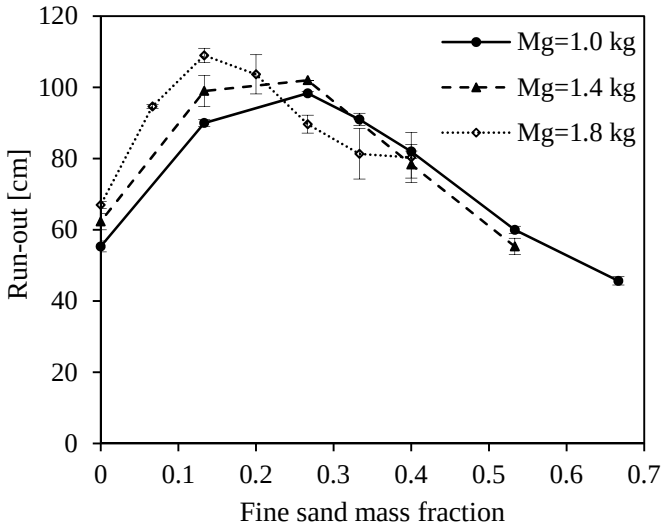

Figure 2.13 Run-out of the main part of the deposit for the composites with various fractions of fine sand on the 15° slope. The error bars show standard error of the average run-out for each test.

The trend of run-outs for the composites in the three series was similar. The run-outs increased with F_f until reaching a peak, and then decreased with further increasing F_f. This suggests that a certain amount of fine sand advanced the mobility of granular flows, and excessive fine sand obstructed their propagation. The reason was that a thin layer of fine sand acted as rollers for the rolling of the gravel, leading to reduce the effective friction resistance during the movement; the interactions between particles became more complicated than they just acted as a single-row roller to lubricate the gravel when excessive fine sand was involved. These rollers were in a dilemma so that the particles were either blocked or forced into sliding. Furthermore, from the point of view of energy, the energy was consumed significantly due to interegranular friction when so excessive fine sand was involved that the gravel was embedded in a matrix of fine sand. This implies that an appropriate proportion of fine particles were partly responsible for the long run-out of rock avalanches.

When F_f was small ($0< F_f \leq 0.2$), the flows with 1.8 kg gravel (dot line, Figure 2.13) exhibited the highest mobility. This implies that the composite containing more coarse particles travelled farther than that with less coarse particles at small F_f. The main cause was that the gravel typically had a high porosity, and the interactions between particles would be reduced by substituting a coarse particle for the same mass of fine particles. Frictional loss was proportional to the surface area of particles available for the interactions, and thus less energy was consumed by intergranular friction when the mass of the gravel increased.

The flow with 1.8 kg gravel at $F_f = 0.13$ (1.8 kg gravel, 0.8 kg coarse sand, and 0.4 kg fine sand) travelled the longest run-out of 109 cm; the maximum run-out of 102 cm was observed for the flow with 1.4 kg gravel at $F_f = 0.27$ (1.4 kg gravel, 0.8 kg coarse sand, and 0.8 kg fine sand), and the peak in run-out was 98.3 cm for the flow with 1.0 kg grave at $F_f = 0.27$ (1.0 kg gravel, 1.2 kg coarse sand, and 0.8 kg fine sand). For the composites with different mass of the gravel, the flows exhibited the highest mobility at different F_f. The interaction of particles with different sizes and shapes became more complicated when internal structure of granular flows was varied. The precise details of interactions between constitute particles are still out of reach.

The flows containing 1.8 kg gravel show a peak in run-out over a range of F_f between

0.1 and 0.2. The peak in run-out extended over a greater range of F_f between 0.1 and 0.3 for the flows containing 1.4 kg gravel, and of F_f between 0.1 and 0.4 for the flows containing 1.0 kg gravel. The peak was sharper in the experiments with 1.8 kg gravel. This suggests that the mobility was more sensitive to the proportion of fine sand when more gravel was involved.

The run-outs of flows on the 10°, 5°, and 0° slope are shown in Figures 2.14, 2.15, and 2.16. The composites also travelled farther than the three mono-materials on these slopes. The trends of run-outs were similar to that on the 15° slope. However, the run-outs on the gentle slopes were shorter than that on the 15° slope. This indicates that the inclination of the lower slope was significantly influenced the mobility of granular composites. The difference in run-out was not significant for a range of F_f on these gentle slopes, comparing with that on the 15° slope. This implies that the effect of the interactions between coarse and fine particles on enhancing the mobility of composites was not fully developed on the gentle slopes, i.e. the rolling motion was difficult to occur on the gentle slopes. On the 5° and 0° slope, the run-outs were almost identical at large F_f(0.3~0.67) regardless of the mass of gravel. This was because the gravel embedded in a matrix of fine sand and was difficult to move on these gentle slopes.

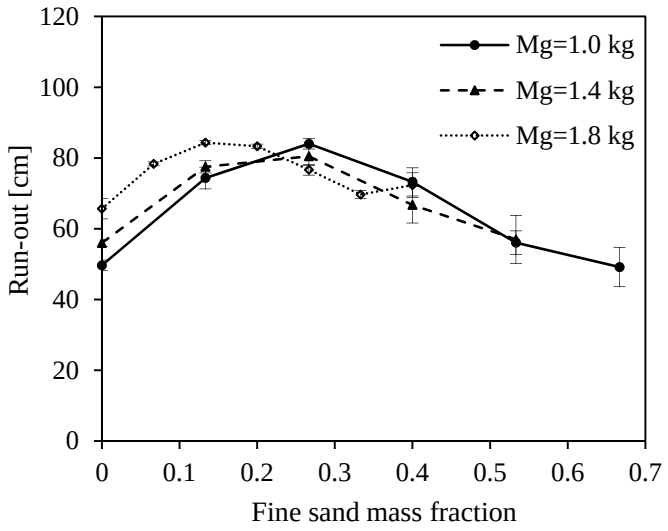

Figure 2.14 Run-out of the main part of the deposit for the composites with various fractions of fine sand on the 10° slope. The error bars show standard error of the average run-out for each test.

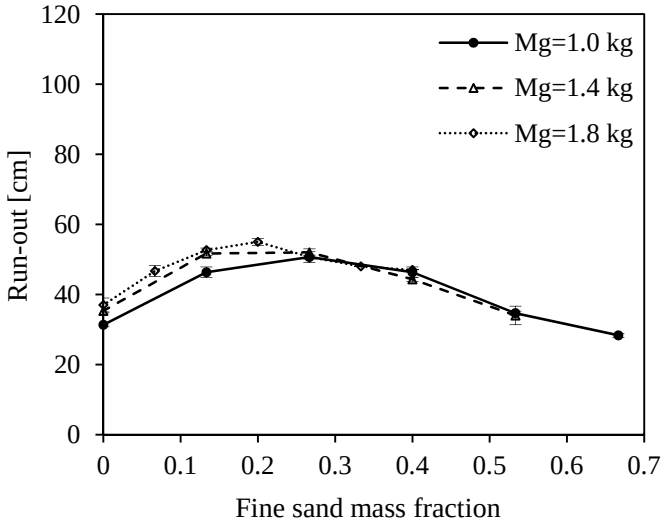

Figure 2.15 Run-out of the main part of the deposit for the composites with various fractions of fine sand on the 5° slope. The error bars show standard error of the average run-out for each test.

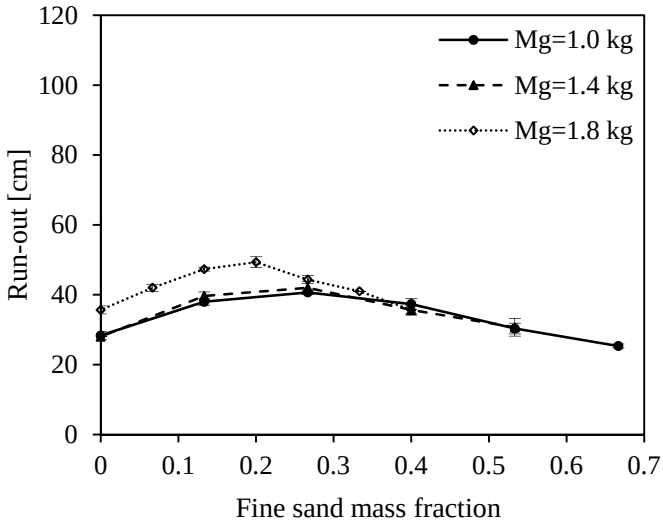

Figure 2.16 Run-out of the main part of the deposit for the composites with various fractions of fine sand on the 0° slope. The error bars show standard error of the average run-out for each test.

Figure 2.17 shows the deposit morphology of the main part of the deposit accumulated

on the lower slope with different inclinations. The three flows, consisted of various constitute particles, were selected for comparison. Each of the three flows typically exhibited the longest run-out in the series with the same mass of the gravel on the 15° slope. The deposit morphologies on the steep and gentle slopes significantly departed from each other. This indicates that the deposit morphology of granular flows was also influenced strongly by the inclination of the lower slope. The deposit profile was much flatter and longer on the steep slopes (15° and 10°) than that on the gentle slopes (5° and 0°). This phenomenon implies that there was a critical inclination of the lower slope between 5° and 10° at which particle motion in flows changed. When the slope was steeper than the critical inclination, the particles were prone to rolling. Otherwise, the particles exhibited sliding motion.

For all composites of coarse and fine particles used in the experiments, the deposits exhibited some common features as follows. First, coarse particles segregated to the surface of fine particles. This phenomenon is also observed frequently in field investigations. Second, the region of maximum concentration of particles was farther from the flow origin on the steeper slope, that is, more materials were transported a long distance. A majority of granular materials accumulated a broad range from the position 20 cm to the position 90 cm on the 15° and 10° slopes. This situation is riskier for human habitation and environmental protection in steep mountain slopes. On the gentle slopes, however, the deposits concentrated a narrow range from the position 0 cm to the position 40 cm. The materials were prone to contribute to add the deposition height rather than the run-out on the gentle slope. Last, the deposit morphologies were almost similar on the same slope for the three flows with different composite components. This implies that the mobility of granular flows was more sensitive to the inclination of the lower slope than granular component.

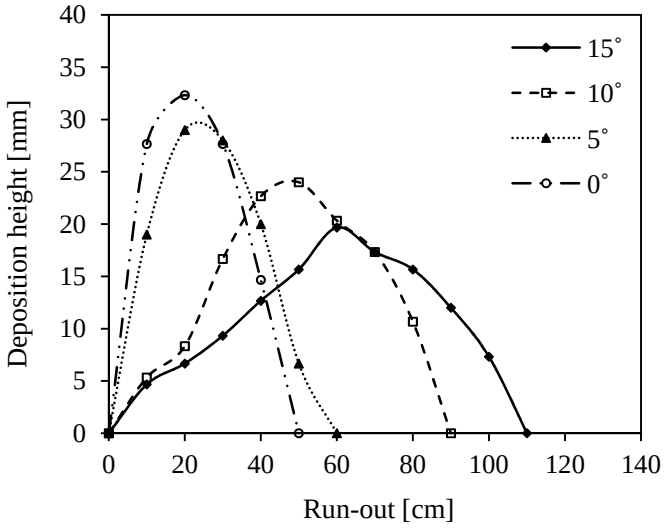

(a)

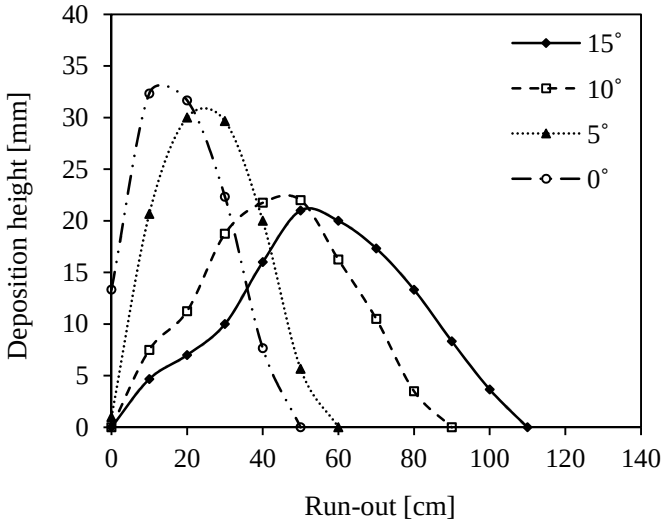

(b)

Figure 2.17 Deposit morphology of the main part of the deposit accumulated on the lower slope with different inclinations: (a) 1.8 kg gravel with F_f = 0.13; (b) 1.4 kg gravel with F_f = 0.27; (c) 1.0 kg gravel with F_f = 0.27 (to be continued)

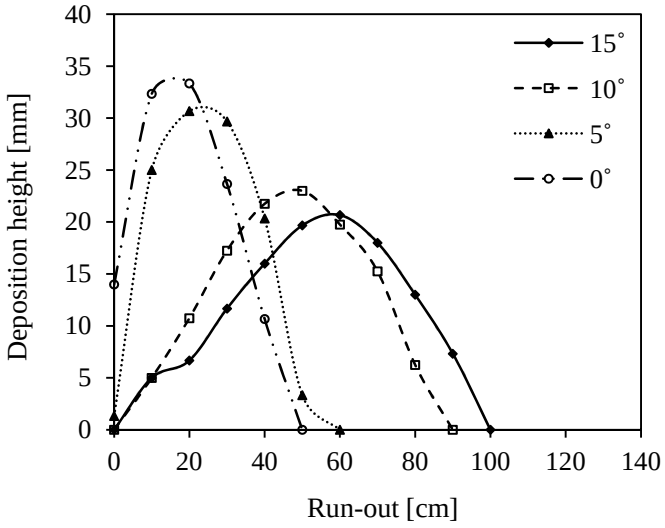

(c)

Figure 2.17 Deposit morphology of the main part of the deposit accumulated on the lower slope with different inclinations: (a) 1.8 kg gravel with F_f = 0.13; (b) 1.4 kg gravel with F_f = 0.27; (c) 1.0 kg gravel with F_f = 0.27 (continued)

2.4 CONCLUSIONS

The flows in a small flume described here varied the proportion of constitute particles but maintained the same total mass to examine the effect of interactions between particles on the mobility of granular flows. Test results indicate that the run-outs of the flows with a wide range of grain sizes were larger than the flows only containing mono-sized particles. The proportion of fine sand strongly influenced the run-out of granular composites. The fine sand was transported with the gravel, and naturally segregated to the base of the flow under gravity. The rolling of fine sand acted as a lubricant for the gravel by the interactions with each other, and thus the friction resistance reduced during the movement. With increasing F_f, a greater proportion of gravel was completely supported by the fine sand, and the run-out reached its peak. This emphasizes that rolling motion was very important in flow propagation, and increasing proportion of rolling to sliding in particle motion reduced energy consumption. However, the run-out decreased with further increasing F_f. This was because intergranular friction dominated which was the primary source of energy loss, and thus limited the propagation of granular flows. Particle interactions played an important role within high-mobility

flows containing a wide range of grain sizes on the dynamics of some landslides and rock avalanches, though precise details of particle interactions is still unknown because the motion of fine particles within the flows is difficult to observe in the tests.

The deposit characteristics on the steep and gentle slopes significantly departed from each other. The deposit profile was much flatter and longer on the steep slopes (15° and 10°) than that on the gentle slopes (5° and 0°). The region of maximum concentration of particles was farther from the flow origin on the steeper slope, i.e., more materials were transported a long distance on steep slope. On the gentle slopes, however, the deposit was more concentrated on the gentle slopes because the materials were prone to contribute to add the deposition height rather than the run-out. The deposit morphologies were almost similar on the same slope for the three flows containing different constitute particles. This implies that the mobility of granular flows was more sensitive to the inclination of the lower slope than granular components.

CHAPTER 3

SMALL FLUME TESTS OF GRANULAR FLOWS ON A SHAKING TABLE

3.1 INTRODUCTION

The destructive impact of earthquakes, in many parts of the world, is greatly enhanced by the triggering of landslides during or after the shaking (Bommer and Rodríguez, 2002). The earthquake-induced landslide has been broadly investigated and discussed in the past. Physical model tests, such as the centrifuge test and the shaking table test, have been widely used to investigate slope dynamic response. The centrifuge test utilizes the gravity force as the scale factor to simulate a prototype slope. Additionally, Wartman et al. (2005) carried out a series of shaking table tests to investigate the mechanisms of seismically induced permanent deformations in slopes, and compared test results with Newmark displacements. Lin and Wang (2006) conducted shaking table tests and numerical analysis to identify the initiation of landslide movement based on nonlinear behavior from acceleration records. Wang and Lin (2011) studied the initiation and displacement of a laboratory slope subjected to seismic load by a series of shaking table tests. These laboratory experiments are used to mainly study dynamic behavior and responses of earthquake-induced landslides. As far as I know, there is little information available in the literature that propagation process and deposit characteristics of earthquake-induced rock avalanches are investigated by shaking table tests.

The most abundant types of earthquake-induced landslides are rockfalls and slides of rock fragments that form on steep slopes. A rockfall occurs when a small rock mass breaks free and disintegrates into blocks that bounce and roll down steep slopes. For the slides of rock fragments, there are several major types according to the size or type of debris generated and distance and speed moved as well, e.g. rock avalanches, debris avalanches, and rockslides. A rock avalanche is the disintegration of a large rock mass on a mountain slope and a rapid movement downhill. Debris avalanches involve the rapid mass movements of rock originating on the slopes. In a rock slide, fragments break away

from the face of a steep slope and fall down its side but do not travel far. The objective of this study is to investigate the run-out of granular flows using a shaking table model test, as a step to study propagation mechanisms and deposit characteristics of earthquake-induced rock avalanches and debris avalanches.

3.2 EXPERIMENTS AND METHODS

3.2.1 Experimental set-up

The two-part flume used in the shaking table tests was the same one presented in Chapter 2 (Figure 2.1). Each slope was 1.5 m in length and 0.18 m in width. The angle of the upper slope was 45°, while that of the lower slope was 10°. The flume was fixed tightly on the shaking table (2.0 m × 1.0 m) by channels to avoid any collapse during the tests.

Granular materials were released by removing a gate covering the entire width of the flume. Each case was repeated five times to guarantee the accuracy, and the run-out was measured after each test. In this chapter, the measurements were also conducted on the main part of the deposit, where a majority of materials accumulated.

3.2.2 Employed materials

Two composites were used, and their particle size distribution is listed in Table 3.1.

Table 3.1 Particle size distribution of granular composites

Granular materials	Mass of composite component [kg]		
	10 ~ 20 [mm]	1 ~ 2 [mm]	0.1 ~ 0.2 [mm]
Coarse particles dominated materials	1.8	0.9	0.3
Fine particles dominated materials	0.3	0.9	1.8

3.2.3 Input sinusoidal wave

The frequency and amplitude of input sinusoidal waves were varied in order to investigate their effects on run-out. In the small flume tests under static conditions mentioned in Chapter 2, the duration of propagation process was less than three seconds from initiation to rest. Therefore, shaking time was three seconds to make sure that the propagation process of experimental flows throughout associated with the shaking. The frequency of input waves was ranging from 2 Hz to 10 Hz in increments of 2 Hz, and the range of the amplitude was from 100 gal to 400 gal in increments of 100 gal.

3.2.4 Shaking subsequence

Two shaking subsequences were designed to simulate different scenarios. In the first shaking subsequence, the materials were released meanwhile sinusoidal waves were input. This consideration was to simulate the propagation process of a large rock mass from a steep slope in conjunction with a long-period seismic shaking. For the propagation process of an existing mass originating on a gentle slope, the second shaking subsequence was designed in which the materials were released and deposited on the lower slope, and then sinusoidal waves were input.

In the first shaking subsequence, the run-out was measured after the test. The difference with the average run-out (65 cm) under static conditions was obtained, as a measurement of enhanced mobility due to the vibration. In the second shaking subsequence, the run-out was measured before and after the shaking, and the difference between them was the increase in run-out due to the shaking. This increase in run-out was because the existing deposit deformed, and particles within the deposit rearranged the conformation and leaded to some consolidation and movement during the shaking.

3.3 EXPERIMENTAL RESULTS

3.3.1 Frequency and amplitude of input waves

Figure 3.1(a) shows that the run-outs of the coarse particles dominated materials reduced with the frequency of input waves. This was because the energy was significantly

dissipated caused by intergranular friction during the high-frequency vibration. The difference in run-out due to various amplitudes was significant in the experiments with a low frequency, and it gradually became not obvious with increasing frequency especially in the experiments with the frequency of 10 Hz. Furthermore, the decrease in run-out with frequency was more significant in the experiments with large amplitude than that with small amplitude. This implies that the run-out was more sensitive to the frequency at large amplitude than at small amplitude.

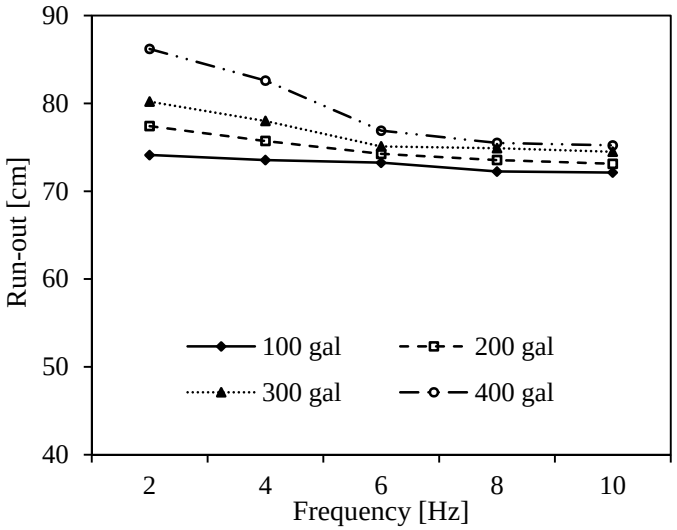

(a)

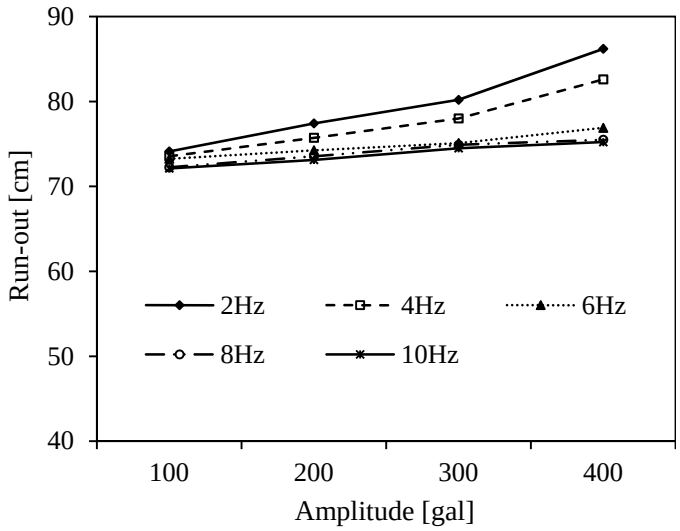

(b)

Figure 3.1 Run-out of coarse particles dominated materials (first shaking subsequence)

The run-out increased with the amplitude (Figure 3.1 (b)). The increase in run-out with the amplitude was more significant at a low frequency than that at a high frequency.

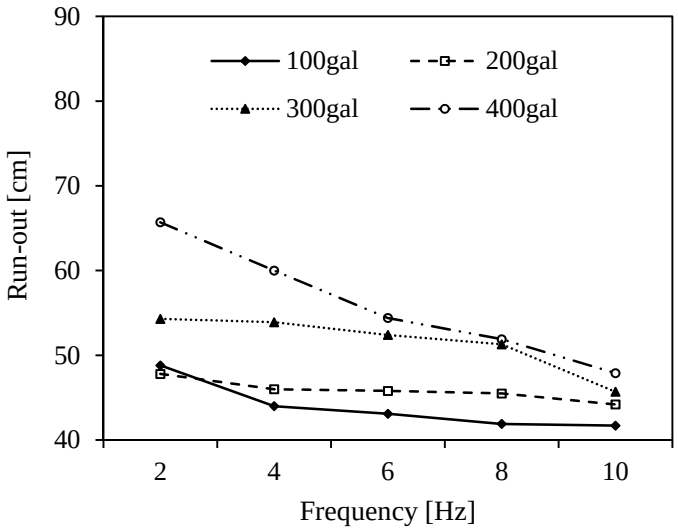

(a)

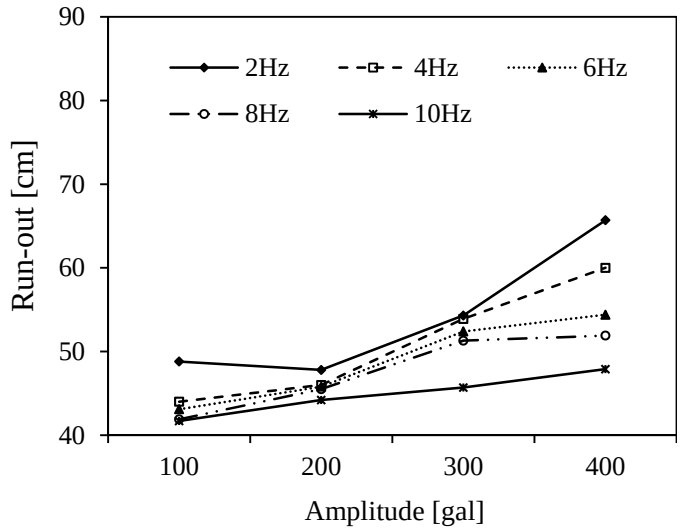

(b)

Figure 3.2 Run-out of fine particles dominated materials (first shaking subsequence)

Similar trends also were observed for the fine particles dominated materials (Figure 3.2). However, the run-out of the fine particles dominated materials was significantly smaller than that of the coarse particles dominated materials under various dynamic conditions. One of the main causes was that intergranular friction greatly dissipated the energy when excessive fine particles were involved. This agreed with the conclusion drawn in Chapter 2 that a flow consisting of enough coarse particles and few fine particles had a high mobility. This also implies that this conclusion held under either static or dynamic conditions.

The decrease in run-out with frequency was more significant for the fine particles dominated materials than that for the coarse particles dominated materials. This was caused by dramatic energy consumption due to intergranular friction during the high-frequency vibration.

3.3.2 Shaking subsequence

The run-out increased due to the vibration in most experiments, comparing with that under static conditions. However, the increase in run-out was not observed at the amplitude of 100 gal. This implies that the vibration with small amplitude was difficult to enhance the mobility of granular flows.

The increase in run-out of the coarse particles dominated materials in the experiments with the amplitude of 200 gal, 300 gal and 400 gal is shown in Figure 3.3. The most significant increase in run-out was observed in the experiments with the frequency of 2 Hz, regardless of the shaking subsequence. The increase in run-out at the amplitude of 200 gal and 300 gal was larger in the first subsequence than that in the second subsequence. This implies that the superposition effect of flow-propagation and seismic acceleration was significant at 200 and 300 gal. In the first shaking subsequence, the materials started to move meanwhile the waves were input. Less energy was consumed by intergranular friction due to the low concentration of the moving mass. In the second shaking subsequence, however, the materials were released and then accumulated on the lower slope. The materials were difficult to move, and more energy was dissipated by intergranular friction due to the high concentration of the deposit. The increase in run-out at the amplitude of 400 gal was smaller in the first subsequence than that in the second

subsequence. This was because the moving mass dramatically collided with the upper slope due to the large amplitude of input waves when they flowed along the upper slope, and the energy was significantly dissipated by the collision between the materials and the upper slope.

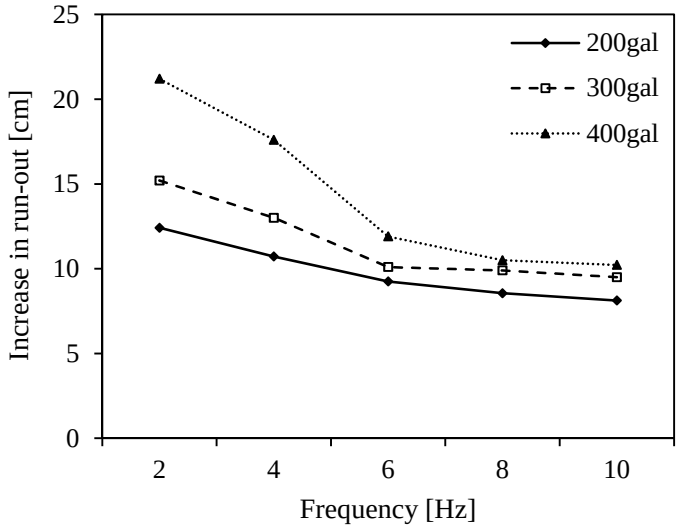

(a)

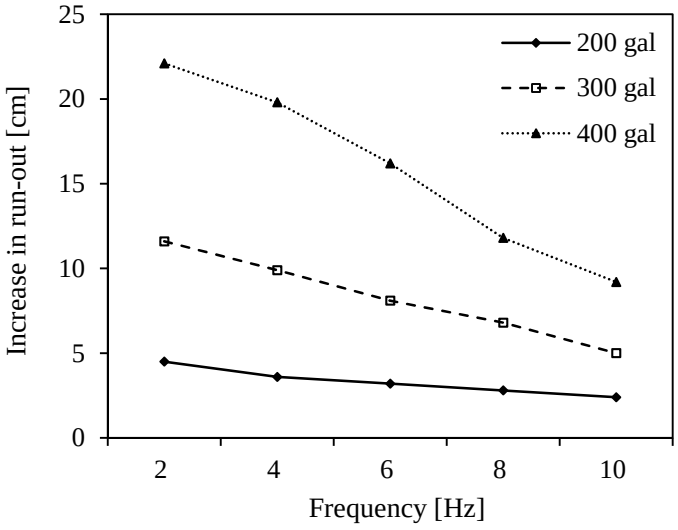

(b)

Figure 3.3 Increase in run-out of the coarse particles dominated materials in different shaking subsequence: (a) the materials were released meanwhile the shaking; (b) the materials were released before the shaking

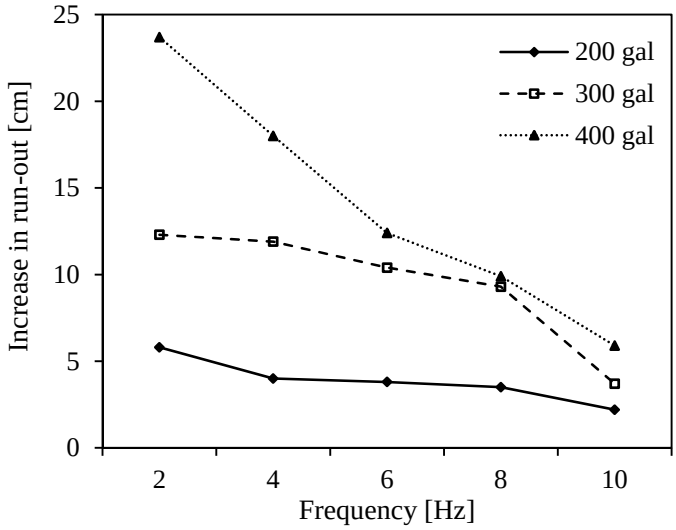

(a)

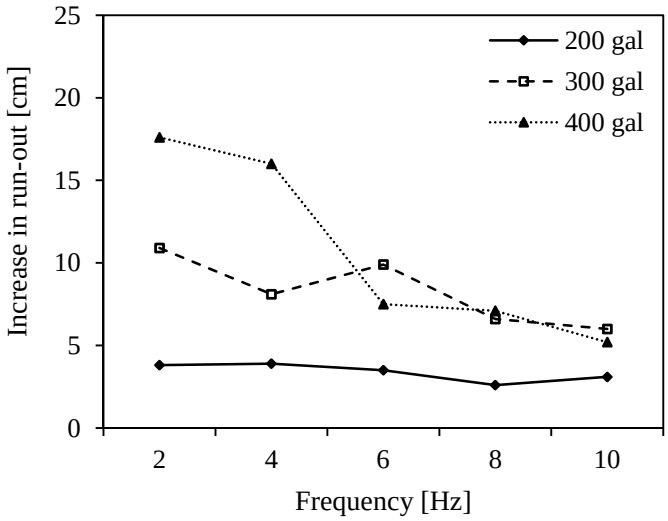

(b)

Figure 3.4 Increase in run-out of the fine particles dominated materials in different shaking subsequence: (a) the materials were released meanwhile the shaking; (b) the materials were released before the shaking

Figure 3.4 shows the increase in run-out of the fine particles dominated materials in the experiments with the amplitude of 200 gal, 300 gal and 400 gal. The increase was

smaller than those of the coarse particles dominated materials in most experiments. This was because the coarse particles embedded in a matrix of the fine particles and was difficult to move even under dynamic conditions. The increase in run-out in the first shaking subsequence was larger than that in the second shaking subsequence in most experiments.

3.4 CONCLUSIONS

A series of shaking table tests was carried out to investigate some potential factors influencing run-out of granular flows released in a small flume under dynamic conditions. The frequency and amplitude of input sinusoidal waves were varied. Two composites were released before/meanwhile the sinusoidal waves were input to simulate debris avalanche/rock avalanche associated with seismic shaking.

Test results show that the run-outs of the two composites increased with decreasing frequency and increasing amplitude. The run-out of the fine particles dominated materials was significantly smaller than that of the coarse particles dominated materials. The decrease in run-out with frequency for the fine particles dominated materials was more significant than that for the coarse particles dominated materials. This was because intergranular friction dramatically dissipated the energy when excessive fine particles were involved. This conclusion agreed with that drawn in Chapter 2 that a composite consisting of enough coarse particles and few fine particles had a high mobility. This conclusion held under either static or dynamic conditions. The increase in run-out due to the shaking was observed in most experiments, except in the series with the amplitude of 100 gal. The increase in run-out when the materials were released meanwhile the sinusoidal waves were input was larger than that when the materials were released before the shaking at the amplitude of 200 gal and 300 gal. This was because more energy was consumed by intergranular friction due to the high concentration of the existing deposit on the lower slope. However, the increase in run-out when the materials were released meanwhile the shaking was smaller than that when the materials were released before the shaking at 400 gal. One of the main causes was that the moving mass dramatically collided with the upper slope at the large amplitude when they flowed along the upper slope.

CHAPTER 4

LARGE FLUME TESTS OF GRANULAR FLOWS

4.1 INTRODUCTION

Rock avalanches pose significant hazards in many parts over the world especially in mountainous areas. Extensive efforts have been directed to protect society from such hazards, and this has interested many researchers. Most attention is aimed at triggering mechanisms, movement dynamics, and material characteristics. From a practical point of view, rock avalanches, which have been extremely costly in human lives and engineering development, are among most dangerous natural granular flows due to their large volume and spreading. From a theoretical point of view, rock-avalanche propagation has been debated strongly because the run-out is often much larger than that would be predicted by a Coulomb slide-block model (Sosio et al., 2008). At present mechanisms involved in these events are thought only understood in broad outlines, and many important questions remain unanswered (Evans et al., 2009).

Experiment plays a significant role in contributing to a better understanding of propagation mechanisms and factors influencing velocity and deposit characteristics (Manzella and Labiouse, 2009). A number of authors have performed small-scale (Acharya et al., 2009; Deangeli, 2008; Manzella and Labiouse, 2008, 2009; Lajeunesse, et al., 2004, 2005; Lube, et al., 2005; Ugai et al., 2009a, 2009b, 2009c, 2010; Valentino et al., 2008; Wang and Sassa, 2001, 2003; Yang et al., 2011b) and large-scale tests (Eckersley, 1990; Moriwaki et al., 2004; Okada and Ochiai, 2008; Okura et al., 2000a; Ugai et al., 2011; Yang et al., 2010, 2011a). It is well known that small-scale tests have problems with scale effects, similarity relations, and disruptive effects of sensors and their cables (Moriwaki et al., 2004). Therefore, a model as close as possible to a natural size is desirable for the purpose of realistically reproducing a rock avalanche phenomenon, even it is difficult to achieve.

Modeling rock-avalanche run-out and deriving associated parameters—velocity and deposit characteristics—can provide guidance to the extent of the potential susceptible

area and get an insight into the propagation mechanisms (Sosio et al., 2008). A majority of previous studies have focused on the effects of various factors influencing run-out and angle of reach because the run-out (or angle of reach) is relatively visual. A velocity evaluation is helpful to analyze the propagation dynamics (e.g. rate-dependent resistance, kinetic energy, duration) and to explain some physical features observed. From a structural engineering and planning point of view, one must properly predict the velocity field of a possible avalanche in order to adequately design buildings, roadways, and rail transportations in mountainous regions and appropriately estimate impact pressures on obstructing buildings that may be hit by an avalanche along its track down a mountain valley (Pusasaini et al., 2005a). Scheidegger (1973) collected some data from the literature and proposed an empirical formula to predict rock-avalanche velocity from a relationship between the volume and velocity. Other researchers (Crosta et al., 2009; Deangeli, 2008; Evans et al., 2009; Okura, 2000b; Pudasaini et al., 2005b; Sosio et al., 2008; Valentino et al., 2008) have used numerical models to simulate rock avalanches and obtain their velocities. However, velocity in tests is difficult to exactly quantify due to the relative indirectness of measurement and the short distance available for its evaluation. Several measurement methods have been offered in order to improve the feasibility of velocity evaluation in tests. Digital image analysis has been used to calculate the velocity of moving materials in laboratory tests, e.g. Acharya et al. (2009), Deangeli (2008), Evans et al. (2009), Moriwaki et al. (2004), Okada and Ochiai (2008), Sosio (2008), Valentino et al. (2008). Manzella and Labiouse (2008, 2009) adopted a fringe-projection method to derive mass-front velocity and deposit characteristics of experimental flows. Therefore, analysis is no longer limited to data such as run-out and friction angle; it also allows considering the velocity in tests. At present, the velocity of the Thurwiesser rock avalanche in the Italian Alps was reported based on digital analysis of broadcast-quality video (Sosio et al., 2008). Jibson et al. (2006) presented a formula to estimate flow velocity based on superelevation, the elevation difference of a channelized deposit between the inside and outside of a curve. Xu et al. (2010) evaluated velocities of some field rock avalanches, e.g. the Niumiangou landslide triggered by the Wenchuan earthquake in China, based on bend superelevation at some key locations, and compared the results with those calculated by the momentum transfer method (Zhang and Liu, 2008) and also the Scheidegger's method (Scheidegger, 1973).

Pudasaini et al. (2005a, 2007), Pudasaini and Hutter (2007), Pudasaini and Kröener

(2008), and Pudasaini and Domnik (2009) have analyzed and presented results on the complete dynamics of sand and gravel flows down chutes and rectangular channels in the laboratory scale from initiation to deposition. The velocity of the moving particles was measured by Particle Image Velocimetry technique. Experimental results were well predicted by the granular avalanche theories they used.

Of particular interest is the work conducted by Manella and Labiouse (2009), who presented the behavior of small-scale, dry granular avalanches. The run-out, width and length of final deposits were measured by the tape, while mass-front velocity and deposit characteristics were derived by fringe-projection method. After mass front entered the accumulation zone, it initially decelerated uniformly due to friction resistance, and subsequently accelerated due to the impulse given by the rear part of moving materials. The authors denoted that this provided experimental evidence to the theory of transfer of momentum described by Van Gassen and Cruden (1989) and also earlier by Heim (1932). However, the energy associated with granular flows is a major concern to avalanche dynamics, rather than momentum (McSaveney, 2002; McSaveney and Davies, 2007; Pudasaini and Domnik, 2009; Crosta et al., 2007; Locat et al., 2003; Kokusho and Ishizawa, 2006). Additionally, Okura et al. (2000a) performed outdoor rockfall experiments with mono-sized blocks (one on top of the other), and denoted that the frequency of collision between blocks increases with the number of blocks.

In spite of many studies, how a rock avalanche is triggered and propagated, and how the run-out or reach angle is affected by material characteristics, drop height, topographic constraints, and other influencing factors, are still poorly understood. There is little information available in the literature about the effect of factors, such as material characteristics of composites, and micro-topography (e.g. the convexity and forest model), on propagation process of rock avalanches.

An aim of this study was to clarify the effect of released materials and topography on mass-front velocity in the direction of movement and deposit characteristics of rock avalanches. For this purpose, a series of tests was carried out with dry, rigid gravel and/or blocks moving down a large inclined flume. Gradation and volume of materials, shape and initial arrangement of blocks, consecutive releases, obstacles, and bottom roughness were varied independently. This chapter presents the influence of these factors on mass-front velocity and deposit characteristics of the rapid, dry granular flows in the

large flume.

4.2 EXPERIMENTS AND METHODS

4.2.1 Experimental set-up

The two-part flume used in the tests was 15.5 m long, 5.7 m high, 1.0 m wide, and 1.0 m deep (Figure 4.1). An upper slope 5.5 m long, inclined at 45° was connected with a lower slope 10.0 m long, inclined at 10°. The inclinations of the upper and lower slopes of the flume were similar to those of the Xiejiadian rock avalanche in Sichuan Province, China (details of field investigation of that rock avalanche are presented by Yang et al., 2009).

Figure 4.1 Experimental set-up

A gate was arranged near the top of the upper slope to control the release of materials. One flume sidewall was made of transparent reinforced PMMA to allow side views of the movement of materials. Two tapes were fixed vertically to the sidewall at 1.0 m intervals to conveniently measure deposition height, and the other was installed along the bottom of the sidewall also as reference targets in order to determine conversion factors.

Table 4.1 Summary of large-scale flume tests

Case No.	Test conditions	Initial geometry	Released materials						
			Cubes [kg]		Cobbles [kg]		Gravel [kg]	Total mass [kg]	Total volume [m^3]
			Large	Small	Large	Small			
1	Matting	Trapezium	200	200	0	0	0	400	0.2975
2	Matting	Triangle	200	200	0	0	0	400	0.2738
3	Matting	Triangle	0	0	0	0	400	400	0.2738
4	Matting	Triangle	200	200	0	0	400	800	0.4802
5	Matting ; Twice	First, trapezium	200	200	0	0	0	800	0.2738
	、	Second, triangle	0	0			400		0.2701
6	Matting ; Twice	First, triangle	0	0	0	0	400	800	0.2701
	、	Second, trapezium	200	200			0		0.2853
8	Matting ; Convexity	Trapezium	200	200	0	0	0	400	0.2800
9	Matting	Triangle	0	0	100	100	0	200	0.1800
10	Matting	Triangle	0	0	200	200	0	400	0.2888
11	Matting ; Convexity	Triangle	0	0	100	100	0	200	0.1800
12	Matting ; Convexity	Triangle	0	0	200	200	0	400	0.2905
13	Matting ; Convexity	Triangle	100	100	0	0	0	200	0.1663
14	Matting	Triangle	0	0	200	200	400	800	0.5000
15	Matting ; Forest model	Triangle	200	200	0	0	400	800	0.5000
16	Matting ; Forest model	Triangle	0	0	200	200	400	800	0.4901
18	No matting	Triangle	200	200	200	200	0	800	0.5408
19	No matting	Triangle	200	200	200	200	400	1200	0.7442
20	No matting; convexity	Trapezium	200	200	0	0	0	400	0.2870
21	No matting; convexity	Triangle	0	0	0	0	400	400	0.2888
22	No matting	Triangle	0	0	0	0	400	400	0.2813

The test conditions varied in the experiments were:

a) Released materials: blocks (cubes and rounded cobbles) and/or gravel;

b) Material volume;

c) Initial arrangement of blocks: trapezium (high and narrow), or triangular (low and

wide);

d) Consecutive releases: first blocks and then gravel, or first gravel and then blocks;

e) Obstacles: the convexity, or forest model;

f) Bottom roughness. In most experiments, a mat was coated on the base of the flume unless otherwise stated.

Despite the difficulty of matching scaling laws, the use of physical modeling enables studies of the influence of factors of interest, by comparing and analyzing one factor at a time. Due to the large quantities of materials employed in this research, the range of studied factors was limited. Table 4.1 shows those cases used for analysis described in this chapter. Case 2 was treated as a benchmark to facilitate the comparison of the results.

4.2.2 Employed material

This study used mono-materials (cubes, cobbles or gravel) and composites of them to examine their effects on mass-front velocity and deposit characteristics. The materials employed for the tests were:

a) Blocks: Cube-shaped granite blocks as shown in Figure 4.2, of either 0.1 m or 0.05 m on each side, were called large cubes or small cubes respectively; rounded blocks with diameter of either about 0.1 m or 0.05 m, were called large cobbles or small cobbles respectively. Released materials had a volume of 0.2738 m^3 in the benchmark case. Thus, corresponding to a failed mass with a volume of 10^5 m^3 in field situation, the scaling of grain size should be approximately 70 times according to the reference (Davies and McSaveney, 1999). The largest-sized block of 0.1 m used in this work corresponded to a large boulder with a diameter of 7 m in the field situation. Such boulders are somewhat too coarse; however, they are frequently observed in field investigations (Xu et al., 2010; Yang et al. 2009). These boulders have distinguished mobility. To examine and highlight effects of these large particles on the movement of granular avalanches, the blocks of 0.1 m were thus employed in this study.

Figure 4.2 Employed cubes

b) Gravel: The grading curve of the gravel (D_{50}=4.0 mm) is presented in Figure 4.3. These grains were also insufficiently fine in scaling down model tests. Actually, it is impossible to represent at very small-scale prototype grains exactly following the scaling law, in order to avoid these extremely fine grains to bind together in a way different from that of corresponding grains in the large-scale situation ascribing to intergranular forces (e.g. cohesive and/or electrostatic force) (Davies and McSaveney, 1999). Davies and McSaveney (1999) used materials with volumes of 0.1, 1.0, 10, and 1000 L in laboratory tests. The three smaller containers were used to drop fine (D_{50}=0.19 mm), well-sorted silica sand, and the largest one was used to drop well-sorted gravel (D_{50}=2.0 mm). The gravel used in this work was close to the situation with the volume of 0.1 L in the tests (Davies and McSaveney, 1999) according to the scaling of grain size between laboratory and field situation. Furthermore, the particle size distribution of the gravel follows a similar manner with those of field rock avalanches reported by e.g. McSaveney and Davies (2007), Dunning (2006). Thus, the gravel used could be idealized as scaled-down representations of corresponding grains in typical large rock avalanches. Internal friction angle of the gravel was 32.5°, which was determined by large direct shear tests as listed in Table 4.2.

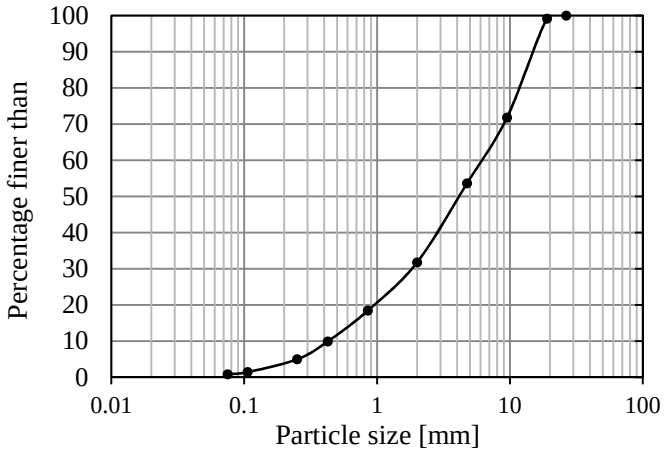

Figure 4.3 Grading curve of the gravel

Table 4.2 Results of large direct shear tests

Interface	Cohesion/Adhesion [kPa]	Friction angle [°]
Gravel	0.056	32.53
Interface between the gravel and the mat	0.442	31.52
Interface between the gravel and the forest model	0.000	38.68
Interface between the gravel and the wood (no matting)	0.089	22.58

To the authors' knowledge, the gravel has been seldom used in model tests, and different kinds of sand or beads have been used according to most literature. One of the main causes is to match the scaling law as close as possible in laboratory tests. Another is that sand is a more suitable material for the validation of numerical models based on fluid mechanics (i.e. grain diameters should be smaller than 1/10 of the flow depth to avoid a 'bounce behavior' and to assure a dense, one-phase flow) (Manzella and Labiouse, 2008). For small-scale laboratory avalanches down chutes and channels, quartz and sand are frequently used because the flow depth can be as small as 3~5 particle diameters (Pudasaini and Hutter, 2007; Pudasaini et al., 2005a, 2007; Pudasaini and Kröner, 2008; Pudasaini and Domnik, 2009). Davies (1997) conducted experiments and found that grain density, grain size, and grain-size distribution have negligible effects on run-out distance, and friction angle, fall geometry, and volume have significant effects.

Fragmentation is a prominent process in the emplacement of field rock avalanches (Davies et al., 1999, Davies and McSaveney, 2002, 2009, Crosta et al., 2007). However, it is not feasible to model the fragmentation process at reduced scale (Davies and McSaveney, 1999). The choice of a characteristic particle size of materials employed in this study did not accurately reproduce that corresponding to natural rock avalanches; the simplification using a well characterized material justified the choice attributing to enough strength of grains without regard to fragmentation from the view point of experimental goals.

4.2.3 Data acquisition

The deposit was divided into two parts based on the accumulation of particles. The first part of the deposit was a coherent main mass, and the second part was the deposit which was a layer one particle height. No account was taken of the second part of the deposit where it is possible to distinguish individual separated particles. Additionally, those blocks, moving beyond the flume and stopping on the horizon, were also not considered as a part of the deposit.

Each test was filmed by three digital video cameras operating at 30 frames per second, as shown in Figure 4.4. Two cameras were positioned at the side of the flume to plot the side outline of moving materials, and the other was placed above the end of the flume at a height of 2.0 m above the horizon in order to record the movement by a frontal perspective.

Travel distance, deposition height, and length of the main part of the deposit were measured manually with the tape. The travel distance was defined as the distance from the gate, which was paralleling to the base of the flume. Mass-front velocity was derived with specific processing from the videos and images recorded during the tests. In this study, the mass-front velocity refers to the velocity of a characteristic point located at the tip of the mass front, such as a certain grain which was possible to identify. The mass front was diffusive, and those particles bounced violently were not considered as a part of the mass front.

The mass-front velocity, hereinafter referred to as the velocity for simplification, was derived as follows. The same characteristic point was tracked in a series of frames

acquired at a known frequency of 30 fps. The travel distance of the characteristic point was obtained with the tape fixed along the bottom of the side wall, and corrected with a conversion factor which allowed for different distances in different images introduced by the shooting angle. The velocity was calculated as the travel distance divided by the time interval of 1/30 s between consecutive frames, and fitted with a smooth curve.

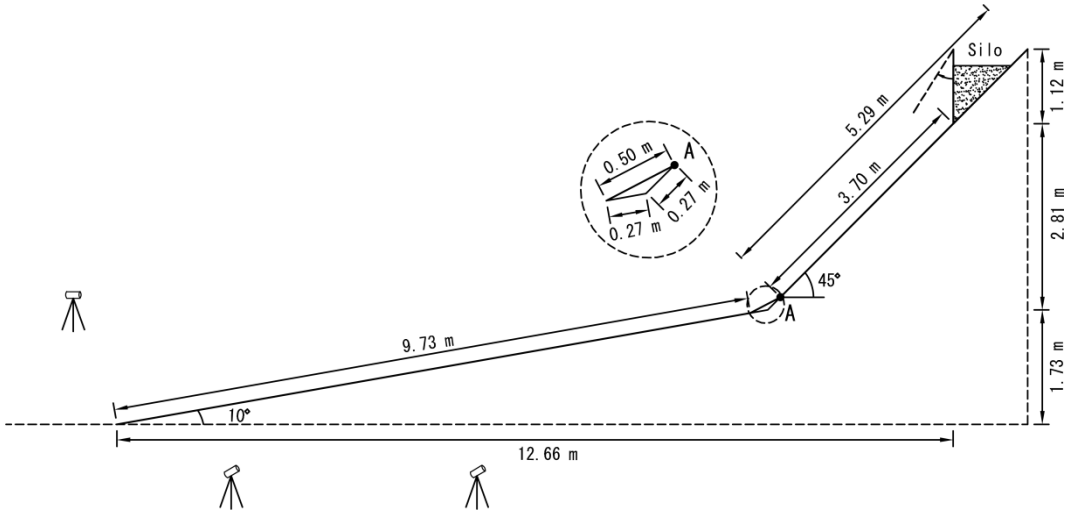

Figure 4.4 Schematic illustration of the model flume and arrangement of cameras

Data acquisition was primarily dependent on the visual resolution, and this was highly sensitive to contrast. Sometimes it was difficult to track the mass front especially in the tests with the gravel because the mass front was diffusive and the boundary of the mass front from the second part was indistinct. In addition, it was also difficult to follow the characteristic point due to dust clouds formed during the movement, and due to light reflection from the transparent sidewall. The accuracy of the measurement depended strongly on the visibility of the tracked characteristic point. The precision of measured distances was about 0.5 mm in images. The scaling of the reference tape was the largest and was about 20 times near the gate. Thus, the precision of the travel distance was 0.01 m, and that of the velocity was about 0.3 ms^{-1}.

When a particular tracked characteristic point became untraceable, another characteristic point was redefined to track and the processing was continued from the

moment that a new point was defined. Additionally, when the flowing layer remained largely invisible in dust clouds especially near the concavity of the flume, the travel distance of a characteristic point in consecutive images was estimated based on the travel distance of the front of the dust. Nonetheless, the preciseness in velocity was still reliable because extremely fine particles were sparse and the duration of the dust was short.

The relationship between the travel distance and velocity was plotted. The trend of velocities and also the peak velocity were observed and compared according to these plots.

4.3 RESULTS AND DISCUSSIONS ABOUT MASS-FRONT VELOCITY

4.3.1 Released materials

4.3.1.1 Mono-materials

Several tests were conducted on mono-materials of cubes in case 2, gravel in case 3, and cobbles in case 10.

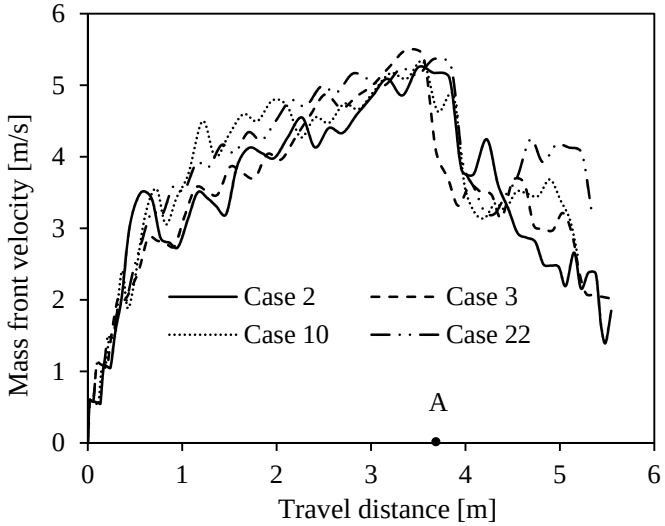

Figure 4.5 Mass-front velocity against travel distance from the gate for cases 2, 3, 10, and 22. (Point A indicates the distinguishing point between the upper and lower portions of the flume.)

Figure 4.5 shows that trends of velocities were similar in the three cases. Herein, the trend of velocities for the cubes is presented in detail. The velocity of cubes, marked by the solid line, increased fluctuatedly when the materials flowed down the flume, showing a peak velocity of 5.3 ms^{-1} at a travel distance of 3.6 m. Afterwards, the velocity showed a sudden drop after the peak velocity due to the energy loss induced by the collision between the materials and the flume. Then, the velocity increased slightly from a certain point within a short time. After that, the mass front decelerated and came to rest slowly. A complete stop is not shown in the plots because the mass front stopped beyond the viewing angle of the camera.

The materials should accelerate until the end of the upper slope at the travel distance of 3.7 m, but the peak velocity was shown at a travel distance of 3.6 m in case 2. This was because the time interval of 1/30 s between consecutive frames was somewhat long relative to a high velocity, and the maximum velocity measured sometimes did not just match the length of the upper slope. The maximum error in the position where the peak velocity appeared was less than 5% compared with the length of the upper slope. A better high-speed camera should be used in order to catch more precise data.

A high velocity and its fluctuation were shown along the upper slope for the cobbles. Videos reveal that cobbles at the surface of the flow were prone to rolling and impact due to their high roundness. Rolling frictional resistance of the cobbles at the surface was lower than sliding frictional resistance at the base, and the velocity at the surface was higher than that at the base. Scrutiny of the videos also shows that subsequent cobbles with the high velocity at the surface gave propulsion to those at the front by the impact. It was possible that opportunities of collision between the cobbles were more than those between the cubes and between gravel. These were the reasons of the high velocity and great fluctuation for the cobbles. One may therefore wonder whether block rolling might be partly responsible for the mobility of natural rock avalanches, and to what extent the results are applicable to a field situation. It is common to observe boulder rolling ahead of the front of a pyroclastic flow as it races down the slope of a stratovolcano, but there is much evidence against rolling motion inside a rock avalanche. Scrutiny reveals that rolling motion occurred at the surface of the granular flows in our tests, and it might exist at the surface of a large rock avalanche.

The velocity reduced at the concavity for the blocks and for the gravel as well. This

was because of added frictional resistance when the materials made contact with the lower slope. The added frictional resistance was caused by a higher overburden stress, which was due to the collision between the materials and the flume when the direction of movement changed. The decrease in velocity was more dramatic for the gravel than for the blocks. For the gravel, part of the energy was dissipated by the friction when the movement direction changed, and another part of the energy was consumed due to the internal deformation. Subsequent gravel-avalanches were allowed to make a perfect inelastic collision, in which energy loss was rather great, with those pre-existing deposit near the concavity. For the blocks, part of the energy was consumed by the friction, and little energy was dissipated by the internal deformation. Subsequent block-flows and pre-existing deposit made a non-perfect elastic collision, in which energy loss was less than the perfect inelastic collision for the gravel. These might be the reasons for the significant decrease in velocity for the gravel.

4.3.1.2 Composites

Figure 4.6 Arrangement of the composite (cubes and gravel) in layer in case 4

Two composites were tested. The first (case 4) was a composite of gravel (400 kg) and cubes (200 kg large cubes and 200 kg small cubes), and the second (case 14) was a composite of gravel (400 kg) and cobbles (200 kg large cobbles and 200 kg small

cobbles). The composite of cubes and gravel was initially arranged as alternating layers of cubes and gravel (as illustrated in Figure 4.6).

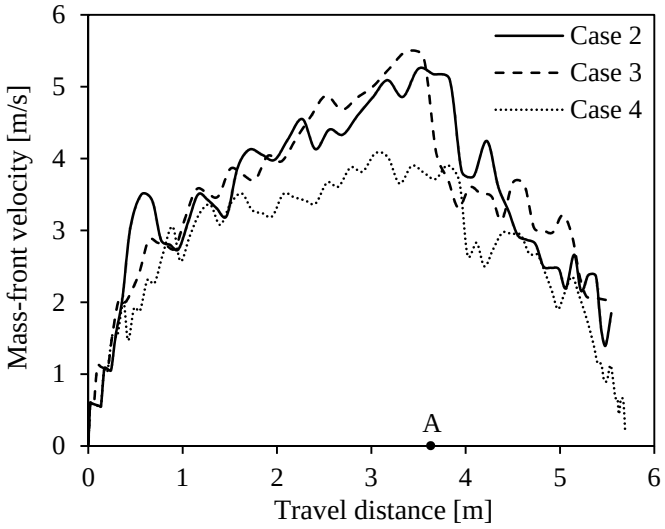

Figure 4.7 Mass-front velocity against travel distance from the gate for cases 2, 3 and 4

The composite of cubes and gravel displayed a rather lower mobility in case 4 than the mono-material of cubes and of gravel (Figure 4.7). The maximum velocities were 5.1 ms^{-1} at a travel distance of 3.84 m for the cubes and 5.4 ms^{-1} at a travel distance of 3.55 m for the gravel respectively, compared with 3.91 ms^{-1} at a travel distance of 3.81 m for the composite of cubes and gravel. The mean velocities along the upper slope were 3.02 ms^{-1} for the cubes, 3.22 ms^{-1} for the gravel, and 2.66 ms^{-1} for the composite, respectively. This implies that the effect of material characteristics on the velocity was not a simple superposition. Scrutiny shows that quite a number of cubes stayed at the rear of the main part of the deposit rather than the mass front, which means, the cubes were difficult to move at the surface of the gravel. It was possible that more energy was consumed by the friction between the cubes and the gravel when the cubes moved upward to the front and stayed at the surface. Pudasaini and Hutter (2007) gave more explanation on segregation during the flow and deposition of the particles by their physical properties. Another cause may have been that the composite had lower porosity, and greater particle concentration was able to consume more energy by intergranular friction. These were the reasons why the velocity was low for the composite of cubes and gravel even when the mass was

increased by about 100%.

An unexpectedly high velocity, almost the same as those of mono-materials, was measured for the composite of cobbles and gravel (case 14, Figure 4.8). The velocity of this composite was considerably higher than that of the composite of cubes and gravel (case 4). Scrutiny of the videos reveals that the cobbles frequently moved upward and forward, and few cobbles stayed at the rear of the main part of the deposit. This phenomenon implies that the cobbles rolled at the surface of the gravel more easily than the cubes. Besides, the surface of cobbles was smoother than that of cubes, and the materials could shear easily internally and also slid easily along the base due to the small internal friction angle. This was not the situation in case 4.

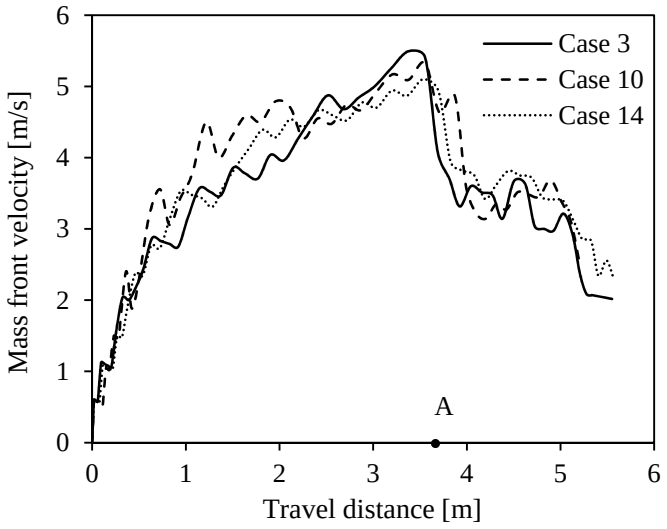

Figure 4.8 Mass-front velocity against travel distance from the gate for cases 3, 10 and 14

4.3.2 Material volume

Cases 9 and 10 employed 200 kg cobbles (100 kg large cobbles and 100 kg small cobbles) and 400 kg cobbles (200 kg large cobbles and 200 kg small cobbles) respectively.

The velocity of the materials with the smaller volume (case 9) was lower than that of the larger volume (case 10), as shown in Figure 4.9. Collisional opportunities increased with the volume in the constrained flume, and rear blocks gave propulsion to make

frontal ones accelerate. Moreover, the high velocity was probably caused by more potential energy involved in the materials with a large volume. Therefore, it is concluded that a large volume was partly accountable for the high velocity of rock avalanches, i.e., the ‘size effect’.

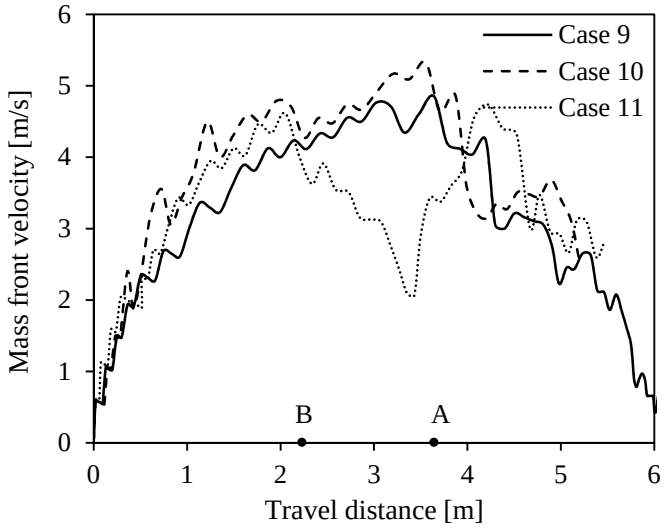

Figure 4.9 Mass-front velocity against travel distance from the gate for cases 9, 10 and 11. (Point B indicates the distinguishing point between the upper portion of the flume and the convexity.)

Okura et al. (2000a) indicated that relative positions among falling blocks are essentially maintained in the downflow direction; the rear blocks cannot pass the front ones and so the blocks maintain their positional relations from rockfall initiation to final deposition. This phenomenon was also frequently observed in our tests and rear particles appeared to propel and accelerate frontal ones. However, it was also revealed by the video recordings that rear particles passed some originally frontal particles and moved far. Releasing mode might be the main cause for the difference from the results by Okura et al. (2000a). In their tests, blocks were arranged in a cube on a falling apparatus which was set on a flat surface at the top of the slope. A prop which was set under the apparatus was pulled out to induce a granular avalanche by the weight of the rocks and the apparatus themselves. When the prop was pulled out, the frontal blocks moved before the rear ones. Therefore, conservation of relative positions of blocks in a moving mass holds.

In our tests, however, the gate was opened when a pin was pulled out, which was set on the upper part of the gate (Figure 4.4); the basal blocks moved first, and then the top ones. Thus, the conservation of relative positions among the blocks was broken.

4.3.3 Initial arrangement

Two types of initial arrangement were designed for blocks by varying the shape of silo. In case 1, blocks were initially arranged in a high and narrow stack (indicated by the word ‘trapezium’ in Table 4.1). In case 2, blocks were initially arranged in a low and wide stack (indicated by the word ‘triangle’ in Table 4.1). The arrangements of the blocks are illustrated in Figures 4.10(a) and 4.10(b).

Figure 4.10 Initial arrangement of blocks: (a) triangle; (b) trapezium

The hypothesis was that the velocity in case 1 would be higher than that in case 2 because the height of original mass center in the ‘high and narrow’ initial arrangement was 1.25 times larger than that in case 2. Potential energy in case 1 was also higher than that in case 2. However, Figure 4.11 shows that the velocity in case 1 was slight lower than that in case 2. The influence of the initial arrangement seems not so significant in

this study. Many researchers reported that fall geometry has a considerably effect on run-out, such as Crosta et al. (2009), Davies (1997), Lajeunesse et al. (2004, 2005), Lube et al. (2005), Manzella and Labiouse (2008). The difference from their results was probably caused by two reasons. First, the height of the trapezium (1.0 m) in case 1 was not much higher than the side of the triangle (0.74 m) in case 2. Second, the materials arranged in the silo firstly moved in the vertical direction and contacted with the base of the silo after the gate was opened. In case 1, the added frictional resistance, caused by a higher overburden stress, consumed more potential energy due to the change in movement direction.

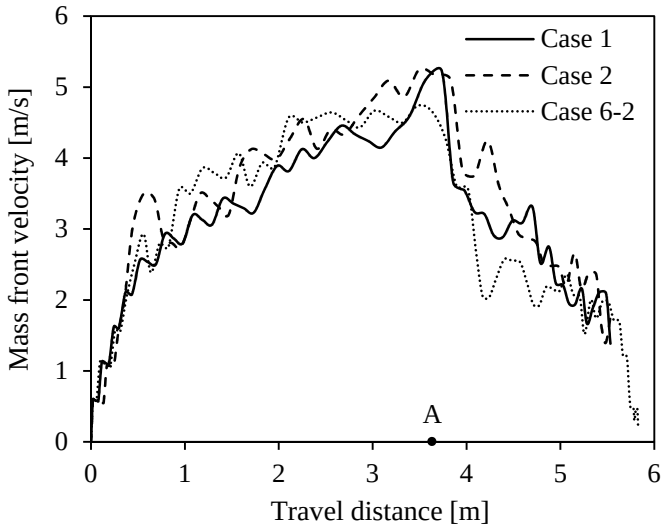

Figure 4.11 Mass-front velocity against travel distance from the gate for cases 1, 2, and 6-2

4.3.4 Consecutive releases

Some factors are not feasible to model in reduced scale tests. Examples of these are those involving environmental conditions not present in the laboratory, such as the presence of a saturated substrate, or ground shaking due to the impact of the avalanche on the ground at the toe of failed slopes (Davies and McSaveney, 1999). From a practical point of view, the presence of a substrate can be simulated by consecutive releases in the laboratory, and pre-existing deposits can be the substrate for subsequent avalanches. The effect of

the substrate on propagation process (e.g. entrainment) can thus be investigated in laboratory tests. Pudasaini and Kröner (2008) successively released different granular materials and stratified depositions in a channel flow very similar to that studied in this chapter.

Cases 5 and 6 were conducted to study the influence of consecutive releases on the velocity, and the order of the release is listed in Table 4.1. Cubes were released first and they deposited on the flume (case 5-1). Gravel was then released subsequently and they travelled over the pre-existing deposit of the cubes (case 5-2). Case 6 followed the same pattern but the release subsequence, i.e., gravel was released first (case 6-1) and then cubes (case 6-2).

Mass front was hard to track and its velocity was not able to be determined in case 5-2 because the second release of the gravel permeated into the pore of the pre-existing deposit of the cubes. This phenomenon demonstrates that the pre-existing coarse deposit had some influence in obstructing of movement of the fine materials.

The velocity was determined in case 6-2 and compared with that in case 2. As shown in Figure 4.11, there was no significant difference in velocity when materials travelled along the upper slope for cases 2 and 6-2, and the velocity in case 6-2 was considerably lower than that in case 2 along the lower slope. One of the main causes was that part of the energy from the second release was absorbed by the pre-existing deposit of the first release, and another part of the energy was used due to entrainment. Entrainment along propagation path is confirmed in field investigations, such as the Xiejiadian rock avalanche (Xu et al., 2010). A soft, erodible substrate was of certain influence on the velocity and ability of entrainment during rapid movement along its propagation path. Additionally, the energy was also consumed by the friction when the cubes slid over the accumulation of the gravel.

4.3.5 Obstacles

It is reasonable that the propagation process of granular avalanches is affected by the locations of topographic constraints and obstacles on the path, such as bends, deflections, channeling, opposite-wall obstruction, and dense forest. These obstructions are defined in detail by Corominas (1996), and Pudasaini and Hutter (2007). Some of these obstructions

are found at the site of the Xiejiadian rock avalanche (Xu et al., 2010). In this study, a sharp convexity in the slope and a dense forest were simulated.

4.3.5.1 The convexity

The schematic plan of the slope convexity is illustrated in Figure 4.12. The sharp convexity was set in case 11. All other conditions were similar to those in case 9.

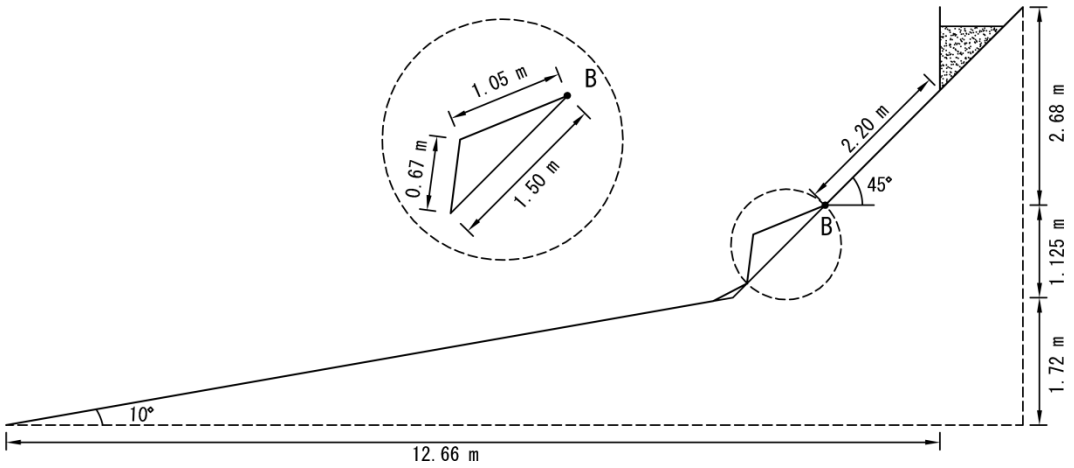

Figure 4.12 Arrangement of obstacle: convexity

The trend of velocities in case 11 significantly departed from that in case 9 (Figure 4. 9). In case 11, the velocity increased when the materials slid along the upper slope, reaching a peak in velocity of 4.6 ms^{-1} when the mass front approached the convexity in the slope. After that, the velocity decreased because the materials travelled across the convexity with a gentle inclination, reaching a low velocity of 2.1 ms^{-1} close to the vertex of the convexity. Some subsequent particles at a relative high velocity gave propulsion to the slowed front, and those propelled frontal particles took a ballistic trajectory from the vertex of the convexity and briefly lost contact with the base of the flume (Figure 4.13). Their velocity increased gradually up to the second peak velocity of 4.7 ms^{-1} at a distance of 4.5 m when the materials finally made contact with the base of the lower slope, compared with the first peak velocity of 4.6 ms^{-1} at the travel distance of 2.4 m. Following this, the velocity decreased greatly due to the added frictional resistance.

Figure 4.13 Materials taking a ballistic trajectory from the vertex of the convexity

The second peak in velocity was shown in case 11 when the materials just landed on the lower slope, even though there was no source of the energy other than that derived from the loss in potential energy. It was attributed to two main reasons. First, part of the energy was conserved when the materials took the ballistic trajectory due to the lack of friction with the flume. It is logical that the low friction is partly responsible for the greater mobility in the actual situation. This is particularly evident for very rough slopes where more abundant, higher and slightly longer ballistic trajectory or jumps occur, which resulted in the high mobility. Second, particles dispersed considerably and individual particle could be distinguished easily when they lost contact with the flume, whereas particles maintained a high concentration when they flowed along the base of the flume, as could be observed in the video recordings. Less energy was consumed by intergranular friction and collision due to the low concentration.

4.3.5.2 Forest model

It is observed in our field investigations, e.g. rock avalanche sites in Sichuan Province, China, that there is a dense forest just after the transition from an abrupt slope to a gentle one. Vegetable is sparse on the surface of the abrupt slope, and crops covered the gentle slope. In order to simulate this scenario, a forest model, 0.9 m long and 1.0 m wide, was

placed in the lower slope from the concavity. 105 model trees with the height of 0.05 m were arranged as shown in Figure 4.14. A composite of cobbles and gravel was released onto the forest model (case 16), compared with case 14 in which all other conditions were the same except it had no forest model.

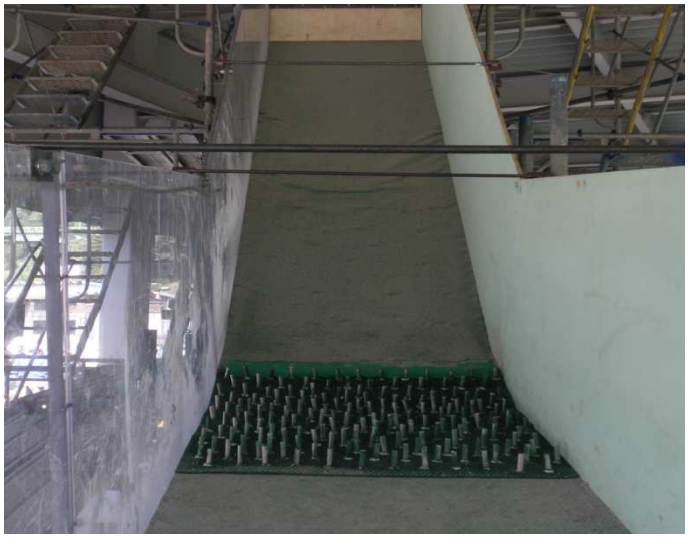

Figure 4.14 Arrangement of obstacle: forest model

The velocity followed rather similar behavior in cases 14 and 16 when the materials flowed along the upper slope. After reaching the peak velocity, the mass front slowed suddenly near the concavity in both cases 14 and 16. The slowing was more remarkable in case 16 than that in case 14, due to the presence of the model forest, as shown in Fig. 16. The mean velocity along the lower slope was 3.26 ms^{-1} in case 14 and 2.3 ms^{-1} in case 16 respectively, which means, the mean velocity reduced by 29.4% as a result of the resistance of the model forest. The velocity increased slightly after the mass front left the forest model in case 16. Some model trees were destroyed and entrained by the moving materials. Comparing with the size of blocks (0.1 m or 0.05 m), the trees with the height of 0.05 m (as the same order of magnitude in the size of blocks, even an order smaller than blocks) were of certain influence on the velocity in the tests. Corominas (1996) noted that the effect of obstacles is appreciated easily because falls developing through forest cover needed to be one or two orders of magnitude larger in volume to display the same tangent of reach angle as unobstructed rockfalls. It is difficult to draw a qualitative

conclusion how the model trees, e.g. their quantity, height, location, and arrangement, influenced the movement of granular flows, however, the result indicates a significant obstruction effect.

A higher velocity was revealed for the composite of cobbles and gravel in case 16 than that for the composite of cubes and gravel in case 15 along the upper and lower slopes. The difference in velocity between the two cases was not so obvious when the materials travelled along the lower slope, as shown in Figure 4.15. This might be due to the obstruction of the forest model, which weakened the effect of block angularity on propagation process.

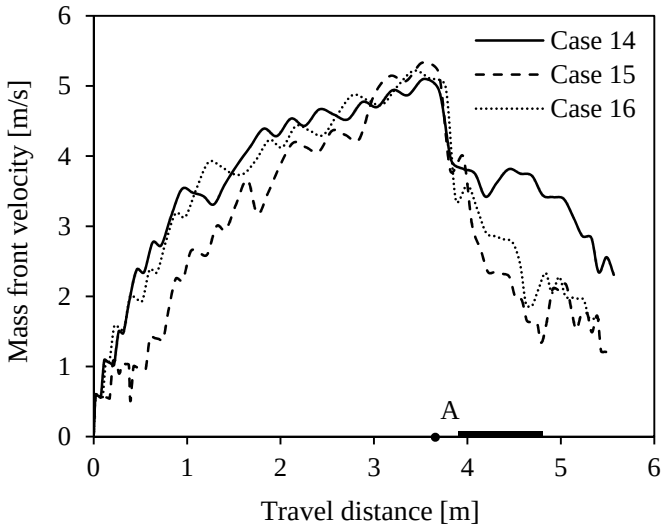

Figure 4.15 Mass-front velocity against travel distance from the gate for cases 14, 15 and 16. (The heavy line on *x*-axis indicates the arrangement of forest model.)

4.3.6 Bottom roughness

Case 22 was performed to examine the effect of bottom roughness referring to case 3.

Cohesion and friction angles were determined for the gravel, and their interface with the mat, forest model, or wood (no matting) by large-scale direct shear tests (Table 4.2). For example, the forest model was fixed on the horizon, and a large shear box filled with the gravel was placed above the forest model. The adhesion and friction angle of the interface between the gravel and the forest model could be measured.

The mass front travelled at a higher velocity in case 22 than in case 3, especially beyond the travel distance of 4.5 m (Figure 4.5). From a geological/geotechnical point of view, this part of the flow region is more important because it explains the real mobility of the flow and the possible thread to settlement. The mean velocity along the lower slope was 2.94 ms^{-1} in case 3 and 3.71 ms^{-1} in case 22, which increased by 26.2% when the mat was absent. The high velocity in case 22 was due to the lower friction between the materials and the flume without matting. For detailed investigations and discussions on the effects of material frictions on the flow dynamics and settlements, we refer to Pudasaini and Hutter (2007) and Pudasaini and Kröner (2008).

4.4 RESULTS AND DISCUSSIONS ABOUT DEPOSIT CHARACTERISTICS

Much previous research has focused on deposit characteristics. Herein the deposit characteristics are also briefly presented.

Figure 4.16 Deposit characteristics of the main part of the deposit in case 4

Vertical segregation was evident, and the blocks that were much larger than the mean

diameter accumulated at the surface of the gravel (Figure 4.16). This is also observed in previous small-scale flume tests as well as in field investigations. See, Pudasaini and Hutter (2007) for detailed discussions on the segregation and the mechanisms generating the segregation in different geophysical mass flows and laboratory granular flows and depositions.

Some factors influencing the characteristics of the main part of the deposit are reported. For laboratory flows of sand and quartz, the deposition processes, characteristics, and dynamics were discussed in detail in Pudasaini and Hutter, 2007; Pudasaini et al., 2005a, 2007; Pudasaini and Kröner, 2008; Pudasaini and Domnik, 2009.

4.4.1 Material volume

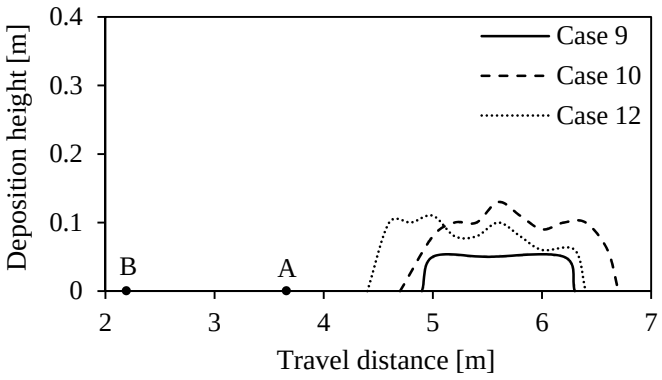

Figure 4.17 Deposit characteristics for cases 9, 10 and 12

As mentioned in section 4.3.2, 200 kg cobbles (100 kg large cobbles and 100 kg small cobbles) and 400 kg cobbles (200 kg large cobbles and 200 kg small cobbles) were employed in cases 9 and 10 respectively. As observed in Figure 4.17, the travel distance in case 10 was longer than that in case 9. The deposition height in case 9 was half of that in case 10, which was attributed to the smaller volume of employed materials in case 9. This result supported the conclusion that run-out is mainly dependent on the volume of involved materials, stated by many researchers, e.g. Corominas, 1996; Davies, 1982; Hsü, 1975; Legros, 2002; Okura et al., 2000a; Scheidegger, 1973; Ugai et al., 2010; Valentino

et al., 2008. The free surface of the deposition in case 9 was smoother than that in case 10. Scrutiny shows that some large cobbles stayed at the surface of the main part of the deposit. There were less opportunities for large cobbles depositing at the surface due to the smaller volume, and this was the possible cause for the smooth surface in case 9.

4.4.2 Obstacles

4.4.2.1 The convexity

In the cases with a convexity, travel distance was defined as the distance travelled along the base of the flume with no convexity to facilitate the comparison with those of other cases.

Cases 10 and 12 were performed under the same conditions except that case 12 was conducted with a convexity. Height and length of the main part of the deposit were closely similar in both cases. Travel distance in case 12 was shorter than that in case 10 (Figure 4.17). The velocity reduced significantly and the energy was dramatically consumed due to the added frictional resistance after the contact with the base of the flume, and the materials deposited soon without moving farther. This was the probable cause for the short travel distance in case 12.

Case 21 was conducted with a convexity, and its reference case was case 22 with no convexity. The two cases were carried out with no matting. Deposition height in case 21 was larger than that in case 22, and length and travel distance were shorter than those in case 22 (Figure 4.18). In case 21, the materials took a ballistic trajectory from the vertex of the convexity and finally made contact with the base of the lower slope, which consumed energy by the added frictional resistance due to the changes in movement direction, and the velocity reduced significantly. The slowed frontal part obstructed the movement of rear particles, and this caused them to decelerate and deposit. This contributed mainly to building up the height of the main part of the deposit. That was the reasons why the main part of the deposit was short and high in case 21.

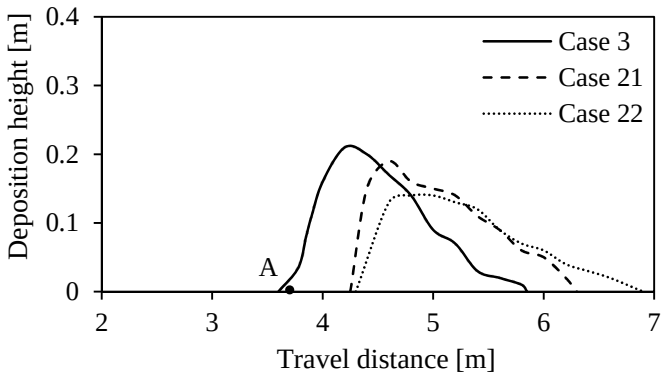

Figure 4.18 Deposit characteristics for cases 3, 21 and 22

4.4.2.2 Forest model

The composite of cubes and gravel was used in cases 4 and 15, with the forest model in case 15. The composite of cobbles and gravel was released in cases 14 and 16, and case 16 had the forest model. As shown in Figure 4.19, the shape of the main part of the deposit was prone to be high and short in the cases with the forest, and low and long in the absence of the forest. This was ascribed to the resistance of the forest model. The materials was obstructed by the model forest and deposited without sliding farther. The travel distances in the cases with the forest were shorter than those in the cases without the forest.

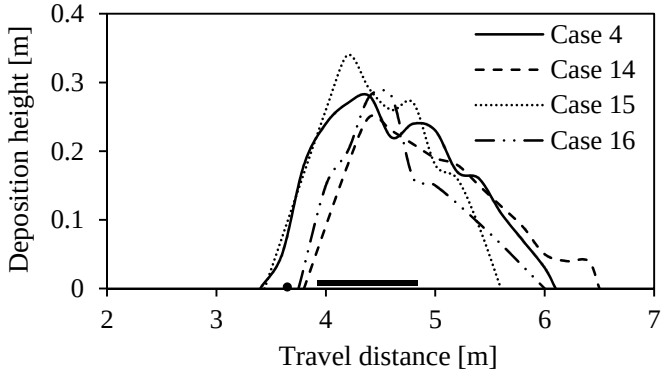

Figure 4.19 Deposit characteristics for cases 4, 14, 15 and 16

4.4.3 Bottom roughness

The deposit shape tended to be short and high due to the presence of matting on the flume base (Figure 4.18). The travel distance in case 22, with the low friction between the materials and the flume, was larger than that in case 3. These results agree with the results presented in Pudasaini and Hutter (2007), Pudasaini and Kröner (2008), for flow of granular materials in different laboratory settings.

4.5 CONCLUSIONS

A series of large flume tests was conducted to clarify some factors influencing mass-front velocity and deposit characteristics of rapid, dry granular flows. Constrained flows were simulated by releasing gravel and/or blocks down a 15.5 m long flume with two slopes of different inclinations in these tests. Test conditions considered in this study were gradation and volume of released materials, shape and initial arrangement of blocks, consecutive releases, obstacles, and bottom roughness. A total of 20 cases with different test conditions were performed.

The velocity was affected significantly by the characteristics and concentration of involved materials. A high velocity and its fluctuation were shown for the cobbles, which were prone to rolling and impact due to their high roundness. The velocity reduced near the concavity for the blocks and for the gravel as well, and the decrease in velocity was more significant for the gravel than that for the blocks. The velocity added up with an increase volume for the cobbles. A composite of cubes and gravel with a large volume displayed a rather lower mobility than a mono-material of cubes and of gravel with a small volume. The velocity of a composite of cobbles and gravel with a large volume was almost the same as a mono-material of cobbles and of gravel with a small volume. The velocity for the case in a high and narrow initial stack was slightly lower than that in a low and wide initial stack, and the influence of the initial arrangement of blocks was not evident in this study.

The progression of granular flows was controlled by the topography, including macro- (e.g. slope mean gradient) and micro-topography (e.g. bottom roughness and obstacle). The velocities in all studied cases reduced by approximately 25% when the materials changed the direction of movement near the concavity of the flume. A soft, erodible

substrate was of certain effect on obstructing of movement of subsequent flows and ability of entrainment along its propagation process. Two peak velocities were shown in the cases with a convexity, which significantly departed from those cases with no convexity. The mass front decelerated when it encountered the convexity, and then accelerated greatly when the materials took a ballistic trajectory from the vertex of the convexity and briefly lost contact with the base of the flume. The forest model obstructed the progression of granular flows. The bottom roughness had an effect upon the velocity.

Travel distance increased with the volume for the cobbles. The movement of materials was affected by micro-topography, such as convexity, forest model, and bottom roughness. Deposit shape was prone to be short and high in these cases; its effect on travel distance was not obvious.

CHAPTER 5

A SIMPLE LUMPED MASS MODEL TO DESCRIBE THE VELOCITY OF GRANULAR FLOWS

5.1 INTRODUCTION

Rock avalanches exhibit much greater mobility than could be predicted using frictional models (Hungr et al., 2001), and the mechanisms involved in these events are still for most part unknown (Manzella and Labiouse, 2009). There are two distinct mechanisms to reduce the friction in granular materials as mentioned in Chapter 1: lubrication or fluidization. Due to numerous practical difficulties related to lubrication and fluidization of a material in motion, particular in geophysical flows, unlubricated (or non-fluidized) friction between coherent sliding bodies is normally treated according to the classical Coulomb law (Pudasaini and Hutter, 2007). Ancey and Meunier (2004) concluded that velocity-dependent sliding cannot convincingly be inferred and the Coulomb model can provide predictions in the velocity and run-out distance in good agreement with field data for most events by a back analysis of 15 documented snow avalanches from field data.

The energy mechanics of geophysical mass flows have attracted the interest of civil engineers at the aspects of avalanche defense, hazard mitigation and disaster planning. Buildings and public spaces need to be designed to withstand at least the total destructive power of avalanches (Pudasaini and Domnik, 2009). Heim (1932) proposed a rigid mass model which is still widely used. The model analyzes basic features like an angle called Fahrböschung (apparent friction angle), the inclination to the horizon of the line joining the crown of the breakaway scar to the most distal deposit along the midstream path of the mass. In Heim's model, a block slides steadily down an incline with constant frictional coefficient, and finally the potential energy is exhausted by friction.

Fahrböschung is a measure of the efficiency of mass movement, and this simple expression can be used to get information about flow characteristics without requiring the full equations of motion or determining the friction parameters from experimental or field observation (Pudasaini and Domnik, 2009).

Kokusho and Ishizawa (2006) and Kokusho et al. (2009, 2011) presented an energy approach to make a simple evaluation for slope failures and subsequent flow deformations. Four energies, i.e., gravitational potential energy, earthquake energy, dissipated energy, and kinetic energy, were considered for the model of a rigid block resting on an inclined plane, and an energy balance was formulated. The earthquake energy was a function of input energy and impedance ratio of the upper layer to the base layer. The input energy was estimated by an empirical equation about the earthquake magnitude and focal distance. Slope displacement can be evaluated by this method if an appropriate friction coefficient of the slope is specified.

McSaveney (2002) numerically simulated the displacement of the center of mass, calculating changes in mass and speed when it lost potential energy to friction, erosion, and viscous and turbulent drag. They concluded that this deforming, sliding-block model gives speeds and duration consistent with other evidence, contrasting with the findings of Voight and Sousa (1994) that simple friction models greatly overestimate speed and underestimate duration.

Legros (2002) analyzed a model of a changing-mass granular flow, using the law of conservation of energy. He concluded that progressive deposition does not allow the center of mass to travel farther than the distance expected for a sliding block, as long as the Coulomb conditions of constant coefficient of friction holds.

In spite of these researches, velocity measurements in the laboratory and their direct comparison with theoretical predictions are still lacking in the literature (Pusasaini et al., 2005a). In this chapter, a simple lumped mass model was proposed based on energy

approach, and its validation was checked by comparing predicted results by this model with the measurements presented in Chapter 4. The model only considered retardation resulted from the constant basal friction, yielded the Coulomb law, between the moving mass and underlying surface. The outcome of this study could be the basis for better predicting the behavior of large rock avalanches by a simple model easy to handle, and calibration of theoretical and numerical models both in engineering practice and field rock avalanches in steep mountain slopes.

5.2 EXPERIMENTS AND METHODS

5.2.1 Experimental set-up

The Wenchuan earthquake, Ms 8.0, which happened along the Longmen Mountain fault zone in southwestern China, triggered a large number of collapse and landslides reported by many researchers (e.g. Huang et al., 2011a; Xu et al., 2011; Sun et al., 2011; Yang et al., 2009). A series of tests was performed to investigate some propagation mechanisms involved in rapid, dry granular flows and to identify factors influencing the mass-front velocity in the large flume. The detailed description of the large flume was presented in Chapter 4.

5.2.2 Experimental conditions

The test conditions were gradation and volume of materials, shape and initial arrangement of blocks, consecutive releases, obstacles, and bottom roughness. Table 4.1 shows the cases analyzed in this chapter; however, other cases, e.g. consecutive releases, were not considered in this study, because the simple lumped mass model was unavailable to describe these tests. For detailed presentation and discussion on the effects of these factors on the velocity, we refer to Yang et al. (2011a).

5.2.3 Experimental results

Test results show that the trend of velocities was similar when the topography was exactly the same. For example, in the case with no convexity, the materials accelerated down the flume, and reached, immediately near the concavity, a peak velocity. When the materials just entered the lower slope, the velocity showed a sudden drop. Finally, the materials gradually came to a rest. When a convexity was introduced, the materials accelerated along the upper slope and reached the first peak in velocity at the concavity. After that, the velocity decreased when the materials travelled across the convexity with a gentle inclination, reaching the lowest velocity close to the vertex of the convexity. Some subsequent particles at a relative higher velocity collided with the slowed front, and propelled frontal particles to take a ballistic trajectory from the vertex of the convexity and briefly lose contact with the base of the flume. The velocity increased gradually up to the second peak immediately before the materials finally made contact with the base of the lower slope. The velocity decreased greatly due to the landing. Finally, the materials came to a rest gradually. A complete stop could not be observed directly from the videos because the mass front stopped beyond the viewing angle of the camera. The velocity was extended to zero with line at the largest travel distance of the main part of the deposit measured by the tape after each test, where mass front was deemed to cease.

5.3 A SIMPLE MODEL FOR THE VALUATION OF VELOCITY

A lumped mass model is presented here to describe the run-out and velocity of the center of mass, and the constant friction between the materials and bottom surface was considered as the only source of energy consumption. The slope configuration in the model was exactly the same as the experimental flume with the two slopes inclined at

different angles. The cases listed in Table 4.1 were reproduced to facilitate the comparison with the test results. Test results indicate that the trend of velocities departed significantly when the bed topography was changed, in particular when a convexity was present. Therefore, the model was constituted under two conditions: the condition of no convexity and that of convexity.

5.3.1 The condition of no convexity

Let us assume a simple case, a block down a slope with two inclinations corresponding to that in the large flume tests. The equation of motion can be written in its simple form

$$a = g(\sin\theta - \mu\cos\theta) \tag{5.1}$$

where, a is the acceleration of the block in its flow direction, g is the acceleration of gravity, θ is the inclination of the slope, and $\mu=tan\varphi$ is the friction coefficient of the block with the basal surface. φ is the friction angle determined by large-scale direct shear tests as listed in Table 4.2.

The velocity v and travel distance s along the upper slope are given by

$$v = g\left(\sin\theta_1 - \mu_1\cos\theta_1\right)t \tag{5.2}$$

$$s = \frac{1}{2}g\left(\sin\theta_1 - \mu_1\cos\theta_1\right)t^2 \tag{5.3}$$

where, μ_1 is the friction coefficient along the upper slope, and θ_1 is the inclination of the upper slope.

Eliminating the variation t, a relationship between the velocity v and travel distance s along the upper slope can be expressed as

$$v = \sqrt{2g\left(\sin\theta_1 - \mu_1\cos\theta_1\right)s} \qquad \left(s < L_1\right) \tag{5.4}$$

The materials reach the distal end of the upper slope at a velocity of v_{L1},

$$v_{L_1} = \sqrt{2g(\sin\theta_1 - \mu_1 \cos\theta_1)L_1} \tag{5.5}$$

where, L_1 is the length of the upper slope.

After that, the materials begin to move at an initial velocity along the lower slope. Here, the initial velocity v_0 is considered as the projection of v_{L1} in the direction paralleling to the lower slope, as illustrated in Figure 5.1, that is,

$$v_0 = v_{L_1} \cos(\theta_1 - \theta_2) \tag{5.6}$$

where, θ_2 is the inclination of the lower slope.

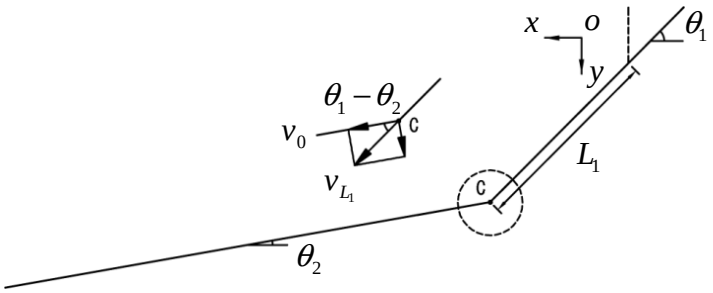

Figure 5.1 Velocity diagram used in the model for the case with no convexity

Equation (5.6) simply follows a momentum transfer assuming a collision problem is involved when the inclination changes; the initial velocity v_0, at which the materials begin to move along the lower slope, resulted from the projection of the velocity just approaching the concavity v_{L1} in the direction paralleling to the lower slope; the velocity in the normal direction is thus neglected.

When the materials move along the lower slope, a relationship between the velocity v

and travel distance s is given by

$$v = \sqrt{v_0^{\,2} + 2g\left(\sin\theta_2 - \mu_2\cos\theta_2\right)\left(s - L_1\right)} \qquad \left(s \geq L_1\right) \tag{5.7}$$

where, μ_2 is the friction coefficient along the lower slope.

5.3.2 The condition of convexity

The velocity and travel distance until the materials approach the vertex of the convexity are the same as those for the case with no convexity.

After the materials reach the vertex of the convexity, they take a ballistic trajectory from the vertex of the convexity and briefly lose contact with the base of the flume, as shown in Figure 4.13. This movement is treated as a projectile motion, without regard to interaction between particles. The velocity v_{L3} at which the materials initially take a ballistic trajectory from the vertex of the convexity is decomposed into the horizontal and vertical directions, and these components are written as, respectively

$$v_{x0} = v_{L_3}\cos\theta_3 \tag{5.8}$$

$$v_{y0} = v_{L_3}\sin\theta_3 \tag{5.9}$$

where, θ_3 is the inclination of the convexity. The velocity diagram in the case with the convexity is illustrated in Figure 5.2.

The materials finally make contact with the base of the lower slope at a velocity of v_{L2}, whose angle to the horizon is given by

$$\alpha = \tan^{-1}\frac{v_{yL_2}}{v_{xL_2}} \tag{5.10}$$

where, v_{xL2} and v_{yL2} is horizontal and vertical component of v_{L2}, respectively.

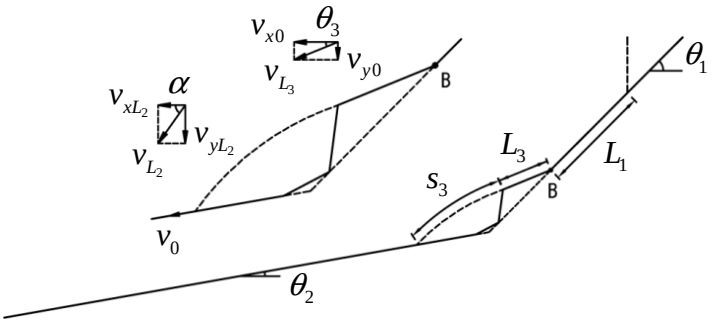

Figure 5.2 Velocity diagram used in the model for the case with the convexity

The velocity v_0' at which the materials flow initially along the lower slope is the projection of v_{L2} at which they land the base

$$v_0' = v_{L_2}\cos\left(\alpha - \theta_2\right) \tag{5.11}$$

When the materials flow along the lower slope, a relationship between the velocity v and travel distance s can be expressed as

$$v = \sqrt{v_0'^2 + 2g\left(\sin\theta_2 - \mu_2\cos\theta_2\right)\left(s - L_1 - L_3 - s_3\right)} \qquad \left(s \geq L_1 + L_3 + s_3\right) \tag{5.12}$$

where, s_3 is the total travel length during the ballistic trajectory, and its increment in the x-direction $\Delta s_{x,i}$, and in the y-direction $\Delta s_{y,i}$ at the time interval Δt can be respectively expressed as follows

$$s_3 = \sum_0^i \sqrt{\Delta s_{x,i}{}^2 + \Delta s_{y,i}{}^2} \tag{5.13}$$

$$\Delta s_{x,i} = v_{x,i-1}\Delta t \tag{5.14}$$

$$\Delta s_{y,i} = v_{y,i-1}\Delta t + \frac{1}{2}g\Delta t^2 \tag{5.15}$$

The velocity during the ballistic trajectory in the x-direction and y-direction can be

respectively given by

$$v_{x,i} = v_{x,i-1} \tag{5.16}$$

$$v_{y,i} = v_{y,i-1} + gt \tag{5.17}$$

5.4 COMPARISON BETWEEN EXPERIMENTAL AND THEORETICAL RESULTS

The experimental results were detailed by Yang et al. (2011a), comparing and analyzing one factor potentially influencing velocity and run-out at a time.

5.4.1 The comparison between predicted and measured velocity

The predicted velocity in each case is shown in Figure 5.3, comparing with the measured velocity. The trend of predicted velocities basically matched those of the measured ones. The predicted velocities were somewhat lower than those measured in most cases. Scrutiny of the videos shows that subsequent particles with a relative higher velocity collided with the slowed front to make them accelerate. The collisions between particles caused the high measured velocity of the mass front and its fluctuation. The simple model could not consider the collisions between particles because the released materials were assumed as a rigid block. This was the reason why the predicted velocity was lower than the measured one. This also implies that continual collisions between particles might be partly responsible for the high velocity and long run-out of natural rock avalanches.

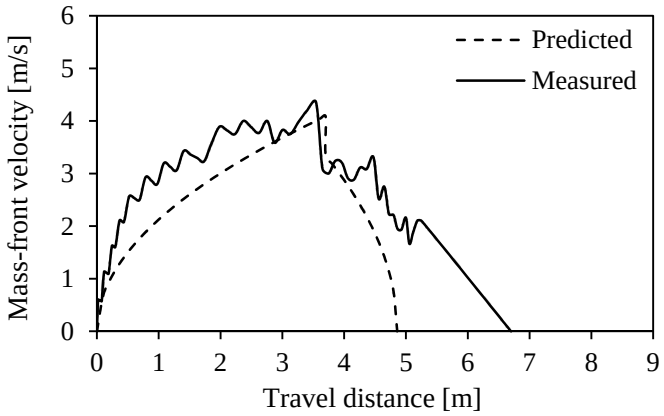

(a) Case 1

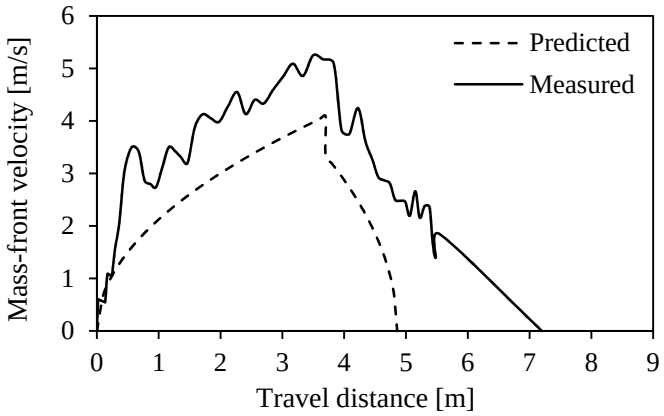

(b) Case 2

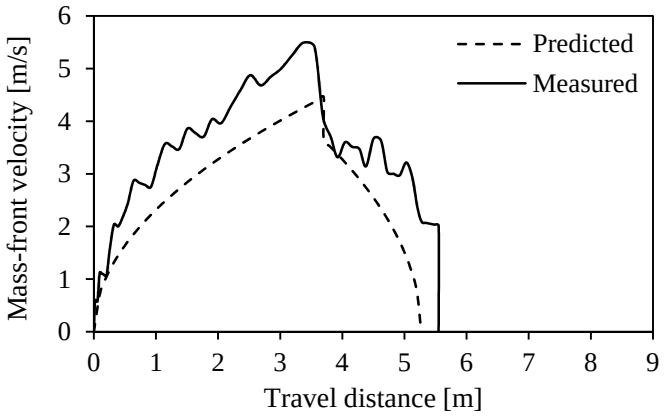

(c) Case 3

Figure 5.3 The comparisons between predicted velocities by this model and measured velocities of granular flows in the large flume tests (to be continued)

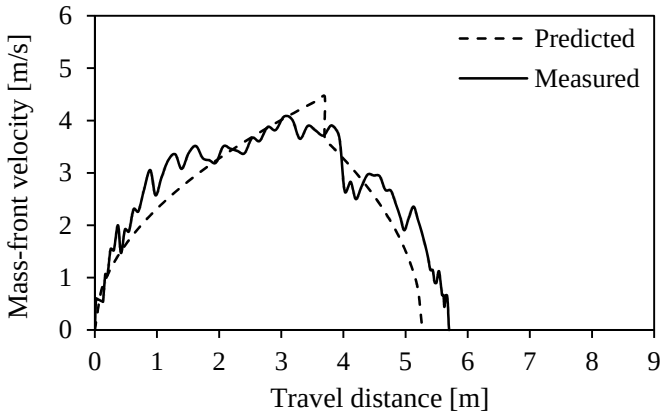

(d) Case 4

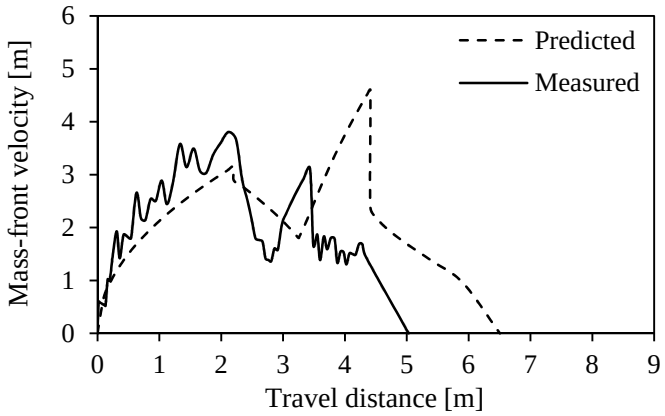

(e) Case 8

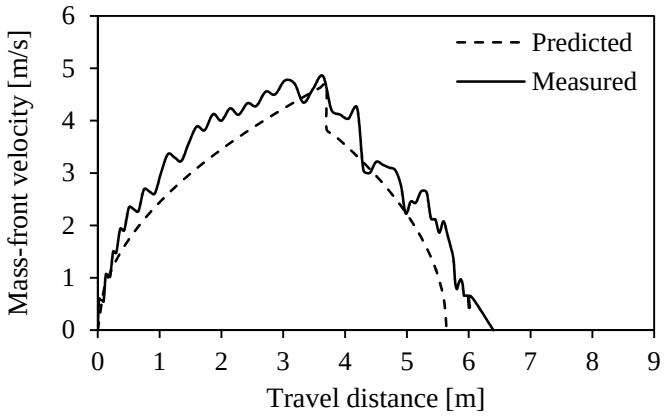

(f) Case 9

Figure 5.3 The comparisons between predicted velocities by this model and measured velocities of granular flows in the large flume tests (continued)

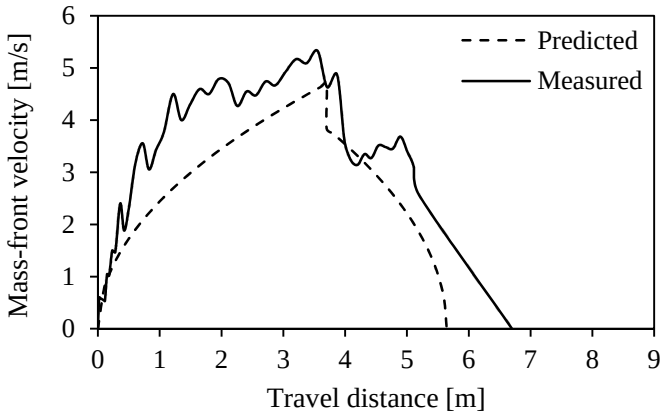

(g) Case 10

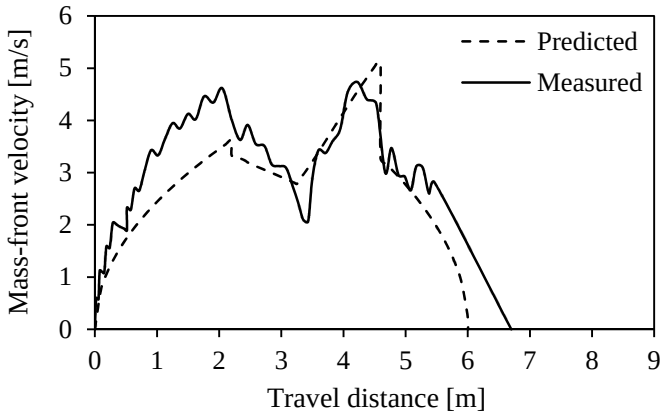

(h) Case 11

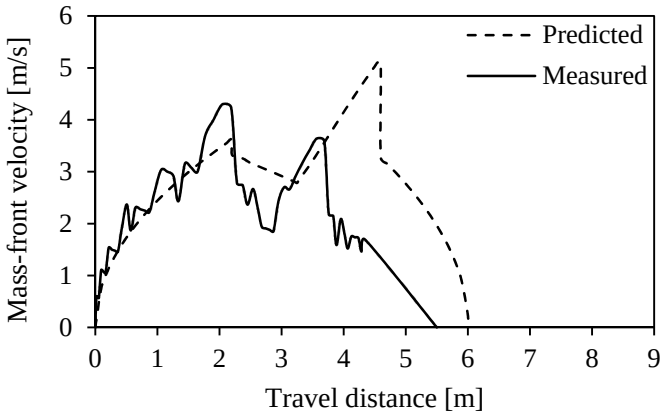

(i) Case 12

Figure 5.3 The comparisons between predicted velocities by this model and measured velocities of granular flows in the large flume tests (continued)

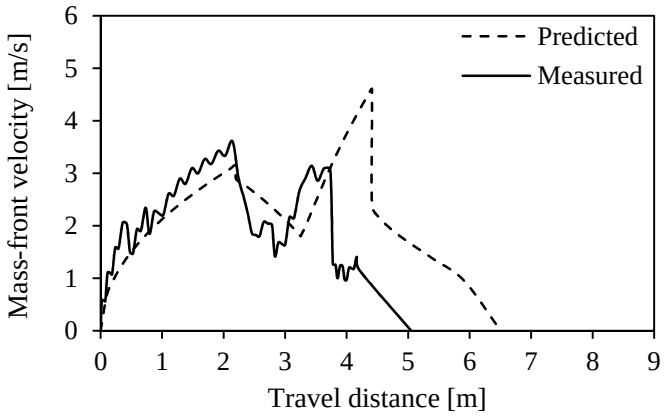

(j) Case 13

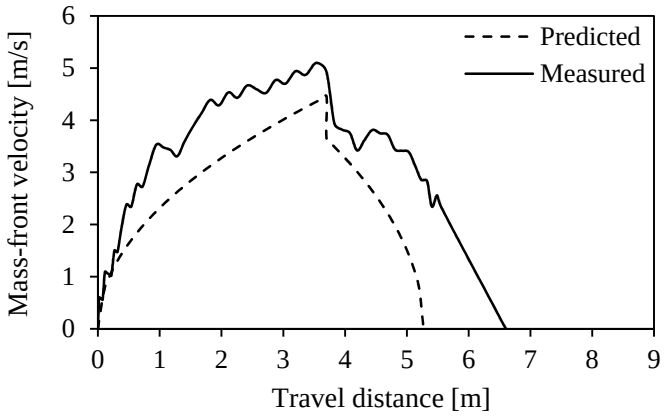

(k) Case 14

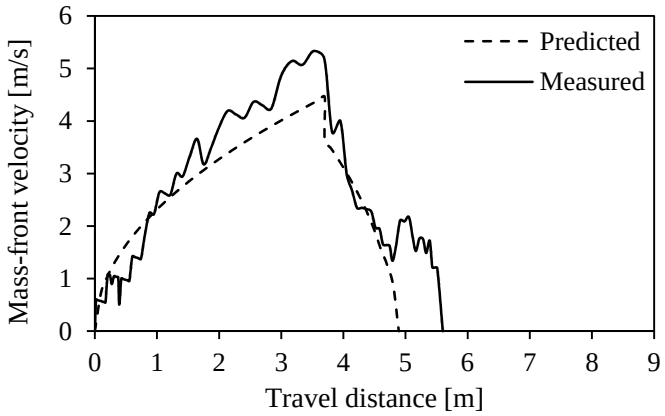

(l) Case 15

Figure 5.3 The comparisons between predicted velocities by this model and measured velocities of granular flows in the large flume tests (continued)

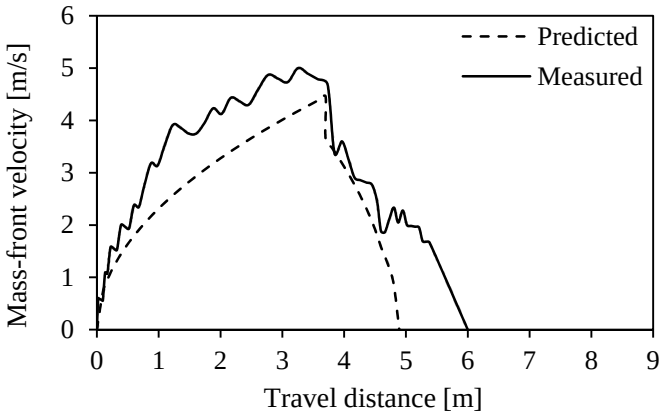

(m) Case 16

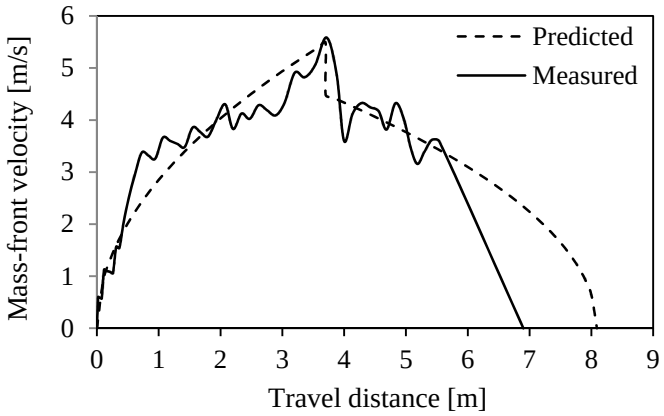

(n) Case 18

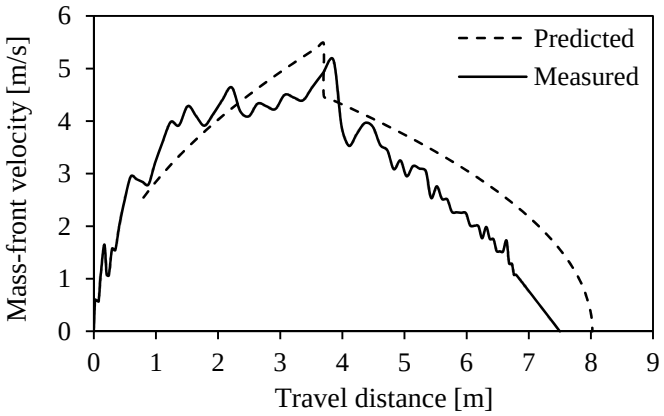

(o) Case 19

Figure 5.3 The comparisons between predicted velocities by this model and measured velocities of granular flows in the large flume tests (continued)

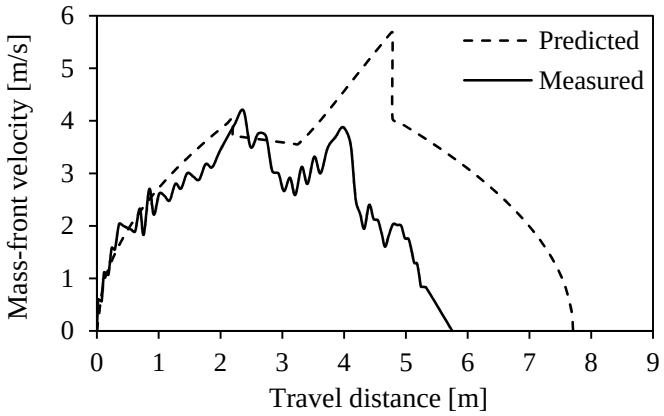

(p) Case 20

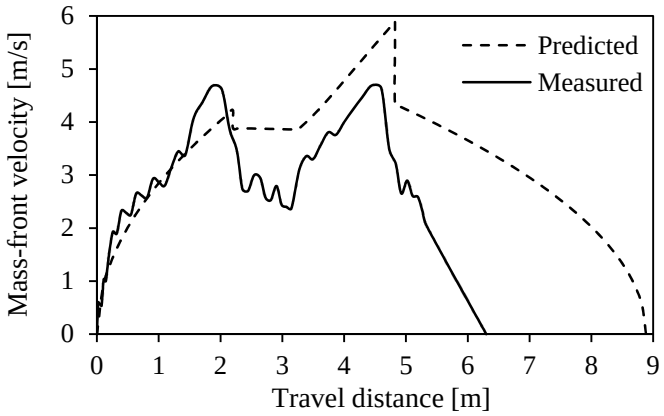

(q) Case 21

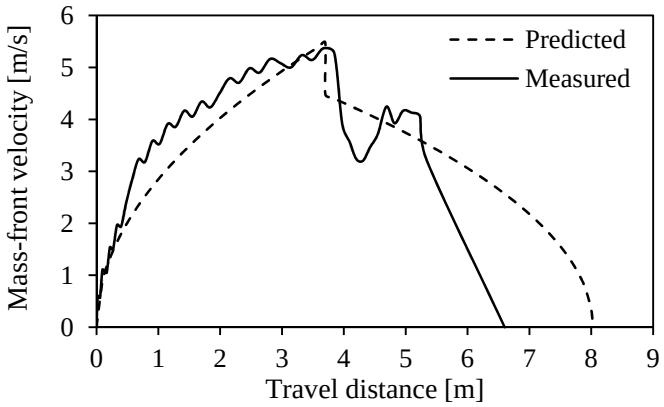

(r) Case 22

Figure 5.3 The comparisons between predicted velocities by this model and measured velocities of granular flows in the large flume tests (continued)

5.4.2 The comparison of the decrease in velocity due to the concavity

Of particular interest is the sudden decrease in velocity near the concavity. After opening the gate, the materials started moving down the flume, quickly acquired large velocity, and formed a rather thin layer of rapidly moving materials. When the materials reached the concavity, the velocity showed a sudden drop, and the flow went through a violent transition from the thin-layered rapid flow with a continuous acceleration over a relatively short region to a rather large deceleration of particles and reorientation of their flow direction. There were several reasons for the considerable decrease in velocity. Part of the energy was dissipated by the collision between the materials and the flume, and secondly due to the added frictional resistance caused by a higher overburden stress when the direction of movement changed. Another part of the energy was also consumed by internal deformation, especially for the flow with the gravel.

The ratio of the velocity immediately after and before the concavity, labeled as R_c for simplification, was a measurement of the decrease in velocity and hence the energy loss when the materials encountered a sudden change in inclination. In this model, as mentioned above, the predicted velocity at which the materials just arrived at the concavity was projected in the direction parallel to the lower slope, to be treated as the initial velocity along the lower slope. Therefore, the predicted R_c was 0.82 when the convexity was absent (R_c=cos(45˚-10˚), where 45° and 10° was the inclination of the upper and the lower slope, respectively, see Figure 4.4). In the case with the convexity, the predicted R_c was 0.92 when the materials encountered the convexity (R_c=cos(45˚-22˚), where 45° and 22° was the inclination of the upper slope and the convexity, see Figure 4.12). The predicted R_c varied only with the change in inclination, and was independent of other factors.

The comparison between the predicted and measured R_c in each case is illustrated in

Figure 5.4. The cases with no convexity are shown on the left, and those with the convexity are on the right. When the convexity was absent, the measured R_c fell within a narrow range of 0.71~0.76. In the cases with the convexity, however, the measured R_c was relatively scattered with the minimum and maximum values between 0.80~0.87. Energy loss was more in the case with no convexity than that with the convexity, which was chiefly caused by the more dramatic change in inclination.

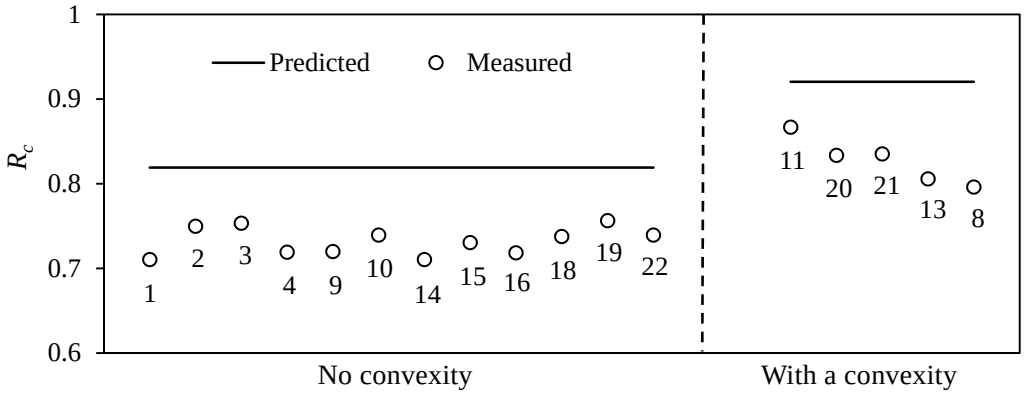

Figure 5.4 Decrease in velocity when the materials changed movement direction due to the variation in slope inclination (Note: Case No. is marked below the legend.)

The average measured R_c was 0.73 in the case where the convexity was absent, and was smaller than the predicted one of 0.82. This implies that more energy was consumed when the materials changed their movement direction. The average measured R_c was 0.83 in the case with the convexity, compared with 0.92 for the predicted one. The measured R_c was smaller than the predicted one for all cases. One of the main reasons was that the simple model took no account of energy loss due to the collisions, and also the added friction resistances between the granular materials and between the granular materials and flume. Another reason was that this lumped mass model failed to consider

the internal deformation of materials.

5.4.3 The comparison of the decrease in velocity due to the landing

The trend of velocities in the case with the convexity significantly departed from that with no convexity. We are mainly interested in the energy loss when the materials finally made contact with the bottom surface of the lower slope. The ratio of the velocity immediately after and before the landing, labeled as R_l, was calculated and compared. In the simple model, as mentioned above, the ballistic trajectory was assumed as the projectile motion for simplification. Incident velocity and its angle with the horizon and the landing location can be determined based on kinematic equations.

The flow was allowed only in the direction parallel to the base of the lower slope after the landing, and the component of the velocity in the direction perpendicular to the lower slope was neglected. The projection of the incident velocity in the direction parallel to the lower slope was thus the initial velocity at which the materials began to flow after the landing. Careful scrutiny reveals that the mass front did not simply follow projectile motion due to the interaction between particles; some particles underwent violent bouncing as the landing and this characteristic is not a feature of this model.

The comparison between the predicted and measured R_l is illustrated in Figure 5.5. The data were widely scattered, and the predicted and measured values greatly differed from each other in cases 8 and 13. One of the probable causes was that there was violent bouncing when the particle contacted with the lower slope, which cannot be reflected in the simple model. Another was that the instant that the particle landed sometimes did not just match with the frequency of the frame edited from the video because the time interval of two consecutive frames is somewhat long (1/30 s) relative to the high landing velocity. These caused that the measured velocity was smaller than that in the predicted one in cases 8 and 13. A higher speed camera should be used in order to capture more

precise data. Except the two scattered cases, the difference between the measured and predicted R_l was estimated to be within 5%.

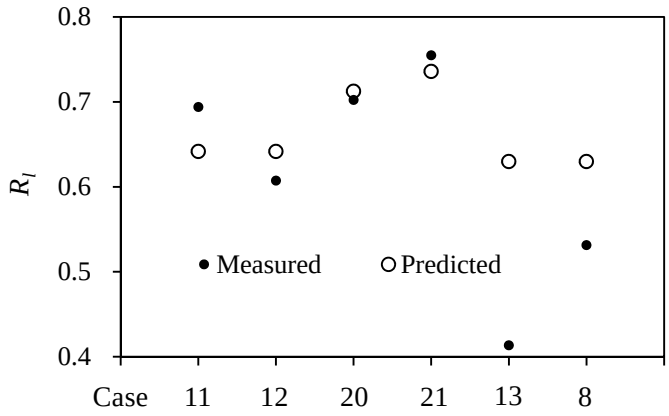

Figure 5.5 Decrease in velocity when the materials finally made contact with the flume

In nine out of twelve cases, the measured run-out was larger than the predicted one when the convexity was absent. This argument might partly account for the importance of collisions between particles. In five out of six cases with the convexity, however, the materials travelled farther in the model than in the test. This was particular evident for any situation in which there are frequent significant changes in movement direction, especially more abundant, higher and slightly longer ballistic trajectories or jumps occurred. The energy was consumed dramatically by the collision, friction, and internal deformation when the flow of materials reoriented, a situation which the simple lumped mass model cannot take account of.

5.5 DISCUSIONS

Although the simple lumped mass model assumed that retardation resulted only from the constant basal friction between the moving mass and underlying surface during the

propagation process, the comparison indicates that predicted results were in reasonable agreement with the measured ones, and the error introduced from the simplification was limited within a range of 10% or less. To our knowledge, such a direct comparison has not been presented before between the predicted velocity by theoretical predictions and the velocity measured in a large flume.

When the model is extended to reproduce natural rock avalanches, the apparent friction angle, rather than the friction angle measured in the laboratory should be used to consider the ‘size effect’. As is known, ‘size effect’ means that the deposits of large rock avalanche with a volume larger than about 10^6-10^7 m^3 will usually extend much farther than smaller ones (e.g. Scheidegger, 1973; Hsü, 1975; Legros, 2002). Large deposits also extend much farther than would be expected using a friction model. The extraordinary long run-out of natural rock avalanches is thus not expected to simply relate to the friction coefficients measured in the laboratory. The apparent friction angle refers the inclination to the horizon of the line joining the top of the breakaway scar and the distal end of the deposit. The tangent of the apparent friction angle is called as apparent friction coefficient, which is a measure of the mobility of moving mass. This simple expression can be used to get information about dynamic characteristics without regard to complicated propagation mechanisms.

Figure 5.6 shows the relationship between the volume and apparent friction coefficient for some natural events (Yang et al., 2012). It shows a trend in reduction of the apparent friction coefficient with the volume, although different mechanisms of motion are involved and scattering of data is high. The volume-dependent apparent friction coefficient is a useful tool to estimate ‘run-out’ or ‘excess travel distance’ in natural rock avalanches, and also served as an important parameter in numerical simulations. The apparent friction coefficient for each case was calculated (Table 4.1). To facilitate the comparison between large and small events, the apparent friction coefficient in the large flume tests is also shown in Figure 5.6. In these tests, the basal friction had a limited

range although the volume of released materials differed by almost five times, because the ‘size effect’ is unavailable in laboratory tests which are really at much smaller scale relative to field events. Using the friction coefficient measured in the large flume tests, which was close to the apparent frictional coefficient, this model can predict the run-out and velocity of granular flows, which generally were consistent with the measured ones.

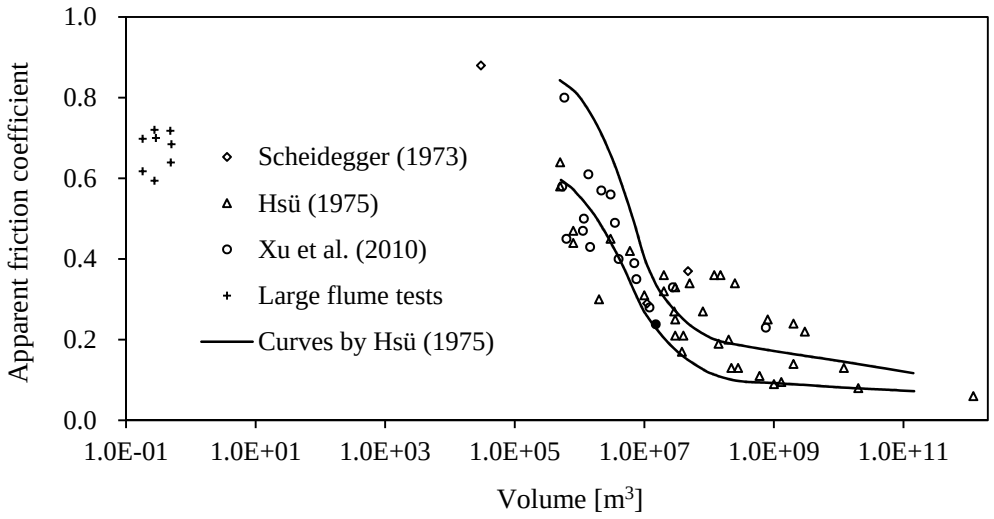

Figure 5.6 Correlation between the volume and apparent friction coefficient

As pointed out by Scheidegger’s (1973), the concept of the apparent friction coefficient obeys the law of conservation of energy. This is basically identical to the model proposed in this chapter. Therefore, if an apparent friction coefficient is used, the model not only could predict the run-out of rock avalanches but also their velocity at a given time during its movement, in which the ‘size effect’ and complex bed topography can be considered.

In addition, observations in the laboratory and in nature show that the rapid flow regime is characterized by more or less uniform velocity profiles with the depth, and the flow state in the rapid flow regime of avalanches is reasonably approximated by a depth integrated dynamical model (e.g. Savage and Hutter, 1989; Denlinger and Iverson, 2004;

Pudasaini et al., 2007). However, the large flume tests clearly demonstrate that the flows were not uniform through the depth, particularly in the region where bed topography suddenly changed. In such a region, there was a considerable momentum transfer in the direction perpendicular to the bottom surface, which cannot be neglected as in the simple lumped mass models. In the model presented in this chapter, the propagation only in the longitudinal direction was taken into account, and the momentum transfer in the direction normal to the bed was thus neglected. This simplification introduced about 10% difference between the predicted and measured decrease in velocity when the materials encountered a sudden change in slope inclination. The difference would be added up with complexity of terrain, e.g. upward the concavity of the surface causing centrifugal acceleration additional to gravity and increasing the reaction of the materials on the surface and hence the available frictional retarding force. Therefore, a fully three-dimensional model is desirable for the purpose of realistically describing the complete three-dimensional intrinsic behavior of granular flows. Highly refined mathematical solutions and a Coulomb-like behavior have been successfully used for a three-dimensional flow description (Denlinger and Iverson, 2001; Iverson and Denlinger, 2001).

The internal deformation also cannot be neglected as in the simple lumped mass models. This becomes apparent when we consider the materials flowing down, impacting on and running out across a slope inclined at a gentler angle, in this situation an overall depth flow changes into a surface boundary layer flow. Furthermore, the model can only provide reasonable approximations to the movement of the center of mass rather than the mass front, which is often the most important aspect of dynamic analysis.

5.6 CONCLUSIONS

This chapter presents a simple lumped mass model to predict the run-out and velocity of

experimental flows released in the large flume presented in Chapter 4, and the comparisons between predicted and measured results allow the following conclusions to be obtained.

(1) The simple lumped mass model based on energy approach could roughly predict the run-out and velocity of granular flows. The predicted velocity was somewhat lower than the measured one because the model neglected the collisions between particles. Subsequent particles with a higher velocity collided with slowed fronts to make them accelerate. This implies that continual collisions were a potential cause for the high velocity and long run-out of large rock avalanches. This simple model can also be extended to predict the run-out and velocity of rock avalanches if the apparent friction coefficient is used, and it assists in the design of safer human habitation and environmental protection.

(2) The presented model predicted a decrease in velocity when the flow changed its movement direction due to the variation in slope inclination. The predicted decrease in velocity was less than the measured one within a reasonable range of no more than 10%. The difference would be added up with the complexity of bed topography, especially when more abundant, higher and slightly longer ballistic trajectories or jumps occurred as observed frequently in field investigations.

(3) For some cases, in which a convexity was introduced, the model also predicted similar trends of velocities as measured in the tests. The materials took a ballistic trajectory from the vertex of the convexity, and reduced dramatically when they finally made contact with the base of the lower slope. The difference between predicted and measured decrease in velocity was estimated with about 5% due to the landing.

CHAPTER 6

NUMERICAL SIMULATIONS BY DISCONTINUOUS DEFORMATION ANALYSIS

6.1 INTRODUCTION

Rock mass is an inhomogeneous, anisotropic geological material consisting of both continuous rock medium and discontinuous components, such as joints, faults, and bedding planes (Ning et al., 2011). Discontinuous rock masses, although formed from a wide range of geological processes, possess the common characteristics of lower shear strength and negligible tensile strength relative to intact rock. The distinct element method (DEM) and discontinuous deformation analysis (DDA) are the two most popular discrete element methods for discontinuous rock mass. Discrete element methods have the advantage of being able to capture the kinematics and dynamics of numerous individual blocks without assuming failure modes (Sitar et al., 2005). In these methods, the domain of interest is treated as an assembly of rigid or deformable blocks/particles, and the contacts among these blocks/particles need to be identified and updated continuously during the entire deformation/motion process and represented by appropriate constitutive models (Jing and Hudson, 2002).

Although both DEM and DDA simulate the behavior of interacting discrete bodies, the two methods are completely different theoretically. In DEM, a rock mass is represented as a block assembly, and joints are treated as interfaces between blocks. Contact forces are computed using a soft contact approach in which the contact is assumed to be deformable. An artificial damping term is required to dissipate energy. The calculations alternate between the application of a force-displacement relationship at all of the contacts and Newton’s second law for all of the blocks. In contrast, DDA, which was originally formulated by Shi (1988), forms a system of algebraic equations based on the principle of minimum potential energy and uses displacements as variables in an implicit formulation. DDA uses standard FEM meshes over blocks, but all of the elements are real isolated blocks bounded by pre-existing discontinuities. DDA adopts a penalty-constraint method

using an opening-closing iterative scheme within each time step to achieve equilibrium of the blocks under contact constrains. The contact between the blocks is assumed to be rigid; thus, no overlapping or interpenetration of the blocks is allowed. Energy consumption occurs due to friction resistance at the contacts.

DDA has emerged as an attractive model for geomechanical problems because other numerical methods cannot easily replace its advantages. The continuum-based method, which is limited to problems in which the slide mass deforms slowly and has few material discontinuities, is clearly not suitable for large deformation situations. Limitations of the explicit DEM include its very small step for numerical stability and the use of artificial damping to absorb the energy generated from the relaxation analysis to maintain equilibrium. Shi (1988) claimed that the energy-based DDA can overcome the two limitations of the force-based DEM. Jing (1998) summarized the following four basic advantages of DDA over DEM: (a) the equilibrium condition is automatically satisfied for quasi-static problems without the use of excessive iteration cycles; (b) the length of the time step can theoretically be larger than that in explicit DEM formulations without inducing numerical instability; (c) there is no contact overlap, which is an important aspect for the simulation of fluid flow in fractured rocks; and (d) it is easy to convert an existing FEM code into a DDA code and include numerous mature FEM techniques without inheriting the limitations of ordinary FEM, such as small deformation, continuous material geometry, and reduced dynamic analysis efficiency. Based on these advantages, this study selected DDA as the analysis method to investigate the behavior of granular flows released in the large flume presented in Chapter 4 and three large landslides triggered by the Wenchuan earthquake.

Though DDA was developed by Shi during the late 1980s, and is thus a relatively new numerical simulation tool, it has been applied to a wide range of problems, and researchers in the DDA community have dedicated a great deal of effort to document the accuracy of this method by performing validation studies (MacLaughlin and Doolin, 2006). MacLaughlin and Doolin (2006) reviewed the validation of DDA with respect to analytical solutions, other numerical techniques, and laboratory and field data. Doolin and Sitar (2002) validated the displacement accuracy of DDA with respect to analytical solutions by studying the behavior of an idealized frictional sliding block under a range of material properties and analysis parameters. Lin et al. (1996) were likely the first researchers to quantitatively compare DDA and DEM. They provided some examples of the application

of DDA to rockfall, slope stability and underground excavation problems. A detailed comparison between DDA and DEM was discussed by Khan (2010) from both theoretical and practical points of view. Tsesarsky et al. (2005) investigated the displacement history of a single block on an incline subjected to sinusoidal loading, and examined the accuracy of DDA by comparing simulation results with analytical solutions and experimental results. Wu (2010) and Wu and Chen (2011) used DDA to simulate two field landslides triggered by the Chi-Chi earthquake in Taiwan. Hatzor et al. (2004) calculated the dynamic deformation of a real jointed rock slope using a fully dynamic version of DDA, and the authors found that in the multi-block case, 2% kinetic damping is necessary to realistically predict damage. Ishikawa et al. (1997) discussed the non-linear deformation behavior of coarse granular materials subjected to both monotonic and cyclic loading, and concluded that DDA is moderately successful in simulating the behavior of railroad ballast and provides better results than FEM for the same problem.

The objective of this chapter is to present some numerical simulations by DDA and investigate propagation mechanisms involved in rock avalanches. DDA was applied to reproduce a series of granular flows released in the large flume to demonstrate the applicability of DDA for realistically describing the behavior of granular flows. The application of DDA was then extended to large events triggered by the Wenchuan earthquake. Suggestion is put forward regarding the determination of a key parameter used in the simulation of field events.

6.2 BASIC MATHEMATICAL FORMULATIONS OF DDA

A general description of the method and formulation of DDA is adapted from Shi and Goodman (1985, 1989) and Shi (1992).

Assuming that each block has constant stresses and strains, the displacement (u, v) in the x- and y-directions at any point (x, y) within a block is the accumulation of displacements induced by six displacement variables: u_0, v_0, r_0, ε_x, ε_y, and γ_{xy}. Summing these six sources of displacement gives

$$\begin{Bmatrix} u \\ v \end{Bmatrix} = \begin{bmatrix} 1 & 0 & -(y-y_0) & (x-x_0) & 0 & (y-y_0)/2 \\ 0 & 1 & (x-x_0) & 0 & (y-y_0) & (x-x_0)/2 \end{bmatrix} [D] \tag{6.1}$$

where

$$[D] = \begin{bmatrix} u_0 & v_0 & r_0 & \varepsilon_x & \varepsilon_y & \gamma_{xy} \end{bmatrix}^T \tag{6.2}$$

(u_0, v_0) is the rigid body translation of the center of gravity (x_0, y_0) of the block; r_0 is the rotation angle of the block with a rotation center at (x_0, y_0), the unit of which is given in radians; and ε_x, ε_y, and γ_{xy} are the normal and shear strains of the block, respectively.

Individual blocks are connected to form a block system by contacts between blocks and displacement constraints on single blocks. For a block system with n blocks, the simultaneous equilibrium equations ($6n \times 6n$) have the following form:

$$\begin{bmatrix} K_{11} & K_{12} & \cdots & K_{1j} & \cdots & K_{1n} \\ K_{21} & K_{22} & \cdots & K_{2j} & \cdots & K_{2n} \\ \vdots & \vdots & & \vdots & & \vdots \\ K_{i1} & K_{i2} & \cdots & K_{ij} & \cdots & K_{in} \\ \vdots & \vdots & & \vdots & & \vdots \\ K_{n1} & K_{n2} & \cdots & K_{nj} & \cdots & K_{nn} \end{bmatrix} \begin{Bmatrix} D_1 \\ D_2 \\ \vdots \\ D_i \\ \vdots \\ D_n \end{Bmatrix} = \begin{Bmatrix} F_1 \\ F_2 \\ \vdots \\ F_i \\ \vdots \\ F_n \end{Bmatrix} \tag{6.3}$$

where D_i represents the displacement variables of block i, and F_i is the load applied to block i distributed to the six displacement variables. The diagonal sub-matrices [K_{ii}] in the coefficient matrix in equation (6.3) represent the sum of the contributing sub-matrices, such as mass, block stiffness, and so on, for the ith block. The off-diagonal sub-matrices [K_{ij}] ($i \neq j$) are 6×6 sub-matrices and represent the sum of the contributing sub-matrices of contacts between block i and block j, as well as other inter-block actions, such as bolting.

The solution of the system of equations is constrained by the system of inequalities associated with block kinematics (no penetration or tension between blocks) and the Mohr-Coulomb joint failure criterion for sliding along the interface, which is the main source of energy consumption. These equilibrium equations, which are derived by minimizing the total potential energy of the block system, are used to determine the displacements. The ith row of equation (6.3) consists of six linear equations of the form

$$\frac{\partial \Pi}{\partial d_{ri}} = 0 \quad (r = 1, \ldots, 6) \tag{6.4}$$

where d_{ri} is the displacement variable of block i. The equations for r = 1 and 2

$$\frac{\partial \Pi}{\partial u_0} = 0, \quad \frac{\partial \Pi}{\partial v_0} = 0 \tag{6.5}$$

represent the equilibrium of the loads and contact forces acting on block *i* in the *x*- and *y*-directions, respectively. The equation for *r* = 3

$$\frac{\partial \Pi}{\partial r_0} = 0 \tag{6.6}$$

represents the moment equilibrium of the loads and contact forces acting on block *i*. The equations for *r* = 4, 5 and 6

$$\frac{\partial \Pi}{\partial \varepsilon_x} = 0, \quad \frac{\partial \Pi}{\partial \varepsilon_y} = 0, \quad \frac{\partial \Pi}{\partial \gamma_{xy}} = 0 \tag{6.7}$$

represent the equilibrium of the external forces and stresses on block *i* in the *x*-, *y*- and shear directions, respectively.

The total potential energy Π is the summation over the potential energies of individual stresses and forces. The potential energy of each force or stress and their differentiations can be calculated separately. The differentiations

$$\frac{\partial^2 \Pi}{\partial d_{ri} \partial d_{sj}} \quad (r, s = 1, \ldots, 6) \tag{6.8}$$

are the coefficients of the unknowns d_{si} in equation (6.3) for variable d_{ri}. Therefore, the terms in equation (6.8) form the 6 × 6 sub-matrix $[K_{ij}]$ in equation (6.3). Equation (6.8) implies that the coefficient matrix $[K]$ of equation (6.3) is symmetric. The differentiations

$$-\frac{\partial \Pi(0)}{\partial d_{ri}} \quad (r = 1, \ldots, 6) \tag{6.9}$$

are the free terms of equation (6.4) after they are shifted to the right. Therefore, all of the terms in equation (6.9) form the 6 × 1 sub-matrix $[F_i]$.

6.3 EXPERIMENTAL SET-UP

The large flume tests were conducted to investigate some of the propagation mechanisms

involved in the rapid, dry, dense granular flows and to identify factors influencing the mass-front velocity of the flows. A detailed description of the large flume tests was presented by Yang et al. (2011a).

The velocity is one of the most important physical quantities for the dynamic characterization of rock avalanches. DDA is used to predict the velocity of granular flows in the large flume, and the comparison between the predicted and measured velocity facilitate to evaluate the precision of DDA.

6.4 LARGE FLUME TEST SIMULATION

The geometry and initial configuration of the numerical model were based on a 2D reproduction of the experimental conditions. Cube-shaped blocks with 0.1 m and 0.05 m sides were called large cubes and small cubes, respectively. Cobbles were simulated by hexagons that were as close as possible in shape to those employed in the tests. The gravel layer was randomly divided into an assembly of polygons with different shapes and sizes. The mechanic properties of the granular materials were measured in the laboratory. Some of the numerical control parameters are as follows: the time step size = 0.001 s, the maximum allowed displacement ratio = 0.00085, the contact spring stiffness = 1×10^6 kN/m, and the factor of over-relaxation = 1.3.

The numerical model reproduced the experimental set-up as close as possible. The main discrepancy was the difference between the plane strain condition in the tests and the 2D nature of the model. In the 2D model, granular elements were treated as 2D polygons, out-of-plane movements were not considered, and the effect of the flume's sidewalls was not taken into account because their roughness was sufficiently small to ensure the flow in 2D conditions.

6.4.1 Released material

6.4.1.1 Mono-materials

In cases 2, 3, and 10, several tests were conducted on the mono-materials of cubes, gravel, and cobbles, respectively. Figure 6.1 illustrates the initial arrangement of the granular

elements in cases 2, 3 and 10.

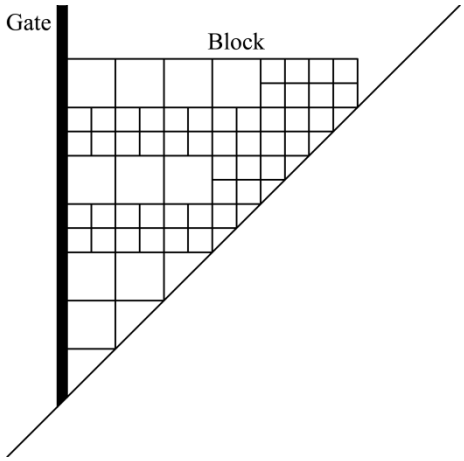

(a) Case 2

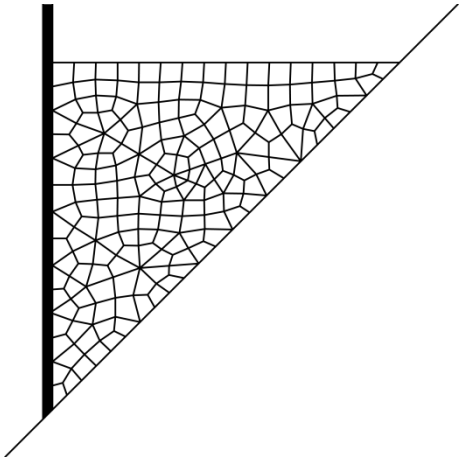

(b) Case 3

Figure 6.1 Initial geometry of the blocks in cases 2, 3 and 10 (to be continued)

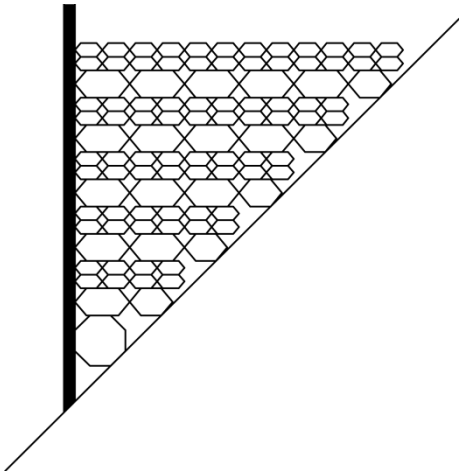

(c) Case 10

Figure 6.1 Initial geometry of the blocks in cases 2, 3 and 10 (continued)

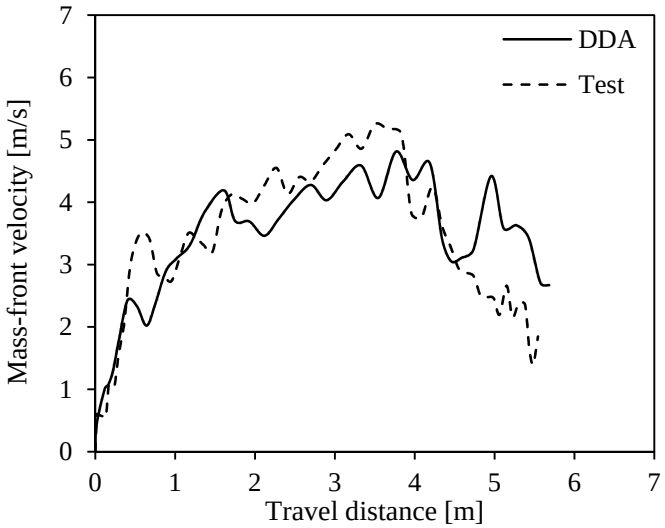

Figure 6.2 Comparison of the simulated and measured velocities in case 2

Figures 6.2, 6.3 and 6.4 show the simulated and measured mass-front velocities for cases 2, 3, and 10, respectively. The trend of the simulated velocities corresponded well with that of the measured velocities. Both the simulated and measured velocities fluctuated due to the propulsion of subsequent particles to the slowed front by impact. DDA accurately reflected this important phenomenon; this was an advantage of DDA over simple lumped mass models in which a moving mass is simplified as a rigid body without regard to

collisions between particles.

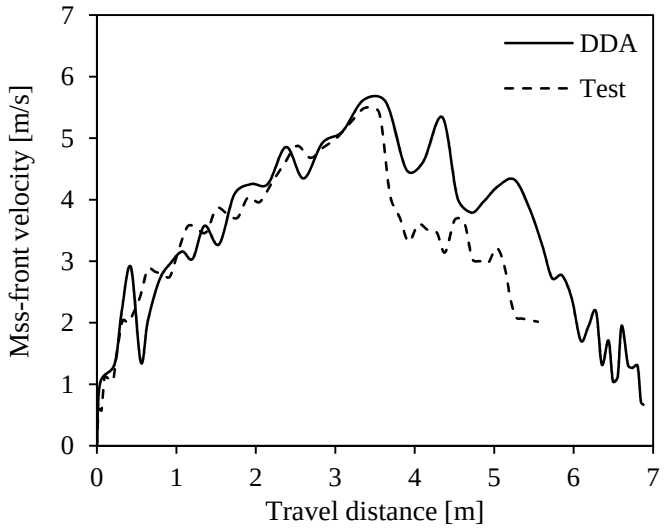

Figure 6.3 Comparison of the simulated and measured velocities in case 3

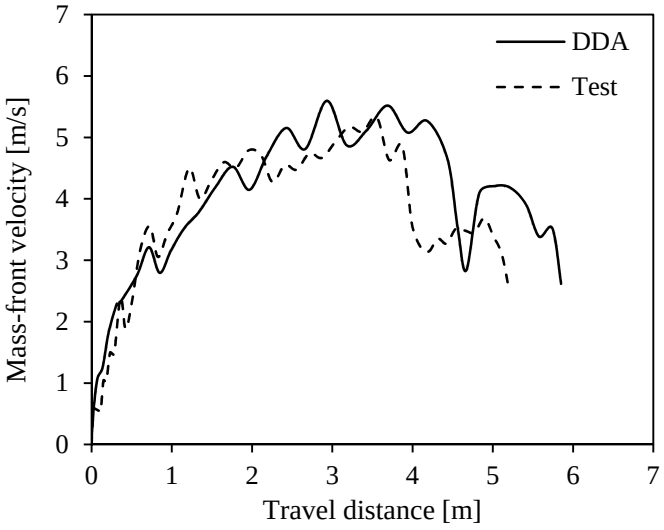

Figure 6.4 Comparison of the simulated and measured velocities in case 10

In case 10, cobbles were also simulated by regular octagons. The simulated velocity for the regular octagons was much higher than that for the hexagons, and also much higher than the velocity measured in the tests. A majority of the octagonal blocks moved beyond the flume and stopped on the horizon, while a different situation occurred in the tests. Thus,

the velocity and run-out were highly sensitive to the shape and angularity of granular elements used in the numerical analysis. This conclusion corresponded with that drawn by Hatzor et al. (2004), who found that the DDA simulation results are extremely sensitive to the geometrical configuration, i.e., the computed mesh. Therefore, the shape and angularity of the blocks had to be determined carefully in the numerical model because the use of unrealistic granular elements may cause the grain behavior to be modeled inaccurately.

6.4.1.2 Composites

Two composites were tested, including a composite of gravel (400 kg) and cubes (200 kg large cubes and 200 kg small cubes) in case 4 and a composite of gravel (400 kg) and cobbles (200 kg large cobbles and 200 kg small cobbles) in case 14.

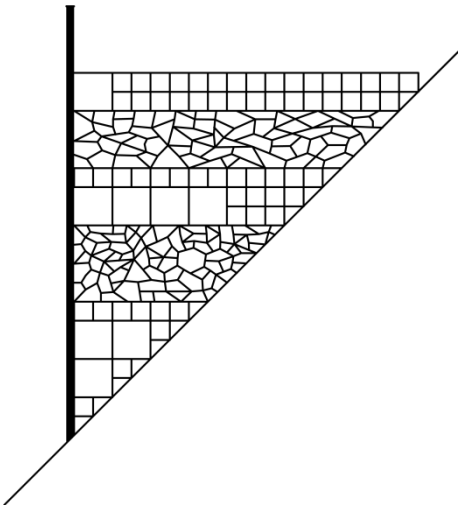

(a) Case 4

Fig. 6.5 Initial geometry of the blocks in cases 4 and 14 (to be continued)

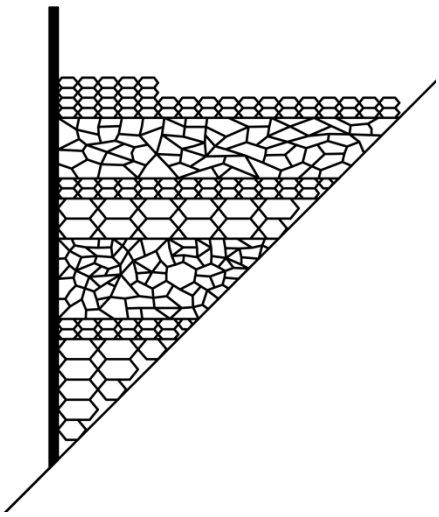

(b) Case 14

Figure 6.5 Initial geometry of the blocks in cases 4 and 14

In case 4, the cube and gravel composite was initially arranged as alternating layers of cubes and gravel (Figure 6.5). A total of 68 cubes were arranged in the position as close as possible to that in the tests. Two layers of gravel were divided into 153 irregular polygons with different shapes and sizes. Though only a few irregular polygons were used in the numerical model and their shape was not exactly the same as that in the tests, the simplification was feasible with the objective of capturing the main features of granular flows.

DDA accurately predicted the low velocity of this composite of cubes and gravel (Figure 6.6). The agreement between the simulation and experiment indicates that DDA effectively described the granular flows. The cube and gravel composite with a large volume displayed a lower mobility than the cube and gravel mono-materials with small volumes because more energy was consumed by intergranular friction between the cubes and gravel. DDA accurately modeled the energy dissipation caused by the friction between particles; this is another advantage of the DDA over simple lump mass models in which retardation only resulted from the constant basal friction between a moving mass and the underlying surface without regard to intergranular friction.

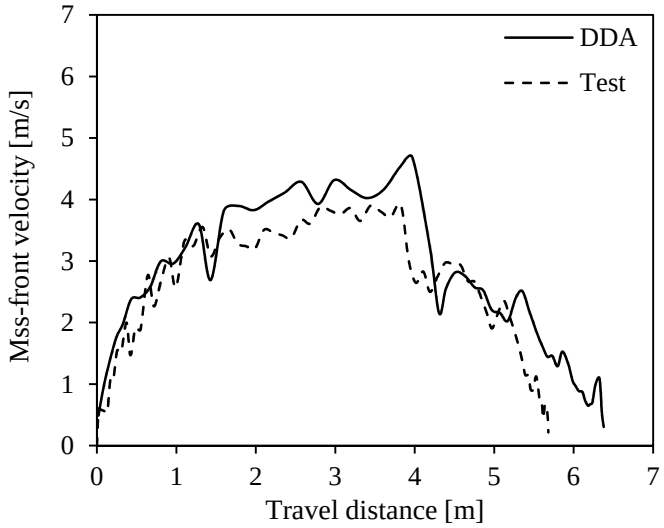

Figure 6.6 Comparison of the simulated and measured velocities in case 4

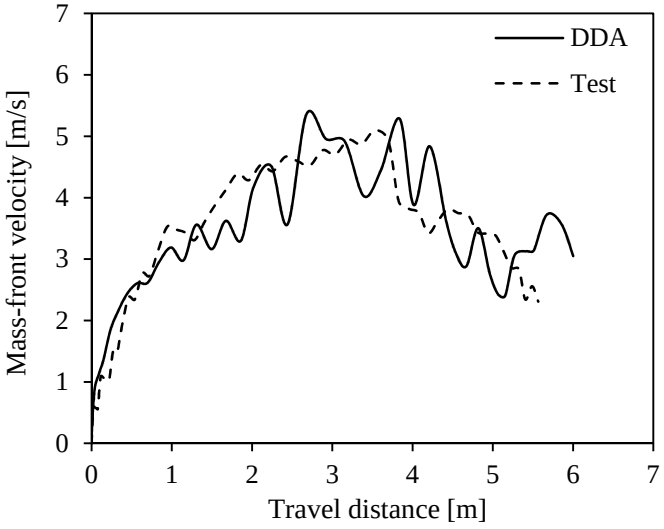

Figure 6.7 Comparison of the simulated and measured velocities in case 14

An unexpectedly high velocity that was almost the same as those for the mono-materials was observed for the cobble and gravel composite in case 14. The velocity of this composite was considerably higher than that of the cube and gravel composite (case 4) because the cobbles rolled on the surface of the gravel more easily than the cubes. The global tendency of the simulated velocities, which are represented by the solid line, coincided with the experimental data, which are represented by the dashed line (case 14, Figure 6.7). However, the simulated velocity fluctuated greatly because the DDA did not

take the energy loss due to the collisions between particles and between particles and the flume into account. Thus, the velocity of the frontal particles increased more significantly when subsequent high-velocity particles provided propulsion to allow them to accelerate. Collisions occurred frequently and considerably dissipated energy. A restitution coefficient had to be introduced to consider the energy loss caused by the collisions. Ma et al. (2011) proposed a modified DDA method to address this problem in simulating rockfalls. The simulated results were compared with test results, and found that the velocity is most accurately predicted using a restitution coefficient of 0.7.

6.4.2 Material volume

Cases 9 and 10 employed 200 kg cobbles (100 kg large cobbles and 100 kg small cobbles) and 400 kg cobbles (200 kg large cobbles and 200 kg small cobbles), respectively.

The velocity of the materials with a smaller volume (case 9, Figure 6.8) was lower than that of the materials with a larger volume (case 10, Figure 6.4). DDA predicted the lower velocity in case 9; this confirms our previous conclusion that the velocity increases with volume for the cobbles.

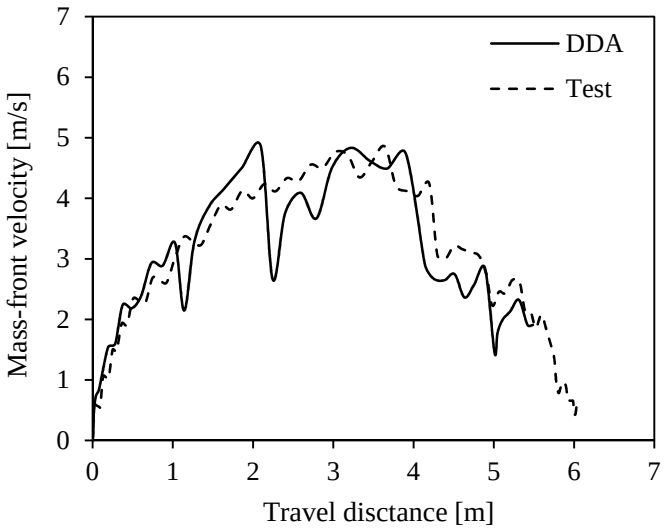

Figure 6.8 Comparison of the simulated and measured velocities in case 9

6.4.3 Obstacles

6.4.3.1 Convexity

A sharp convexity was used in case 11. The velocity trends, showing two peak velocities, significantly departed from the cases in which there was no convexity. The consistency between the simulated and measured velocities in this case (Figure 6.9) indicates that DDA was capable of describing the propagation behavior of granular flows even when the bed topography changed significantly.

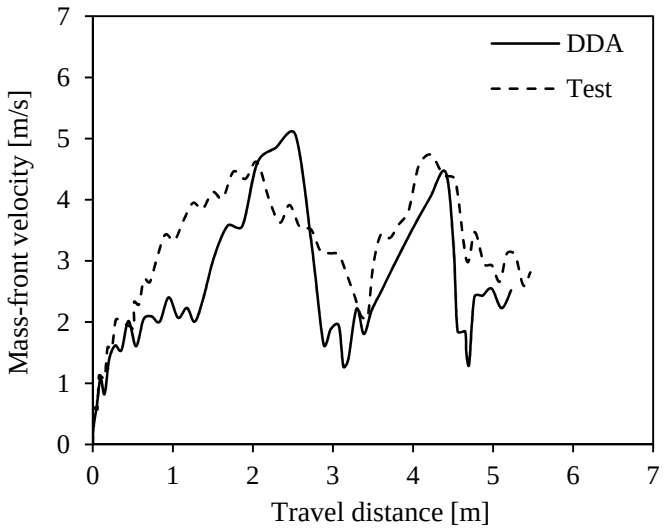

Figure 6.9 Comparison of the simulated and measured velocities in case 11

6.4.3.2 Forest model

A 0.9 m long and 1.0 m wide forest model was placed on the slope after the concavity. A cobble and gravel composite was released onto the forest model (case 16).

The friction angle of the model forest was 38.68°, which was determined by large direct shear tests (Yang et al., 2011a). DDA reflected the obstruction of the propagation movement of granular flows due to the forest. Immediately after the concavity, the velocity dropped more significantly than in the previous case due to the resistance of the model forest, as illustrated in Figure 6.10.

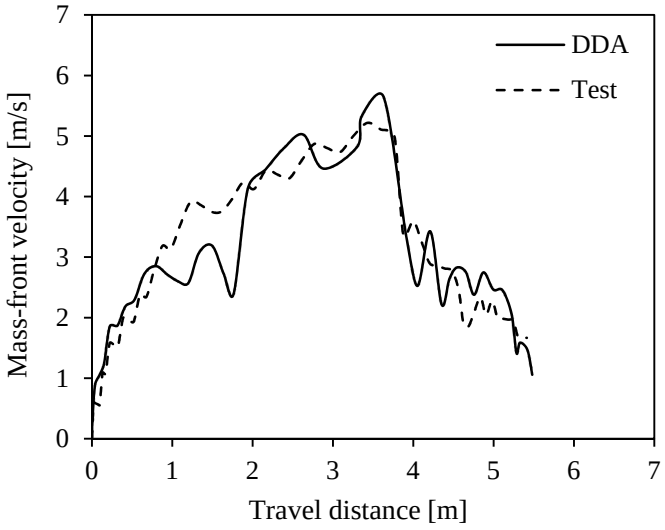

Figure 6.10 Comparison of the simulated and measured velocities in case 16

The comparison of the simulated and measured velocities indicates that DDA can satisfactorily reproduce granular flows in the large flume tests. In the next section, the numerical model will be applied to reproduce three large landslides triggered by the Wenchuan earthquake.

6.5 SIMULATIONS OF LARGE ROCK AVALANCHES

In this section, we extended the application of DDA to the reproduction of three large events triggered by the Wenchuan earthquake on May 12th, 2008, which were selected due to their relevance and the relatively large amount of data recorded before and after the failure.

6.5.1 The Donghekou rock avalanche

The Donghekou rock avalanche buried 7 villages and killed 780 people. It was a typical rapid, long run-out rock avalanche with an altitude difference of 540 m between the toe and main scarp, a sliding distance of 2,270 m, and a volume of 15 million m^3 (Xu et al., 2010). The landslide consisted of sandstone, shale, and schist from the Cambrian age, and was located approximately 4 km from the active fault-rupture (Yin et al., 2009).

After the event, a valley bottom of 1.08 km^2 was covered with deposit with a maximum thickness of 60 m, and an impounded lake with a capacity of 250 million m^3 was formed (Huang et al., 2011b).

It is somewhat difficult to compare a 2D simulation with a 3D field case. Certain assumptions were made to capture the main features of the large rock avalanche. Blocks were treated as 2D quadrilaterals; the failed mass was assumed to be completely disintegrated before it moved without regard to fragmentation during the propagation process; the lateral constraint was neglected; and the initial geometry of the failed mass and initial topography of the sliding surface were highly simplified. Despite these assumptions, a 2D simulation is helpful for understanding the propagation mechanisms and behavior. A sketch of the DDA model of the slope is shown in Figure 6.11. The 170 quadrilaterals composing the failed mass were randomly generated.

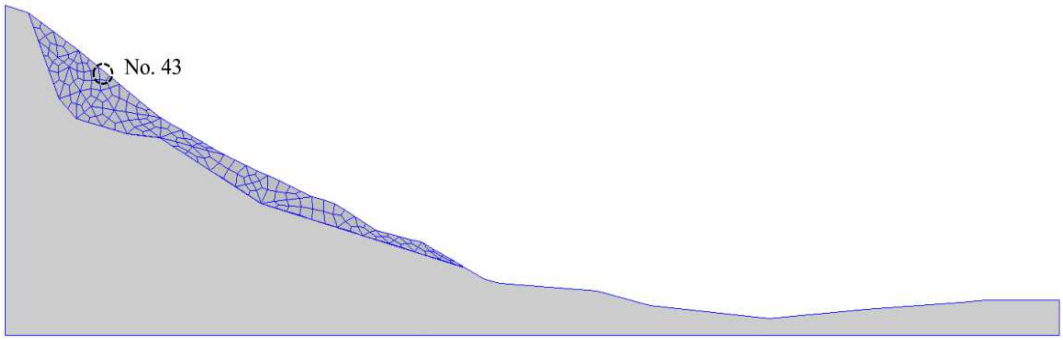

Figure 6.11 Block geometry in the DDA simulation for the Donghekou rock avalanche

The failed mass had an initial horizontal velocity to briefly consider earthquake energy. The initial horizontal velocity was 1 m/s, based on the effects of topographic amplification, seismic horizontal peak velocity, and distance to faults. Another similar case was also performed in which the avalanche was only triggered by the gravity, and the initial velocity was not considered. Comparing these two cases allows the effect of earthquake energy on the final deposit to be investigated. The laboratory-measured mechanical properties were reported by Huang et al. (2009), and the main numerical control parameters are as follows: the time step size = 0.01 s, the maximum allowed displacement ratio = 0.0015, the contact spring stiffness = 5×10^8 kN/m, and the factor of over-relaxation = 1.3.

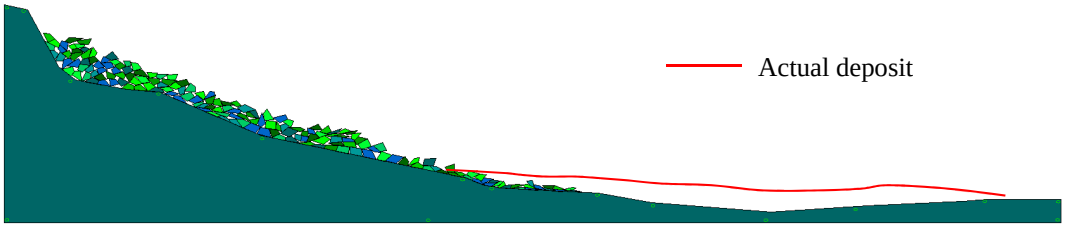

Figure 6.12 Calculated final deposit of the Donghekou rock avalanche when measured friction coefficient was used

The calculated deposit was combined with the actual final deposit observed in the field, as illustrated in Figure 6.12. The sliding mass remained in approximately the same place at 200 s (20,000 time steps) after the inception of motion. The calculated run-out was much shorter than the actual run-out. The trial calculations show that simulation results were significantly affected by friction coefficient. The friction coefficient measured in the laboratory was difficult to reproduce the extremely long run-out of the rock avalanche. This implies that the 'size effect' should be considered in the simulation of field events. The 'size effect' means that the deposits of a natural rock avalanche with a volume larger than 10^6~10^7 m^3 typically extend much farther than those of smaller avalanches and extend much farther than the deposits simulated by a friction model (e.g. Scheidegger, 1973; Hsü, 1975; Erismann and Abele, 2001). The long run-out is thus not expected to relate to the friction coefficient measured in the laboratory. To account for this discrepancy, the apparent friction coefficient, a measure of the mobility of the rock avalanche, is the tangent of the apparent friction angle and refers to the inclination to the horizon of the line joining the top of the breakaway scar and the distal end of the deposit. The apparent friction coefficient was typically much smaller than the measured friction coefficient for large rock avalanches. Figure 6.13 illustrates the relationship between the volume and apparent friction coefficient for some natural events (including the Donghekou rock avalanche, which is represented by a solid circle). To allow these events to be more easily compared, the apparent friction coefficients in the large flume tests are also plotted in Figure 6.13.

The apparent friction coefficient of 0.238 (Xu et al., 2010) was used. The failed mass had an initial velocity of 1 m/s in one case, and the initial velocity was not considered in the second case. When the apparent friction coefficient was used, the calculated deposit

corresponded well with the actual deposit in both cases (Figure 6.14). Whether the apparent friction coefficient can be served as a reasonable parameter in reproducing the actual deposit of field rock avalanches must be further confirmed. Furthermore, the comparison of the two cases implies that the effect of earthquake energy was not apparent on the final deposit. This ambiguity may confirm the statement proposed by Kokusho et al. (2009) that the contribution of earthquake energy is still indirectly important through the reduction of the friction coefficient through cyclic loading instead of directly through the supply of the driving energy.

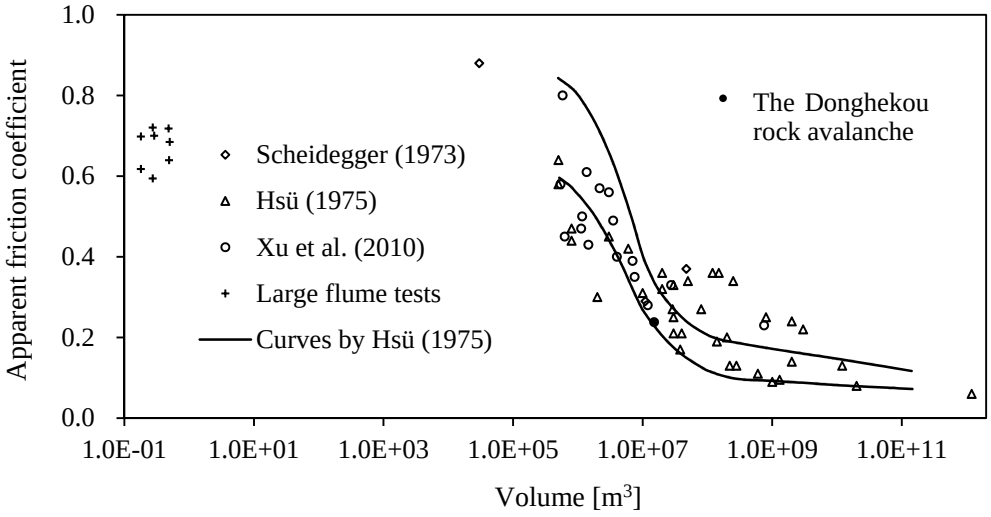

Figure 6.13 Correlation between the volume and apparent friction coefficient

It is worth noting that the friction coefficient measured in the laboratory served as an appropriate parameter in the simulation of the large flume tests, which reasonably predicted the velocity of those granular flows. This was because the volume of granular materials released in the large flume tests was much smaller than 10^6 m^3, and the 'size effect' was unavailable. For field events, however, a volume-dependent apparent friction coefficient should be used to consider the 'size effect'. This result was confirmed by the Davies and McSaveney's conclusion (1999) that granular avalanches with volumes ranging from 10^{-4} m^3 to approximately 10^5 m^3 show consistent run-out behavior, but the run-out behaviors of those with volumes greater than 10^6-10^7 m^3 differ significantly from those at smaller scales.

Figure 6.15 shows the failure process from initiation to rest. Xu et al. (2010) and Yin et al. (2009) stated that a rapid throwing occurred during triggering period. Surprisingly, however, a rapid throwing from the upper gentle platform was not observed in our simulation. Instead, the entire failed mass slid nearly undisturbed, and the debris exhibited similar strata as the source.

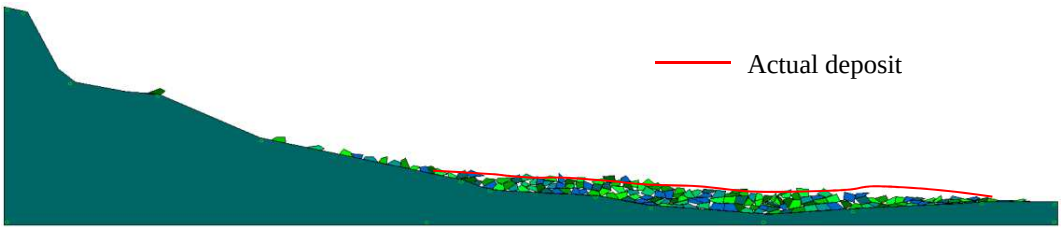

(a) With an initial velocity

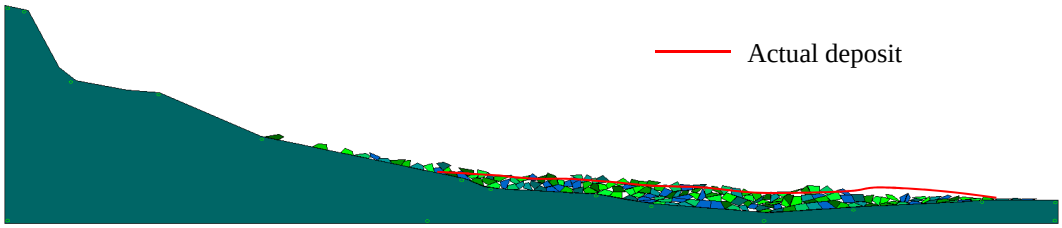

(b) No initial velocity

Figure 6.14 Calculated final deposit of the Donghekou rock avalanche when apparent friction coefficient was used

The maximum simulated velocity among the sliding blocks was 60.2 ms^{-1}, and this block (No. 43) was located near the slope surface, as shown in Figure 6.11. This block traveled 447 m from its initial position, reaching the maximum velocity at an elapsed time of 19.7 s. This block accelerated and bounced due to the propulsion provided by subsequent blocks with higher velocities. Continuous propulsion was one of the potential causes for the high velocities and long run-outs of field rock avalanches.

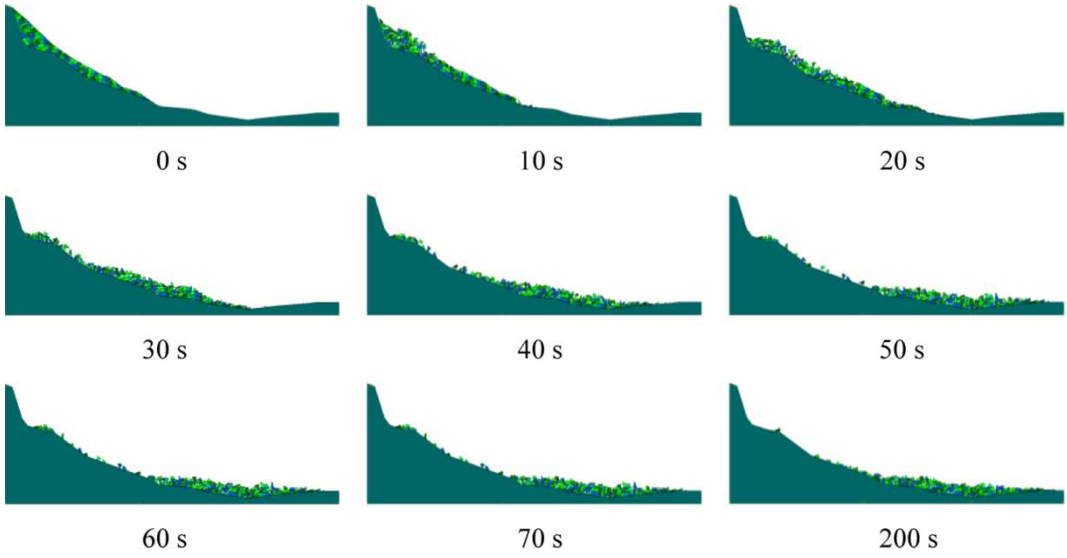

Figure 6.15 Failure process of the Donghekou rock avalanche

6.5.2 The Xinbei middle school landslide

The Xinbei middle school landslide buried at least 1,000 students and teachers (Xinhua News Agency, 2008). The landslide was a complex of ancient landslide and cliff with a length of 650 m, a breadth of 200 m, an average thickness of 40 m, an altitude difference of 300 m, and a volume of approximately 2.4×10^6 m^3 (Huang et al., 2010). The bedrock mainly consisted of thick limestone of Upper Devonian and Lower Carboniferous Periods. This landslide totally destroyed a three-storied school building in the Xinbei Middle School and adjacent building due to its huge impulsive force. In the leading edge of the landslide, there was ground ballooning along the former main street and took the lives of nearly 500 people, it might be related to the break thrust formed by the seism tectonic line (Huang et al., 2010).

The failed mass was randomly divided into 206 polygons (Figure 6.16). The main numerical control parameters, i.e., time step size, maximum allowed displacement ratio, contact spring stiffness, and factor of over-relaxation, were the same as those used for the simulation of the Donghekou rock avalanche. The apparent friction coefficient of this landslide was 0.625.

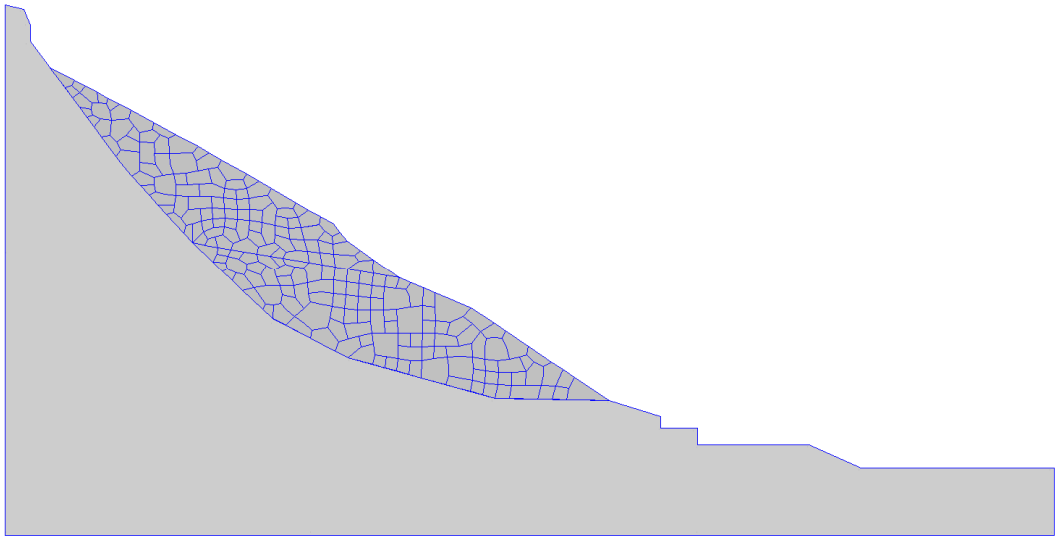

Figure 6.16 Block geometry in the DDA simulation for the Xinbei middle school landslide

The calculated deposit was combined with the actual final deposit observed in the field, as illustrated in Figure 6.17. The calculated deposit was similar to the actual deposit.

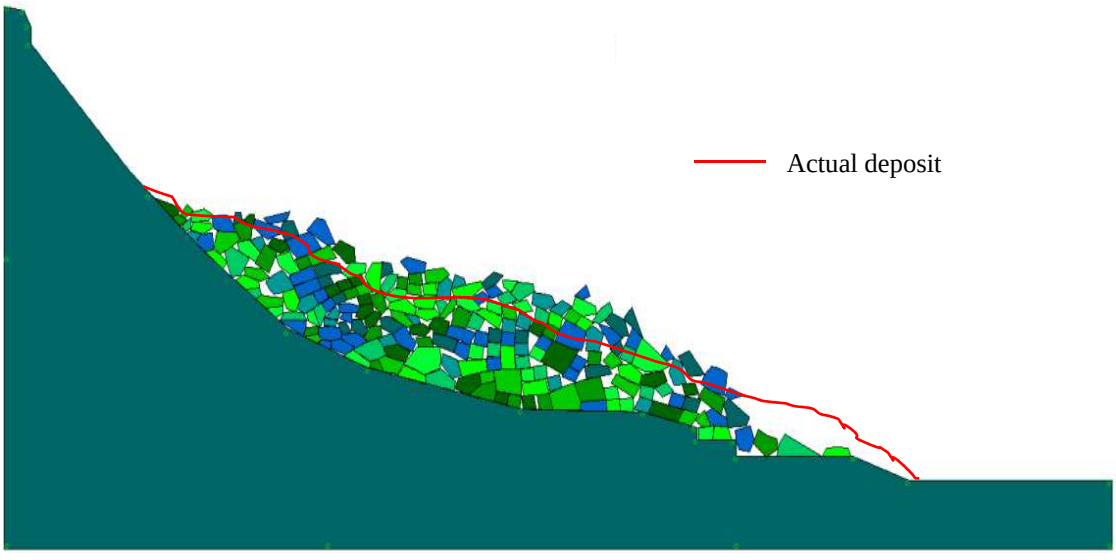

Figure 6.17 Calculated final deposit of the Xinbei middle school landslide when apparent friction coefficient was used

6.5.3 The Shibangou rock avalanche

The Shibangou rock avalanche was a large rock avalanche with a volume of 4.5 million m^3, which buried a village and blocked the Qingzhu River, forming an impounded lake. The altitude difference between the toe and main scarp was 240 m. The deposit covered an area of 3.5×10^5 m^2, with an average thickness of 15 m.

The 176 quadrilaterals composing the failed mass were randomly generated (Figure 6.18). The main numerical control parameters, i.e., time step size, maximum allowed displacement ratio, contact spring stiffness, and factor of over-relaxation, were the same as those used for the simulation of the Donghekou rock avalanche. The apparent friction coefficient of this avalanche was 0.268.

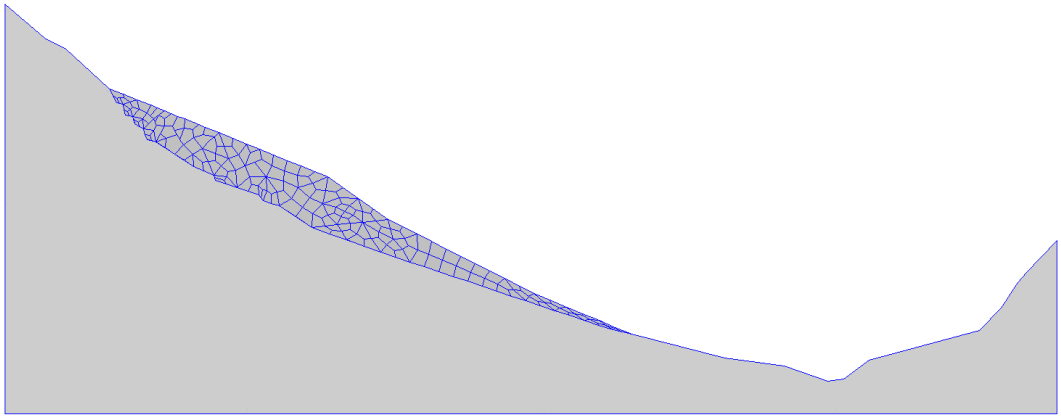

Figure 6.18 Block geometry in the DDA simulation for the Shibangou rock avalanche

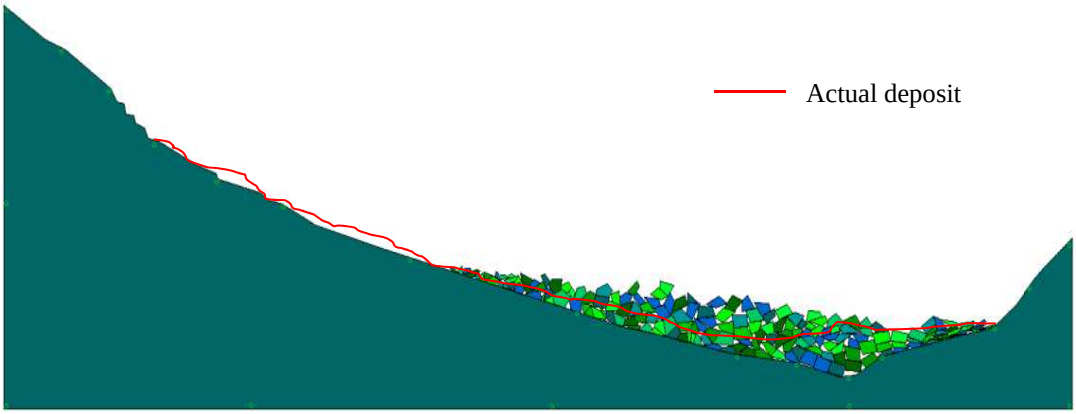

Figure 6.19 Calculated final deposit of the Shibangou rock avalanche when apparent friction coefficient was used

The calculated deposit agreed well with the actual deposit observed in the field, as illustrated in Figure 6.19.

6.6 CONCLUSIONS

In this chapter, certain granular flows released in the large flume and natural rock avalanches triggered by the Wenchuan earthquake were accurately simulated by DDA. Their velocities and deposit characteristics were obtained by this numerical method and then compared with measurements. The comparisons indicate that the DDA simulation was satisfactory, and the differences between the simulations and measurements were limited to an acceptable range.

DDA captured the main features of granular flows in the large flume tests, and the simulated velocity corresponded well with that measured in the tests. Energy dissipation caused by intergranular friction was accurately described in DDA. Collisions between particles, which were one of the possible reasons for the high velocity and long run-out, were also reflected realistically. However, energy loss caused by the collisions was not taken into account in DDA. This caused that the simulated mass-front velocity to fluctuate more than that measured in the tests. Furthermore, the simulated results were highly sensitive to the shape and angularity of granular elements; thus, the use of realistic elements was important for obtaining reliable results.

The friction coefficient strongly influenced the simulation results for the large rock avalanches. The calculated deposit was only similar to the actual deposit when the apparent friction coefficient, which was determined by field investigation, was used instead of the friction coefficient measured in the laboratory. In contrast, for the large flume tests, the measured friction coefficient served as an available parameter to predict the velocity of experimental granular flows. Furthermore, the calculated deposit was similar regardless of the initial horizontal velocity. This implies that the final deposit was mainly determined by the potential energy of the failed mass and was not significantly influenced by the earthquake energy.

CHAPTER 7

STABILITY OF JOINTED ROCK SLOPES INVESTIGATED BY SHAKING TABLE TESTS

7.1 INTRODUCTION

A rock mass is a largely discontinuous, inhomogeneous, anisotropic, and non-elastic material in nature (Harrison and Hudson, 2000). Rock formations usually contain naturally occurring fractures or planes of weakness such as bedding planes, faults, fissures, joints and other mechanical defects (Khan, 2010). 'Jointed rock' is usually used to describe the rock mass which contains these mechanical defects. The stability of rock slopes is mainly governed by the geometrical and strength characteristics of these defects, i.e., jointed behavior, rather than by the mechanical properties of intact rock (Giani, 1992; Hoek and Bray, 1981; Einstein et al., 1983).

The stability of jointed rock slopes is more vulnerable when the slopes are situated in earthquake prone areas, and engineering practices have shown that the instability and destroy of rock engineering always related to dynamic loads. Earthquakes with a very small magnitude may trigger a failure in slopes in jointed rock masses which are perfectly stable otherwise (Latha and Garaga, 2010). From the point of view of dynamic stability, it is very important to investigate the dynamic response of jointed rock slopes subjected to seismic shaking.

Experiments play an important role in contributing to a better understanding of failure mechanisms involved in jointed rock slopes. McBride and Scheele (2001) studied a model slope consisted of 50 blocks, and compared the failure pattern observed in the experiments with DDA numerical simulation. Li et al. (2005) also carried out physical model tests to study the stability of jointed rock slopes, and compared the failure mode and factor of safety with those predicted by DEM.

The dynamic analysis of slopes in rock masses also has been studied using physical model tests and numerical simulations. Ai et al. (2010) conducted explosion model tests

to investigate the dynamic response of consequent rock slope under seismic loading. Other researchers (e.g. Hatzor et al., 2004; Bhasin and Kaynia, 2004; Sosio et al., 2008) simulated dynamic behavior of jointed rock slopes by various numerical analysis. Despite of these studies, failure mechanisms in rock masses associated with seismic shaking are still unknown. There is little information available in the literature about the failure mode and dynamic response of jointed rock slopes investigated by shaking table tests. This chapter presents some shaking table tests to study failure process of jointed rock slopes associated with seismic shaking.

7.2 EXPERIMENTAL SET-UP

Experimental set-up employed in this study is showed in Figure 7.1. A frame was fixed tightly over a shaking table (2.0 m × 1.0 m). The back wall was covered with a white plastic film to achieve a better contrast in the photographs. A piece of polyfoam with a thickness of approximately 5 cm was mounted on the right sidewall of the frame in order to absorb the energy impacted by the right sidewall during the shaking. The base of the frame was covered three layers of blocks to limit boundary layer effects. Concrete blocks with the same dimensions of 45 mm long and a cross section of 25 mm × 25 mm were used. Jointed rock slopes were stacked with different joint configurations: horizontal and vertical straight joints, or joints inclined at 45°. A rock slope with straight joints was treated as a benchmark to facilitate the comparison with other cases.

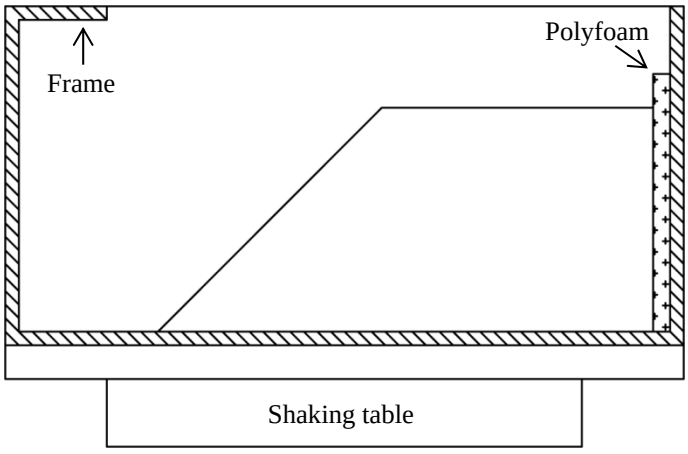

Figure 7.1 Experimental set-up

The model slope was subjected to sinusoidal waves with a peak acceleration of 300 gal and a frequency of 5 Hz, which were applied to the base of the slope and allowed to propagate upwards. Sensors were attached to some blocks to measure the acceleration and evaluate the amplification effect. A high-speed digital video camera was operated at 210 fps to record the movement and failure process by a frontal perspective, and another digital video camera was positioned at the side of the shaking table in order to capture the side outline of moving blocks.

7.3 EXPERIMENTAL RESULTS

7.3.1 A slope with straight joints

7.3.1.1 Benchmark

The slope configuration of the benchmark is shown in Figure 7.2.

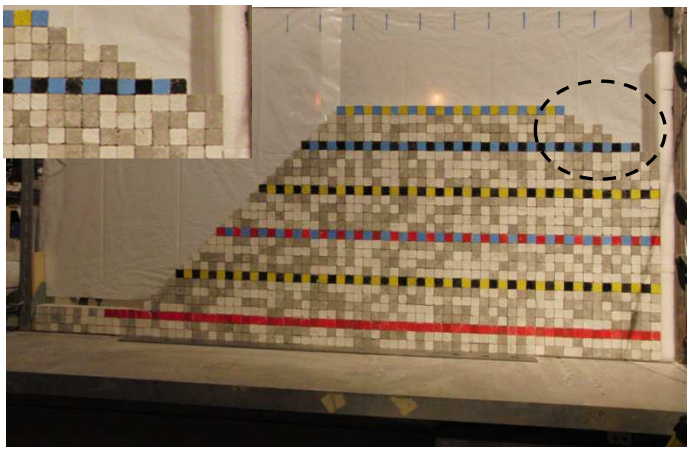

Figure 7.2 A rock slope model with straight joints (benchmark)

The failure process of the benchmark is reported herein (Figure 7.3). First, some cracks appeared at the slope surface usually with a depth of five blocks about 12.5 cm due to the inertia force induced by the sinusoidal waves. Second, when the slope moved

in the opposite direction, some of such cracks closed; however, other cracks kept open although their width became small. The cracks widened and propagated into the slope when the second sinusoidal wave reached. Third, when the acceleration of the wave increased, the cracks further enlarged, and toppling occurred and some blocks rotated. Last, a large failure occurred. Shaking table tests show that the failure was largely influenced by the joint configuration. Significantly different failure pattern was observed in the shaking table tests if vertical joints near the slope surface were discontinuous especially when the length of the vertical discontinuous joints was within the depth of five blocks. This was because the cracks were difficult to propagate in the direction of depth.

(a) Some cracks appeared at slope surface

Figure 7.3 Failure process of the benchmark case (to be continued)

(b) Cracks widened and propagated into the slope

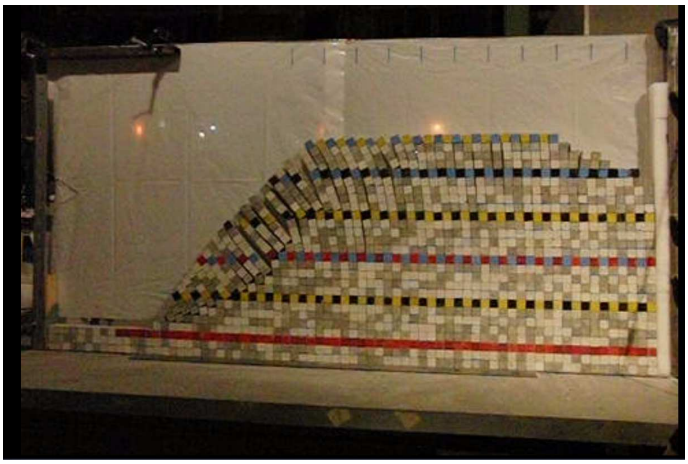

(c) Toppling started

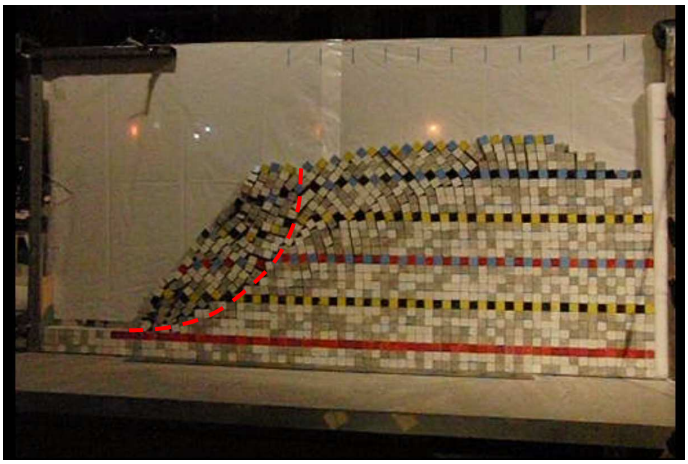

(d) The slope failed

Figure 7.3 Failure process of the benchmark case (continued)

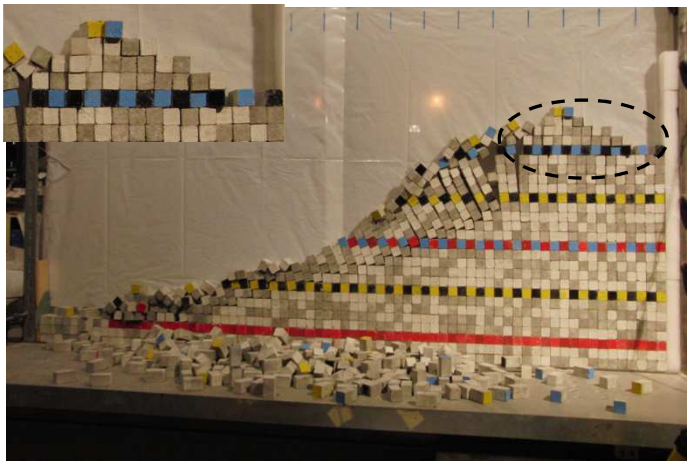

(e) The slope failed completely

Figure 7.3 Failure process of the benchmark case (continued)

7.3.1.2 A slope with one free face

In most experiments, the configuration of the slope crest was similar to that in the benchmark, i.e., with two free faces (Figure 7.2). This consideration was to eliminate the effect of the frame on the stability of the slope by impact during the shaking. In this case, however, a slope with one free face was designed to facilitate the investigation the effect of the impact by the frame (Figure 7.4(a)), in which all other conditions were similar to those in the benchmark except the configuration of the slope crest.

Figure 7.4(b) shows the photography of the slope with one free face after failure. The failure surface was deeper in this case than that in the benchmark. This was due to the impact between the slope crest and the frame during the shaking.

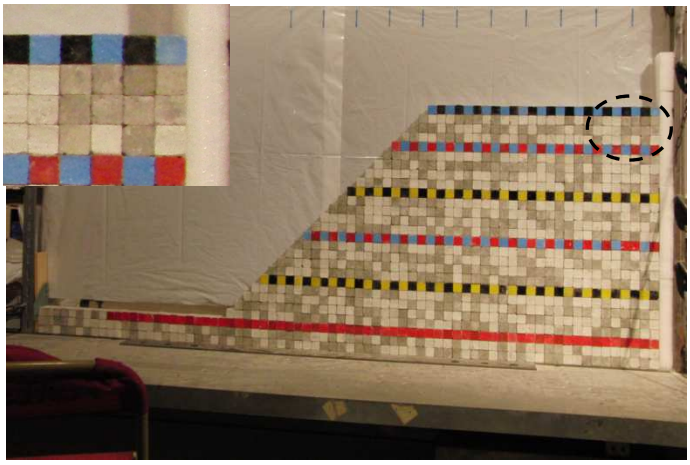

(a) Before failure

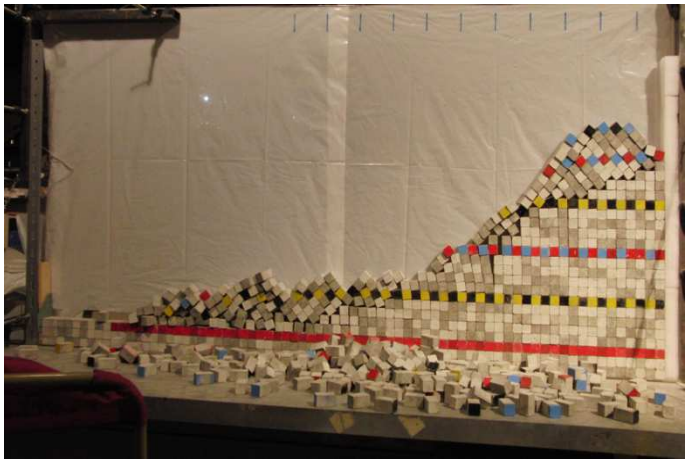

(b) After failure

Figure 7.4 A slope with one free face

7.3.2 A slope with joints inclined at 45°

7.3.2.1 With supporting

Another joint configuration was inclined at 45°. At the bottom of the slope, a wood slab was fixed to avoid any collapse of the blocks laid on the bottom before the shaking (Figure 7.5). The slope did not fail under sinusoidal waves with a peak acceleration of 300 gal and a frequency of 5 Hz.

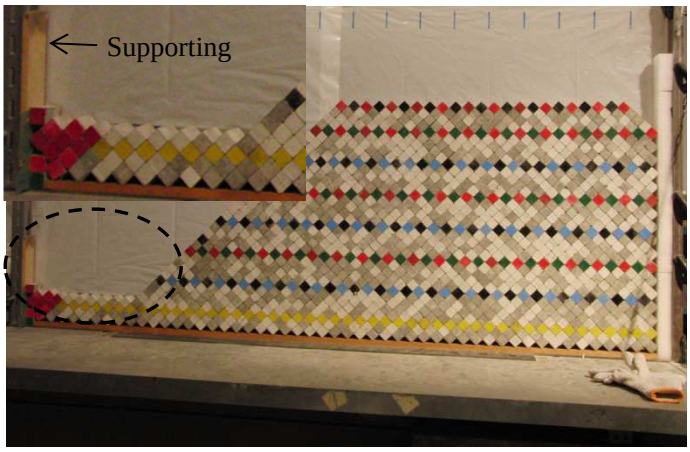

Figure 7.5 A rock slope model with 45° inclined joints (with supporting)

7.3.2.2 No supporting

In this case, there was no supporting at the bottom of the slope (Figure 7.6(a)).

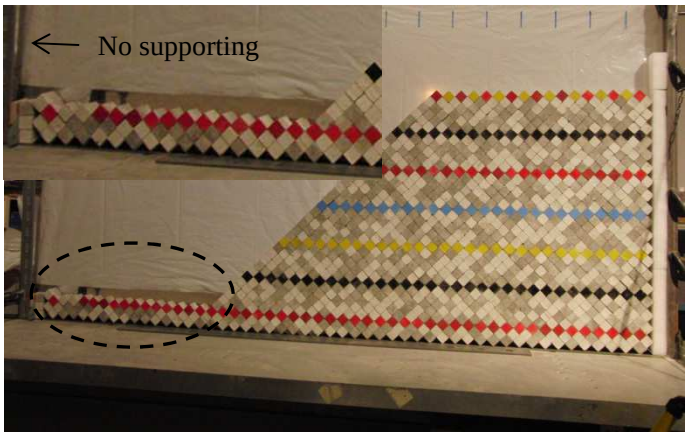

(a) Before failure

Figure 7.6 A rock slope model with 45° inclined joints (no supporting) (to be continued)

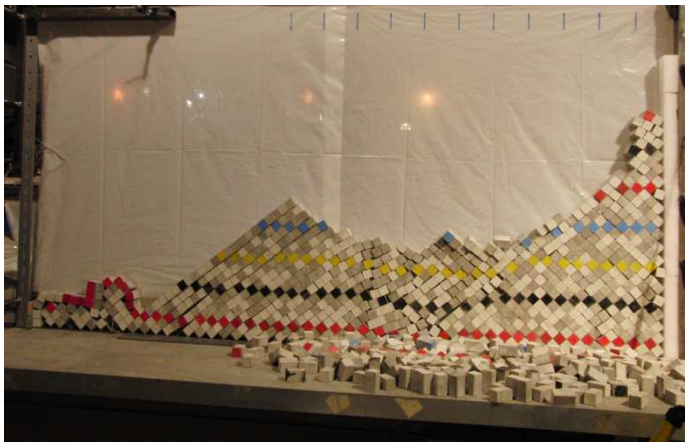

(b) After failure

Figure 7.6 A rock slope model with 45° inclined joints (no supporting) (continued)

The failure involved gradual buckling of the blocks near the toe of the slope, followed by almost wholly downward and leftward movement of the slope, and correspondingly the blocks higher up on the slope failed along a weak interlayer.

7.4 CONCLUSIONS

To give a demonstrative overview of the generally complex process of slope failure associated with seismic shaking, a series of shaking table tests was performed. These tests give a qualitative description of various failure modes: sliding, toppling, and buckling. These qualitative descriptions provide a basis for a quantitative description, such as limit equilibrium or numerical analysis that is properly constrained and meaningful. Shaking table tests show that the failure was largely influenced by the joint configuration. Significantly different failure pattern was observed in the shaking table tests if vertical joints near the slope surface were discontinuous especially when the length of the vertical discontinuous joints was within the depth of five blocks. This was because the cracks were difficult to propagate in the direction of depth.

CHAPTER 8

SUMMARY AND CONCLUSIONS

Rock avalanches pose significant hazards in many parts over the world especially in mountainous areas. Understanding the propagation mechanisms from imitation to rest is extremely important for hazard mapping of mountainous regions, for the prevention, reduction, and mitigation of the natural hazards causing devastating damage of property and claiming the lives of the people on a large scale. In order to investigate propagation mechanisms and deposit characteristics involved in rock avalanches, a series of fundamental studies, including laboratory experiments, theoretical predictions, and numerical simulations, has been performed. Based on these work, some conclusions are obtained in this study.

In Chapter 2, small flume tests were carried out to study the effect of interactions between constitute particles on the mobility of granular flows. Test results indicate that the run-outs of the flows with a wide range of grain sizes were larger than those of the flows only containing mono-sized particles. The proportion of fine sand strongly influenced the run-out of granular composites. The fine sand was transported with the gravel, and segregated naturally to the base of the flow under gravity. The rolling of fine sand acted as a lubricant for the gravel by the interactions with each other, and thus the friction resistance reduced during the movement. With increasing mass of fine sand, a greater proportion of gravel was completely supported by the fine sand, and the run-out reached its peak. This emphasizes that rolling motion was very important in flow propagation, and increasing proportion of rolling to sliding in particle motion reduced energy consumption. However, the run-out decreased with further increasing mass of fine sand. This was because intergranular friction dominated which was the primary source of energy loss, and thus limited the propagation of granular flows. The deposit morphology on the steep and gentle slopes significantly departed from each other. The deposit profile was much flatter and longer on the steep slopes (15° and 10°) than that on the gentle slopes (5° and 0°). The region of maximum concentration of particles was farther from the flow origin on the steeper slope, i.e., more materials were transported a long distance

on the steep slope. On the gentle slopes, however, the deposit was more concentrated because the materials were prone to contribute to add the deposition height rather than the run-out. The deposit morphologies were almost similar on the same slope for the three flows containing different constitute particles. This implies that the enhanced mobility of granular flows was more sensitive to the inclination of the lower slope than granular components.

In Chapter 3, a series of shaking table tests was conducted to investigate some potential factors influencing the run-out of granular flows released in a small flume under dynamic conditions. Test results show that the run-outs of the two composites increased with decreasing frequency and increasing amplitude. The run-out of the fine particles dominated materials was significantly smaller than that of the coarse particles dominated materials. The decrease in run-out with the frequency for the fine particles dominated materials was more significant than that for the coarse particles dominated materials. This was because intergranular friction dramatically dissipated the energy when excessive fine particles were involved. This conclusion agreed with that drawn in Chapter 2. This implies that coarse materials had a higher mobility than fine materials under static and dynamic conditions. The increase in run-out due to the shaking was observed in most experiments, except in the series with the amplitude of 100 gal. The increase in run-out when the materials were released meanwhile the sinusoidal waves were input was larger than that when the materials were released before the shaking at the amplitude of 200 gal and 300 gal. This was because more energy was consumed by intergranular friction due to the high concentration of the existing deposit on the lower slope. However, the increase in run-out when the materials were released meanwhile the shaking was smaller than that when the materials were released before the shaking at 400 gal. One of the main causes was that the moving mass dramatically collided with the upper slope at the large amplitude when they flowed along the upper slope.

In Chapter 4, granular flows were released in a large flume to clarify some factors influencing mass-front velocity and deposit characteristics. The mass-front velocity was affected significantly by the characteristics and concentration of involved materials. A high velocity and its fluctuation were shown for cobbles, which were prone to rolling and impact due to their high roundness. The velocity reduced near the concavity for blocks and for gravel as well, and the decrease in velocity was more significant for the gravel than that for the blocks. The velocity added up with the volume for the cobbles. A

composite of cubes and gravel with a large volume displayed a rather lower mobility than a mono-material of the cubes and of the gravel with a small volume. The velocity of a composite of cobbles and gravel with a large volume was almost the same as a mono-material of the cobbles and of the gravel with a small volume. The velocity for the case in a high and narrow initial stack was slightly lower than that in a low and wide initial stack. The progression of granular flows was controlled by the topography, including macro-topography (e.g. slope mean gradient) and micro-topography (e.g. bottom roughness and obstacle). The velocities in all studied cases reduced by approximately 25% when the materials changed the direction of movement near the concavity of the flume. A soft, erodible substrate was of certain effect on obstructing of movement of subsequent flows and ability of entrainment along its propagation process. Two peak velocities were shown in the cases with a convexity, which significantly departed from those cases in the absence of the convexity. The mass front decelerated when it encountered the convexity, and then accelerated greatly when the materials took a ballistic trajectory from the vertex of the convexity and briefly lost contact with the base of the flume. The forest model obstructed the progression of granular flows. The bottom roughness had an effect upon the velocity. Travel distance increased with the volume of released materials. The movement of materials was affected by micro-topography, such as convexity, forest model, and bottom roughness, and deposit shape was prone to be short and high. However, its effect on travel distance was not obvious.

In Chapter 5, a simple lumped mass model was proposed to describe the velocity of granular flows. The model based on energy approach could roughly predict the velocity of granular flows in the large flume. The predicted velocity was somewhat lower than the measured one because the model neglected collisions between particles. Subsequent particles with a higher velocity collided with slowed fronts to make them accelerate. This implies that continual collisions were a potential cause for high velocities and long run-outs of large rock avalanches. The presented model predicted a decrease in velocity when the flow changed its movement direction due to the variation in slope inclination. The predicted decrease in velocity was less than the measured one within a reasonable range of no more than 10%. The difference would be added up with the complexity of bed topography, especially when more abundant, higher and slightly longer ballistic trajectories or jumps occurred as in field investigations. For some cases, in which a

convexity was introduced, the model also predicted the similar trend of velocities as measured one in the tests. The materials took a ballistic trajectory from the vertex of the convexity, and reduced dramatically when they finally made contact with the base of the lower slope. The difference between predicted and measured decrease in velocity was estimated with approximately 5% due to the landing. This model can be also extended to predict the run-out and velocity of rock avalanches if the apparent friction coefficient is used, and it assists in the design of safer human habitation and environmental protection.

In Chapter 6, some experimental flows presented in Chapter 4 and three large rock avalanches were reproduced by discontinuous deformation analysis. DDA captured the main features of granular flows in the large flume tests, and the simulated velocity corresponded well with that measured in the tests. Energy dissipation caused by intergranular friction was accurately described in DDA. Collisions between particles, which were one of the possible reasons for the high velocity and long run-out, were also reflected realistically. However, energy loss caused by these collisions was not taken into account in DDA, causing the simulated mass-front velocity to fluctuate more than that measured in the tests. Furthermore, the simulated results were highly sensitive to the shape and angularity of granular elements; thus, the use of realistic elements was important for obtaining reliable results. The friction coefficient strongly influenced the simulation results for the large rock avalanches. The calculated deposit was only similar to the actual deposit when the apparent friction coefficient, which was determined by field investigation, was used instead of the friction coefficient measured in the laboratory. In contrast, for the large flume tests, the measured friction coefficient served as an available parameter to predict the velocity of experimental granular flows. Furthermore, the calculated deposit was similar regardless of the initial horizontal velocity. This implies that the final deposit was mainly determined by the potential energy of the failed mass and was not significantly influenced by the earthquake energy.

In Chapter 7, to give a demonstrative overview of the generally complex process of slope failure associated with seismic shaking, a series of shaking table tests was performed. These tests give a qualitative description of various failure modes: sliding, toppling, and buckling. These qualitative descriptions provide a basic for a quantitative description, such as limit equilibrium or numerical analysis that is properly constrained and meaningful. Shaking table tests show that the failure was largely influenced by the joint configuration. Significantly different failure pattern was observed in the shaking

table tests if vertical joints near the slope surface were discontinuous especially when the length of the vertical discontinuous joints was within the depth of five blocks. This was because the cracks were difficult to propagate in the direction of depth.

The most general aim of this work was to deepen the knowledge on rock avalanche behavior and to open some perspectives for further advancement of the research in this field. I hope to have given a contribution to the knowledge of some aspects associated with propagation mechanisms involved in rock avalanches. As previously note, interactions between constitute particles influenced the mobility of granular flows. A thin layer of fine particles acted as rollers for the rolling of coarse particles, and the effective friction resistance was reduced during the movement; when excessive fine particles were involved, however, coarse particles were embedded in a matrix of the fine particles so that the particles were either blocked or forced into sliding. Rolling motion was thus very important in flow propagation, and increasing proportion of rolling to sliding in particle motion reduced energy consumption and enhanced the mobility of granular flows. Furthermore, subsequent particles with a higher velocity gave propulsion to these at the front by impact, and thus continued collisions were partly responsible for the high mobility of rock avalanches. Size effect should be considered to realistically reproduce large rock avalanches by theoretic model and numerical analysis.

Though an extensive set of factors influencing the velocity and run-out of experimental granular flows has been taken into consideration, the range of studied factors was limited in this research due to the limit of space and time. Some factors such as the angularity and grain size of granular materials have been found to have influences on the propagation of granular flows and needs be considered in future tests. The present lumped mass model should be extended to the reproduction of field rock avalanches to check its applicability. Furthermore, the conclusion that the apparent friction coefficient served as a reasonable parameter for the reproduction of large events needs to be further confirmed by simulating a number of large events.

There are still many challenges to be met in the field of avalanche research. The main intention of future researches in this field should be directed towards modeling and solving the real problems so as to minimize the casualties and hazards induced by natural avalanches. This includes knowledge and understanding from the initiation, propagation, to deposition. Ultimately, we can set up a system, or a set of systems linked to form a

network that are enable the observation and collection of detailed information about the location and level of rock avalanches, region prone to be hit, etc., for a safer world.

REFERENCES

Acharya G, Davies T, Bowman E (2009). The influence of shallow landslide on sediment supply: A flume-based investigation using sandy soil. *Eng. Geol.*, 109: 161-169.

Ai C, Feng C, Li SH, Zhao AP (2010). Experimental research on dynamic response of consequent rock slope under seismic loading. *Chinese Journal of Rock Mechanics and Engineering*, 29(9): 1825-1832 (in Chinese).

Ancey C, Meunier M (2004). Estimating bulk rheological properties of flowing snow avalanches from field data. *J. Geophys. Res.*, 109: F01004.

Balmforth NJ, Kerswell RR (2005). Granular collapse in two dimensions. *J. Fluid Mech.*, 538: 399-428.

Bhasin R, Kaynia AM (2004). Static and dynamic simulation of a 700-m high rock slope in western Norway. *Eng. Geol.*, 71: 213-226.

Bommer JJ, Rodríguez CE (2002). Earthquake-induced landslides in Central America. *Eng. Geol.*, 63: 189-220.

Bouchut F, Westdickenberg M (2004). Gravity driven shallow water models for arbitrary topography. *Comm. Math. Sci.*, 2: 359-389.

Campbell CS (1989). Self-lubrication for long runout landslides. *J. Geol.*, 97: 653-665.

Campbell CS, Cleary PW, Hopkins M (1995). Large-scale landslide simulations: global deformation, velocities and basal friction. *J. Geophys. Res.*, 100: 8267-8273.

Collins GS, Melosh HJ (2003). Acoustic fluidization and the extraordinary mobility of sturzstroms. *J. Geophys. Res.*, 108(B10): 2473.

Corominas J (1996). The angle of reach as a mobility index for small and large landslide. *Can. Geotech. J.*, 33: 260-271.

Crosta GB, Frattini P, Fusi N (2007). Fragmentation in the Val Pola rock avalanche,

Italian Alps. *J. Geophys. Res.*, 112: F01006.

Crosta GB, Imposimato S, Roddeman D (2009). Numerical modeling of 2-D granular step collapse on erodible and nonerodible surface. *J. Geophys. Res.*, 114: F03020.

Davies TR (1982). Spreading of rock avalanche debris by mechanical fluidization. *Rock Mech.*, 15: 9-24.

Davies TR (1997). Runout of dry granular avalanches. Department of Natural Resources Engineering, Lincoln University, Canterbury, New Zealand.

Davies TR, McSaveney MJ (1999). Runout of dry granular avalanches. *Can. Geotech. J.*, 36: 313-320.

Davies TR, McSaveney MJ (2002). Dynamic simulation of the motion of fragmentation rock avalanches. *Can. Geotech. J.*, 39: 789-798.

Davies TR, McSaveney MJ (2009). The role of rock fragmentation in the motion of large landslides. *Eng. Geol.*, 109: 67-79.

Davies TR, McSaveney MJ, Hodgson KA (1999). A fragmentation-spreading model for long-runout rock avalanches. *Can. Geotech. J.*, 36: 1096-1110.

Deangeli C (2008). Laboratory granular flows generated by slope failures. *Rock Mech. Rock Eng.*, 41(1): 199-217.

Denlinger RP, Iverson RM (2001). Flow of variably fluidized granular masses across three-dimensional terrain: 2. Numerical predictions and experimental tests. *J. Geophys. Res.*, 106: 553-566.

Denlinger RP, Iverson RM (2004). Granular avalanches across irregular three-dimensional terrain, 1. Theory and computation. *J. Geophys. Res.*, 109: F01014.

Doolin DM, Sitar N (2002). Displacement accuracy of discontinuous deformation analysis method applied to sliding block. *J. Eng. Mech.*, 128: 1158-1168.

Dunning SA (2006). The grain size distribution of rock-avalanche deposits in valley-confined settings. *Italian Journal of Engineering Geology and Environment*, Special issue 1: 117-121.

Eckersley D (1990). Instrumented laboratory flowslides. *Géotechnique*, 40(3): 489-502.

Einstein HH, Veneziano D, Baecher GB, O'Reilly (1983). The effect of discontinuity persistence on rock slope stability. *Int. J. Rock Mech. Min. Sci.* & *Geomech. Abstr.*, 20(5): 227-236.

Erismann TH (1979). Mechanisms of large landslides. *Rock Mech.*, 12: 15-46.

Erismann TH, Abele G (2001). Dynamics of rockslides and rockfalls. Berlin, Springer, pp.12.

Evans S, Tutubalina O, Drobyshev V, Chernomorets S, McDougall S, Petrakov D, Hungr O (2009). Catastrophic detachment and high-velocity long-runout flow of Kolka Glacier, Caucasus Mountains, Russia in 2002. *Geomorphology*, 105: 314-321.

Fily M, Bourdelles B, Dedieu JP, Sergent C (1997). Comparison of in situ and landsat thematic mapper derived snow grain characteristics in the Alps. *Remote Sens. Environ.*, 59: 452-460.

Genevois R, Ghirotti M (2005). The 1963 Vaiont landslide. *Giornale di Geologia Applicata*, 1: 41-52.

Giani GP (1992). Rock slope stability analysis. Balkema, Rotterdam.

Goguel J (1978). Scale-dependent rockslides mechanisms, with emphasis on the role of pore fluid vaporization. In: Voight B (Ed.), Rockslides and Avalanches. 1: Natural Phenomena. Elsevier, Amsterdam, pp.693-705.

Habib P (1976). Production of gaseous pore pressure during rock slides. *Rock Mech.*, 7: 193-197.

Harrison JP, Hudson JA (2000). Engineering rock mechanics. Part 2: illustrative workable examples. In: Sarkka, P. and Eloranta, P. Editors, Oxford: Pergamon.

Hatzor YH, Arzi AA, Zaslavsky Y, Shapira A (2004). Dynamic stability analysis of jointed rock slopes using the DDA method: King Herod's Palace, Masada, Israel. *Int. J. Rock Mech. Min. Sci.*, 41: 813–832.

Heim A (1932). Bergsturz und Meschenleben. *Frets und Wasmuth*, 218.

Hoek E, Bray JW (1981). Rock slope engineering. 3rd ed., Institute of Mining and Metallurgy, London, UK.

Hsü KJ (1975). Catastrophic debris streams (Sturzstroms) generated by rockfalls. *Geol. Soc. Am. Bull.*, 86: 129-140.

Huang RQ (2009). Geohazard assessment of the Wenchuan earthquake. Chinese Science Press, Beijing, pp. 408 (in Chinese).

Huang Y, Chen W, Liu JY (2010). Secondary geological hazard analysis in Beichuan after the Wenchuan earthquake and recommendations for reconstruction. *Environ Earth Sci.*, doi: 10.1007/s12665-010-0612-5.

Huang RQ, Xu Q, Huo JJ (2011a). Mechanism and geo-mechanics models of landslides triggered by 5.12 Wenchuan earthquake. *Journal of Mountain Science*, 8(2): 200-210.

Huang Y, Zhang WJ, Xu Q, Xie P, Hao L (2011b). Run-out analysis of flow-like landslides triggered by the Ms 8.0 2008 Wenchuan earthquake using smoothed particle hydrodynamics. *Landslides*, doi: 10.1007/s10346-011-0285-5.

Hungr O, Evans SG, Bovis M, Hutchinson JN (2001). Review of the classification landslides of the flow type. *Environ. Eng. Geosci.*, VII: 221-238.

Ishikawa T, Ohnishi Y, Namura A (1997). DDA applied to deformation analysis of coarse granular materials (ballast). In: Ohnishi Y, editor. *Proc. 2nd Int. Conf. on Analysis of Discontinuous Deformation*. Japan Institute of Systems Research: Kyoto, Japan: 253-262.

Iverson RM, Denlinger RP (2001). Flow of variably fluidized granular masses across three-dimensional terrain: 1. Coulomb mixture theory. *J. Geophys. Res.*, 106: 537-552.

Jibson RW, Harp EL, Schulz W, Keefer DK (2006). Large rock avalanches triggered by the M 7.9 Denali Fault, Alaska, earthquake of 3 November 2002. *Eng. Geol.*, 83: 144-160.

Jing L (1998). Formulation of discontinuous deformation analysis (DDA)—an implicit discrete element model for block system. *Eng. Geol.*, 49: 371-381.

Jing L, Hudson JA (2002). Numerical methods in rock mechanics. *Int. J. Rock Mech. Min. Sci.*, 39: 409-427.

Kent PE (1966). The transport mechanism in catastrophic rockfalls. *J. Geol.*, 74: 79-83.

Khan MS (2010). Investigation of discontinuous deformation analysis for application in jointed rock masses. PhD thesis, University of Toronto, Canada.

Kokusho T, Ishizawa T (2006). Energy approach for earthquake induced slope failure evaluation. *Soil Dyn. Earthq. Eng.*, 26: 221-230.

Kokusho T, Ishizawa T, Koizumi K (2011). Energy approach to seismically induced slope failure and its application to case histories. *Eng. Geol.*, 122: 115-128.

Kokusho T, Ishizawa T, Nishida K (2009). Travel distance of failed slopes during 2004 Chutsu earthquake and its evaluation in terms of energy. *Soil Dyn. Earthq. Eng.*, 29: 1159-1169.

Lajeunesse E, Mangeney-Castelnau A, Vilotte JP (2004). Spreading of a granular mass on a horizontal plane. *Phys. Fluids*, 16(7): 2371-2381.

Lajeunesse E, Monnier JB, Homsy GM (2005). Granular slumping on a horizontal surface. *Phys. Fluids*, 17: 203302.

Latha GM, Garaga A (2010). Seismic stability analysis of a Himalayan rock slope. *Rock Mech. Rock Eng.*, 43: 831-843.

Legros F (2002). The mobility of long-runout landslides. *Eng. Geol.*, 63: 301-331.

Li SH, Lian ZZ, Wang JG (2005). Effect of rock mass structure and block size on the slope stability. *Engineering and Materials Science*, 48: 1-17.

Lin CT, Amadei B, Jung J, Dwyer J (1996). Extensions of discontinuous deformation analysis for jointed rock masses. *Int. J. Rock Mech. Min. Sci. Geomech. Abstr.*, 33(7): 671-694.

Lin ML, Wang KL (2006). Seismic slope behavior in a large-scale shaking table model test. *Eng. Geol.*, 86: 118-133.

Locat P, Couture R, Locat J, Leroueil S (2003). Assessment of the fragmentation energy in rock avalanche. *Proc. 3rd Can. Conf. on Geotechnique and Natural Hazards*: 301-308.

Lube G, Huppert HE, Sparks RSJ, Freundt A (2005). Collapses of two-dimensional granular columns. *Phys. Rev. E*, 72: 041301.

Lube G, Huppert HE, Sparks RSJ, Hallworth MA (2004). Axisymmetric collapses of granular columns. *J. Fluid Mech.*, 508: 175-199.

Ma GC, Matsuyama H, Nishiyama S, Ohnishi Y (2011). Practical studies on rockfall simulation by DDA. *J. Rock Mech. Geotech. Eng.*, 3(1): 57-63.

MacLaughlin MM, Doolin DM (2006). Review of validation of the discontinuous deformation analysis (DDA) method. *Int. J. Numer. Anal. Meth. Geomech.*, 30: 271-305.

Manzella I, Labiouse V (2008). Qualitative analysis of rock avalanches propagation by means of physical modeling of non-constrained gravel flows. *Rock Mech. Rock Eng.*, 41(1): 133-151.

Manzella I, Labiouse V (2009). Flow experiments with gravel and blocks at small scale to investigate parameters and mechanisms involved in rock avalanches. *Eng. Geol.*, 109: 146-158.

McBride AT, Scheele F (2001). Validation of discontinuous deformation analysis using a physical model. *Proc. Structural and Engineering and Mechanics Conf.*, vol. 1, Cape Town, South Africa, 719-726.

Mcsaveney MJ (2002). Recent rockfalls and rock avalanches in Mount Cook National Park, New Zealand, In Catastrophic landslides: effects, occurrence, and mechanisms. Reviews in Engineering Geology edited by S.G. Evans, J.V. DeGraff, Geological Society of America Reviews in Engineering Geology, XV: 35-70.

Mcsaveney MJ, Davies TH (2007). Rockslides and their motion. *Progress in landslide science*, Part II: 113-133.

Melosh HJ (1979). Acoustic fluidization-a new geologic process. *J. Geophys. Res.*, 84: 7513-7520.

Möbius ME, Lauderdale BE, Nagel SR, Jaeger HM (2001). Size separation of granular particles. *Nature*, 414: 270.

Moriwaki H, Inokuchi T, Hattanji T, Sassa K, Ochiai H, Wang GH (2004). Failure processes in a full-scale landslide experiment using a rainfall simulator. *Landslides*, 1: 277-288.

Ning YJ, Yang J, An XM, Ma GW (2011). Modelling rock fracturing and blast-induced rock mass failure via advanced discretisation within the discontinuous deformation analysis framework. *Comput. Geotech.*, 38: 40-49.

Okada Y, Ochiai H (2008). Flow characteristics of 2-phase granular mass flows from model flume tests. *Eng. Geol.*, 97: 1-14.

Okura Y, Kitahara H, Sammori T, Kawanami A (2000a). The effects of rockfall volume on runout distance. *Eng. Geol.*, 58: 109-124.

Okura Y, Kitahara H, Sammori T (2000b). Fluidization in dry landslides. *Eng. Geol.*, 56: 347-360.

Phillips JC, Hogg AJ, Kerswell RR, Thomas NH (2006). Enhanced mobility of granular mixtures of fine and coarse particles. *Earth Planet. Sci. Lett.*, 246: 466-480.

Pudasaini SP, Domnik B (2009). Energy considerations in accelerating rapid shear granular flows. *Nonlin. Processes Geophys.*, 16: 399-407.

Pudasaini SP, Hsiau SS, Wang YQ, Hutter K (2005a). Velocity measurements in dry granular avalanches using particle image velocimetry technique and comparison with theoretical predictions. *Phys. Fluids*, 17: 093301.

Pudasaini SP, Hutter K (2007). Avalanche dynamics: dynamics of rapid flows of dense granular avalanches. Springer-Verlag, Berlin.

Pudasaini SP, Hutter K, Huiau SS, Tai SC, Wang YQ, Katzenbach R (2007). Rapid flow of dry granular materials down inclined chutes impinging on rigid walls. *Phys. Fluids*, 19: 053302.

Pudasaini SP, Kröner C (2008). Shock waves in rapid flows of dense granular materials: Theoretical predictions and experimental results. *Phys. Rev. E*, 78: 041308.

Pudasaini SP, Wang Y, Hutter K (2005b). Modelling debris flows down general channels. *Nat. Hazard Earth Sys.*, 5: 799-819.

Roche O, Gilbertson MA, Phillips JC, Sparks RSJ (2006). The influence of particle size on the flow of initially fluidized powders. *Power Technology*, 166: 167-174.

Sassa K, Fukuoka H, Scarascia-Mugnozza G, Evans S, (1996). Earthquake-induced-landslides: distribution, motion and mechanisms. Special issue for the great Hanshin Earthquake Disasters. *Soils and Foundations*, 53-64.

Savage SB, Hutter K (1989). The motion of a finite mass of granular material down a rough incline. *J. Fluid Mech.*, 199: 177-215.

Savage SB, Lun CKK (1988). Particle size segregation in inclined chute flow of dry cohesionless granular solids. *J. Fluid Mech.*, 189: 311-335.

Scheidegger AE (1973). On the prediction of the reach and velocity of catastrophic landslides. *Rock Mech.*, 5: 231-236.

Shi GH (1988). Discontinuous deformation analysis. PhD thesis, University of California, Berkeley, USA.

Shi GH (1992). Discontinuous deformation analysis: A new numerical model for the statics and dynamics of deformable block structures. *Eng. Comput.*, 9: 157-168.

Shi GH, Goodman RE (1985). Two dimensional discontinuous deformation analysis. *Int. J. Numer. Anal. Meth. Geomech.*, 9: 541-556.

Shi GH, Goodman RE (1989). Generalization of two-dimensional discontinuous deformation analysis for forward modeling. *Int. J. Numer. Anal. Meth. Geomech.*, 13: 359-380.

Shreve RL (1968a). The Blackhawk landslide. *Geol. Soc. Am.*, Spec. Pap. 108: 1-47.

Shreve RL (1968b). Leakage and fluidisation in air-layer lubricated avalanches. *Geol. Soc. Am. Bull.*, 79: 653-658.

Sitar N, MacLaughlin MM, Doolin DM (2005). Influence of kinematics on landslide mobility and failure mode. *J. Geotech. Geoenviron. Eng.*, 131(6): 716-728.

Sosio R, Crosta G, Hungr O (2008). Complete dynamic modeling calibration for the Thurwieser rock avalanche (Italian Central Alps). *Eng*. *Geol*., 100: 11-26.

Sun P, Zhang YS, Shi JS, Chen LW (2011). Analysis on the dynamical process of Donghekou rockslide-debris flow triggered by 5.12 Wenchuan earthquake. *Journal of Mountain Science*, 8(2): 140-148.

Tsesarsky M, Hatzor YH, Sitar N (2005). Dynamic Displacement of a Block on an Inclined Plane: Analytical, Experimental and DDA Results. *Rock Mech*. *Rock Eng*., 38(2): 153-167.

Ugai K, Yang QQ, Cai F, Xu Q, Ahmed A, Su ZM, Yamada M (2009a). Laboratory flume experiment for rock avalanches. *Proc*. *Int*. *Symp*. *on Rock Mechanics*, HongKong.

Ugai K, Yang QQ, Cai F, Xu Q, Ahmed A, Su ZM, Yamada M (2009b). Laboratory flume experiment for rock avalanches. *Proc*. *44th Japan Nat*. *Conf*. *on Geotechnical Engineering*, 1577-1578.

Ugai K, Yang QQ, Cai F, Xu Q, Ahmed A, Su ZM, Yamada M (2009c). Shaking table tests of laboratory flume for rock avalanche, *Proc*. 4*8th Japan Nat*. *Conf*. *on Landslide*, 174-175.

Ugai K, Yang QQ, Cai F, Xu Q, Ahmed A, Su ZM, Yamada M (2010). Laboratory Flume Static and Dynamic Experiment for Rock Avalanches. *Proc*. *Geo-Shanghai* 2010, Soil Dynamics and Earthquake Engineering, Geotechnical Special Publication, ASCE, No. 201, pp. 278-287.

Ugai K, Yang QQ, Cai F, Yamada M, Huang RQ, Xu Q (2011). Fundamental study on mechanism of rock avalanche. *Journal of the Japan Landslide Society*, 48(1): 12-22 (In Japanese).

Valentino R, Barla G, Montrasio L (2008). Experimental analysis and micromechanical modeling of dry granular flow and impacts in laboratory flume tests. *Rock Mech*. *Rock Eng*., 41(1): 153-177.

Van Gassen W, Cruden DM (1989). Momentum transfer and friction in the debris of rock avalanches. *Can*. *Geotech*. *J*., 26: 623-628.

Voight B, Janda RJ, Glicken H, Douglass PM (1983). Nature and mechanics of the Mount St. Helens rockslide-avalanche of May 1980. *Géotechnique,* 33: 243-273.

Voight B, Sousa J (1994). Lessons from Ontake-san: A comparative analysis of debris avalanche dynamics. *Eng*. *Geol*., 38: 262-297.

Wartman J, Seed R, Bray J (2005). Shaking table modeling of seismically induced deformation in slopes. *J*. *Geotech*. *Geoenviron*. *Eng*., 131(5): 610-622.

Wang KL, Lin ML (2011). Initiation and displacement of landslide induced by earthquake—a study of shaking table model slope test. *Eng*. *Geol*., 122: 106-144.

Wang GH, Sassa K (2001). Factors affecting rainfall-induced flowslides in laboratory flume tests. *Géotechnique,* 51 (7): 587-599.

Wang GH, Sassa K (2003). Pore-pressure generation and movement of rainfall-induced landslide: effects of grain size and fine-particle content. *Eng*. *Geol*., 69: 109-125.

Wu JH (2010). Seismic landslide simulations in discontinuous deformation analysis. *Comput*. *Geotech*., 37: 594-601.

Wu JH, Chen CH (2011). Application of DDA to simulate characteristics of the Tsaoling landslide. *Comput*. *Geotech*., 38: 741-750.

Xinhua News Agency (2008). At least 1,000 students buried in China county worst hit by quake. http://news.xinhuanet.com/english/2008-05/13/content_8157648.htm.

Xu Q, Pei X, Huang RQ (2010). Large-scale landslides induced by the Wenchuan Earthquake. Chinese Science Press, Beijing, pp.408-422 (in Chinese).

Xu Q, Zhang S, Li WL (2011). Spatial distribution of large-scale landslides induced by the 5.12 Wenchuan earthquake. *Journal of Mountain Science*, 8(2): 246-260.

Yang QQ, Cai F, Ugai K, Su ZM, Huang RQ, Xu Q (2012). A simple lumped mass model to describe velocity of granular flows in a large flume. *Journal of Mountain Science*, 9(2): 221-231.

Yang QQ, Cai F, Ugai K, Yamada M, Ahmed A, Huang RQ, Xu Q (2011a). Some factors affecting mass-front velocity of rapid dry granular flows in a large flume. *Eng*. *Geol*.,

122: 249-260.

Yang QQ, Keizo Ugai, Cai F, Su ZM. Yamada M (2011b). Small-scale flume test under dynamic condition for rock avalanches. *GeoHunan Int*. *Conf*. II: Emerging Technologies for Design, Construction, Rehabilitation, and Inspections of Transportation Infrastructures, ASCE, pp.165-172.

Yang QQ, Keizo Ugai, Cai F, Yamada M (2010). The effect of released material on mass front velocity of rock avalanches. *Proc*. *45th Japan Nat*. *Conf*. *on Geotechnical Engineering*, 1638-1639.

Yang Q, Su ZM, Ugai K, Cai F, Yamada M (2009). Recent landslide disasters induced by earthquakes. *J*. *Singapore Eng*., Jan: 36-38.

Yin YP, Wang FW, Sun P (2009). Landslide hazards triggered by the 2008 Wenchuan earthquake, Sichuan, China. *Landslides*, 6: 139-151.

Zhang ZY, Liu HC (2008). Large-scale landslide group at Longyang hydropower station and Chana landslide, Qinghai province, in catastrophic landslides in China. Chinese Science Press, Beijing. pp.129-133 (In Chinese).

ACKNOWLEDGEMENTS

No person can complete the requirements for a doctoral degree without a tremendous amount of assistance and support from colleagues and family. I am certainly no exception. I am most grateful to my supervisor, Prof. Ugai Keizo for giving me the great opportunity to study and earn my doctoral degree, and for his persistence, guidance, and encouragement during my research.

I sincerely thank my dissertation committee members, Prof. Shimizu Yoshihiko, Prof. Ugai Keizo, Prof. Wakai Akihiko, Prof. Watari Hisaki, and Prof. Uzaki Kennichi for thoroughly reviewing my work and for their helpful comments and suggestions.

I gratefully acknowledge Prof. Cai Fei for his insightful advice and invaluable guidance. His in-depth review, comments, and suggestions have been very helpful in shaping this dissertation. Without his patient help, this study would not be smoothly finished.

Gratefulness is extended to Prof. Wakai Akihiko for his valuable help and discussions. In addition, thanks are also extended to my fellow students, Mr. Xu Lingyu, Dr. Ahmed Aly as well as the other students of this laboratory for their company, encouragement, and friendship.

I thank Dr. Yamada Masao for his help in conducting the large flume tests, which is an important part in this research. I also would like to thank Mr. Matsuda Kohei for his assistance in performing the small flume tests under static conditions.

I wish to express my acknowledgement to Prof. Xu Linrong in Central South University for his continuous encouragement to work always towards academic excellence and quality research. I am grateful to Prof. Huang Runqiu and Prof. Xu Qiang in Chengdu University of Technology for their support and suggestions.

I owe many thanks to my friends, either in Japan or in China, for their care and support.

I gratefully acknowledge the financial supports provided by China Scholarship

Council during my stay at Gunma University.

A special gratitude is expressed to Dr. Su Zhiman, for his unconditional love and for enjoying this wonderful life together with me.

Last, but not least, my deepest heartfelt appreciation is given to my father, mother, and grandmother for being the sources of determination, motivation, and encouragement leading towards my life.